CORRELATING THE NANOSCALE MECHANICAL AND CHEMICAL PROPERTIES OF KNOCKOUT MICE BONES

by

NADIRE BERIL KAVUKCUOGLU

A Dissertation submitted to the

Graduate School-New Brunswick

Rutgers, The State University of New Jersey

in partial fulfillment of the requirements

for the degree of

Doctor of Philosophy

Graduate Program in Materials Science and Engineering

written under the direction of

Professor Adrian B. Mann

and approved by

_____

_____

_____

_____

New Brunswick, New Jersey

May, 2007

ABSTRACT OF DISSERTATION

CORRELATING THE NANOSCALE MECHANICAL AND CHEMICAL PROPERTIES OF KNOCKOUT MICE BONES

By NADIRE BERIL KAVUKCUOGLU

Dissertation Director:

Professor Adrian B. Mann

Bone is a mineral-organic composite where the organic matrix is mainly type I collagen plus small amounts of non-collagenous proteins including osteopontin (OPN), osteocalcin (OC) and fibrillin 2 (Fbn2). Mature bone undergoes remodeling continually so new bone is formed and old bone resorbed. Uncoupling between the bone resorption and bone formation causes an overall loss of bone mass and leads to diseases like osteoporosis and osteopenia. These are characterized by structural deterioration of the bone tissue and an increased risk of fracture. The non-collagenous bone proteins are known to have a role in regulating bone turnover and to affect the structural integrity of bone. OPN and OC play

a key role in bone resorption and formation, while absence of Fbn-2 causes a connective tissue disorder (congenital contractural arachnodactyly) and has been associated with decreased bone mass.

In this thesis nanoindentation and Raman-microspectroscopy techniques were used to investigate and correlate the mechanical and chemical properties of cortical femoral bones from OPN deficient (OPN-/-), OC deficient (OC-/-) and Fbn-2 deficient (Fbn2-/-) mice and their age, sex and background matched wild-type controls (OPN+/+, OC+/+ and Fbn2+/+). For OPN the hardness (H) and elastic modulus (E) of under 12 week OPN-/- bones were significantly lower than for OPN+/+ bones, but Raman showed no significant difference. Mechanical properties of bones from mice older than 12 weeks were not significantly different with genotype. However, mineralization and crystallinity from >50 week OPN-/- bones were significantly higher than for OPN+/+ bones. Mechanical properties of OPN-/- bones showed no variation with age, but mineralization, crystallinity and type-B carbonate substitution increased for both genotypes. For OC-/- intra-bone analyses showed that the hardness and crystallinity of the bones were significantly higher, especially in the mid-cortical sections, compared to OC+/+ bones. Fbn2-/- bones had significantly lower hardness and elastic modulus compared to Fbn2+/+ bones, but the crystallinity was higher. Type-B carbonate substitution decreased significantly in OC-/- and Fbn2-/- bones compared to their wild-type controls.

The thesis has provided new insight into how non-collagenous proteins affect the nanomechanics and chemistry of bone tissue. This information will assist in the development of new treatments for osteopenia/osteoporosis.

PREFACE

This thesis is based on research conducted in the Department of Materials Science and Engineering, Rutgers University, New Jersey, USA. The samples used in this study were provided by the Department of Cell Biology and Neuroscience (Rutgers University), Center of Alcohol Studies (Rutgers University) and Hospital for Special Surgery, NY

This thesis is based on the following papers:

1. Effects of Osteopontin Defficiency and Aging on Nanomechanics of Mouse Bone. N. B. Kavukcuoglu, D. Denhardt, N. Guzelsu, A.B. Mann; In Press, Journal of Biomedical Materials Research, 2006

2. Raman Microspectroscopic Analysis of Age Related Changes in Osteopontin Deficient Mouse Bones. N. B. Kavukcuoglu, D. Denhardt, A.B. Mann; submitted to Calcified Tissue International 2007

3. Nanomechanics and Raman Spectroscopy of Osteocalcin and Fibrillin 2 Knock-Out Mouse Bones. N.B.Kavukcuoglu, P.Patterson-Buckendahl, E. Arteaga-Solis, S. Lee-Arteaga, F.Ramirez, A.B.Mann; submitted to Journal of Materials Science, December 2006.

4. Effects of Osteopontin on Nanomechanics and Microstructure of Mouse Bones. B. Kavukcuoglu P, C. West, D. Denhardt, A.B. Mann; Materials Research Society Proceedings 2004; vol. 844, p. 99-104

5. Nanomechanics of Knockout Mouse Bones, N. B. Kavukcuoglu, A.B. Mann; In Press, Materials Research Society Proceedings 2006.

DEDICATION

In loving memory of my father and my aunt…

ACKNOWLEDGEMENTS

I am truly grateful to so many people who have been a part of my graduate life and who made this thesis possible.

First and foremost, I would like to thank my advisor Dr. Adrian Mann for his guidance and patience throughout my PhD studies. His door was always open when I needed his advice. His clear and simple explanations for complicated problems helped me find my way through this thesis. I am thankful for his encouragement and support as an advisor and as a friend during the hardest times in my life in the past few years. He is the best advisor and teacher I could have wished for.

I would like to thank my committee members, Dr. Guzelsu, Dr. Cosandey and Dr. Matthewson for their valuable suggestions. I am grateful to Dr. Denhardt, Dr. Buckendahl and Dr. Ramirez for helpful discussions and providing the samples which literally made this thesis possible.

I would like to thank my friends, my office mates, Milca and Syeda. They shared every moment, good and bad, with me. I don't know how they stand but they listened to my endless stories about my thesis or my children and they have always been extremely supportive. Many, many thanks to: Selin, Burak, Tuna, Volkan, Bekir and Omer for the enjoyable lunch times and great weekends.

I can’t thank enough my cousins Nevin and Mohsen. They have become my second family. They have been by my side every time I needed, giving me so much love and support. I know I am very lucky to have them in my life.

I am thankful to my mother for her endless love without which I would have been lost. She is everything I want to be.

Finally, I would like to thank my wonderful family. My husband, for walking with me through life and taking care of me, and my daughters, my rain and sunshine, for bringing all the love and happiness. My life is perfect when I am with them.

Table of Contents

Abstract of Dissertation ii

Preface iv

Dedication vi

Acknowledgements vii

Table of Contents ix

List of Tables xii

List of Figures xiii

1 INTRODUCTION 1

1.1 BONE: STRUCTURE AND COMPOSITION 1

1.1.1 The Hierarchical Structure of Bone 1

1.2 BONE CELLS AND THEIR FUNCTIONS 6

1.2.1 OSTEOCLASTS 6

1.2.2 OSTEOBLASTS 7

1.2.3 BONE REMODELING 8

1.3 NON-COLLAGENOUS BONE MATRIX PROTEINS 10

2 CHARACTERIZATION TECHNIQUES 13

2.1 MECHANICAL CHARACTERIZATION 13

2.1.1 HARDNESS TESTING 13

2.1.2 NANOINDENTATION 15

2.1.3 NANOINDENTATION MEASUREMENTS ON BONE 25

2.1.4 DYNAMIC MECHANICAL ANALYSIS OF BONE 30

2.2 CHEMICAL CHARACTERIZATION 31

2.2.1 RAMAN SPECTROSCOPY 31

2.2.2 RAMAN SPECTROSCOPY ON BONE 33

3 CONCLUSIONS 40

4 REFERENCES 42

Appendix I – Five Publication Forming Basis of Thesis 48

I.1 Effects of Osteopontin Defficiency and Aging on Nanomechanics of Mouse Bone. In Press, Journal of Biomedical Materials Research, 2006……...49

I.2 Raman Microspectroscopic Analysis of Age Related Changes in Osteopontin Deficient Mouse Bones.; submitted to Calcified Tissue International 2007……73

I.3 Nanomechanics and Raman Spectroscopy of Osteocalcin and Fibrillin 2 Knock-Out Mouse Bones.; submitted to Journal of Materials Science, December 2006…….99

I.4 Effects of Osteopontin on Nanomechanics and Microstructure of Mouse Bones; Materials Research Society Proceedings 2004; vol. 844, p. 99-104……126

I.5 Nanomechanics of Knockout Mouse Bones; In Press, Materials Research Society Proceedings 2006…….138

Curriculum Vita……..…….……148

List of Tables

Table 1.1: Mineral analysis of transgenic and knock-out mice reveal the functions of bone matrix proteins[18] 11

Table 2.1 Raman band assignments 34

List of Figures

Figure 1.1 Hierarchical levels of femur are: cortical and cancelous bone; osteons and trabeculae; lamella; collagen fibrils; and collagen molecules,mineral crystals and water. (Figure taken from Rho *et al.*[3]) 2

Figure 1.2 TEM micrographs of Level 1: isolated crystals (left) and collagen fibril (right). Level 2: mineralized collagen fibril. Level 3: thin section of mineralized tendon Level 4: four fibril array patterns organization. Level 5: SEM micrograph of a single osteon. Level 6: light micrograph of femur. Level 7: whole bovine bone (scale:10cm).(Figure taken from Weiner *et al.*[2]) 3

Figure 1.3 Illustration of the mineral-collagen composite structure. Mineral particles are believed to be nucleated at sites which are in register with the 67 nm period of the axial stagger of collagen molecules. (Figure taken from Fratzl *et al.*[7])..... 4

Figure 1.4 Life cycle of osteoclast. Mononuclear hematopoietic precursor fuses with other precursors to form osteoclast cells that attaches to the bone surface and initiates resorption. After bone resorption, osteoclast undergoes apoptosis. (Figure is taken from Sims *et al.*[1])..... 7

Figure 1.5 Osteoblasts proliferate and differentiate from undifferentiate mesenchymal cells. After bone formation, the mature osteoblasts can no longer proliferate but differentiated into an osteocyte embedded in the bone matrix or set into a lining cell on the bone surface. (Figure is taken from Sims *et al.*[1])..... 8

Figure 1.6 Sequence of events involved in bone remodeling. Activation-resorption-formation (ARF) sequence of cellular events. (Figure is taken from Sims *et al*. [1])..... 9

Figure 2.1 Schematic illustration of an instrumented indentation system (Figure taken from Vanladingham M.R.[25]) 15

Figure 2.2 Load-displacement curves for; (a) Elastic Solid; (b) brittle solid; (c) ductile solid; (d) crystalline solid; (e) britle solid with cracking during loading; and (f) polymer exhibiting creep..... 17

Figure 2.3 Shematic Illustration of s section through an axisymmetric indentation from Oliver and Pharr (1992) 18

Figure 2.4 Typical force-displacement curve for nanoindentation after Oliver and Pharr (1992). 19

Figure 2.5 Schematic illustration of a dynamic model for an instrumented indentation system. (Figure from Vanlandingham M.R. [25]) 23

Figure 2.6 Schematic representation of Raman scattering and Rayleigh scattering. 32

Figure 2.7 Typical raman spectra of cortical mouse bone femora..... 35

1 INTRODUCTION

1.1 BONE: STRUCTURE AND COMPOSITION

Bone is a specialized connective tissue that makes up the skeletal system together with cartilage. Main roles of the bone tissue in skeletal system are:[1]

1. Mechanical: Transmits the force of muscular contraction from one part of the body to another during movement.

2. Protective: Bone is a hard and rigid tissue that enables the skeleton to maintain the shape of the body. It has a protective function for vital organs and bone marrow.

3. Metabolic: Bone serves as a reservoir for ions, especially calcium and phosphate, for the maintenance of serum homeostasis

1.1.1 The Hierarchical Structure of Bone

Bone has a complex structure which can be described in terms of hierarchical levels of organization.[2,3] The schematic hierarchical organization and the electron microscopy pictures of six levels of hierarchy are shown in Figures 1.1 and 1.2 respectively.

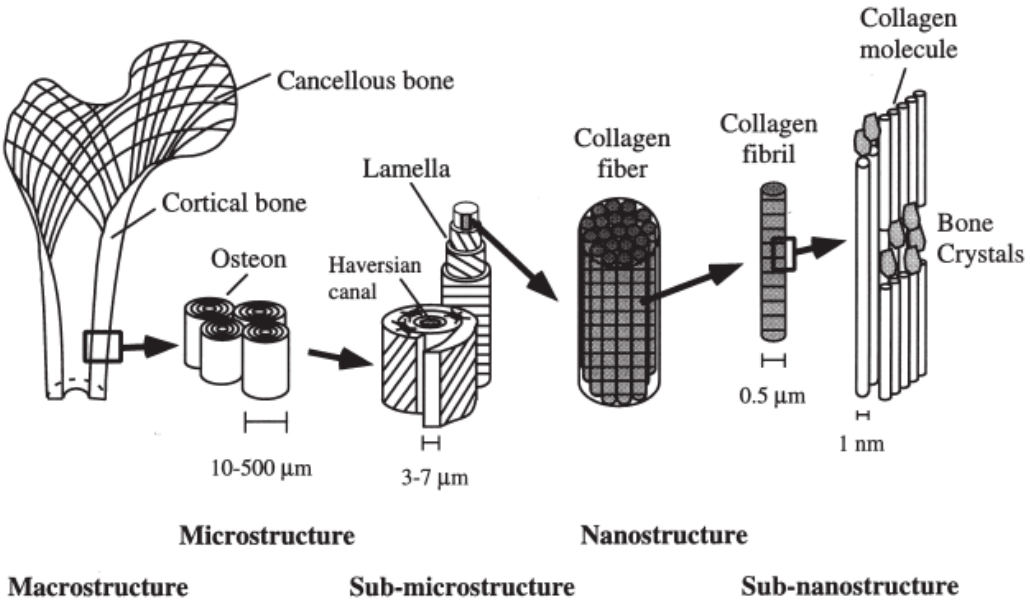

Figure 1.1 Hierarchical levels of femur are: cortical and cancelous bone; osteons and trabeculae; lamella; collagen fibrils; and collagen molecules,mineral crystals and water. (Figure taken from Rho *et al*.[3])

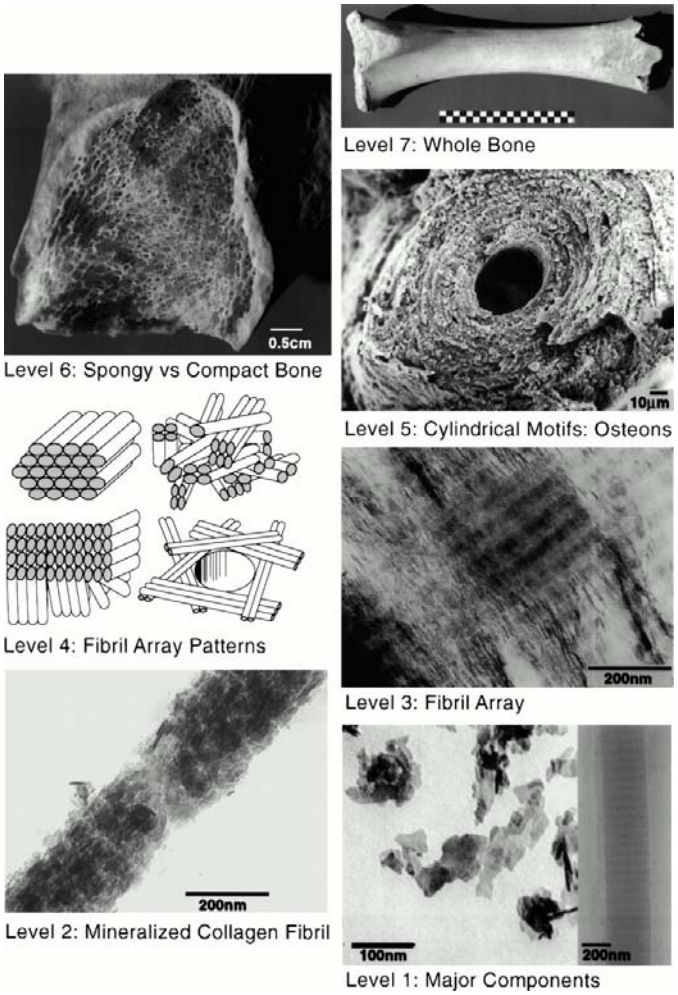

Figure 1.2 TEM micrographs of Level 1: isolated crystals (left) and collagen fibril (right). Level 2: mineralized collagen fibril. Level 3: thin section of mineralized tendon Level 4: four fibril array patterns organization. Level 5: SEM micrograph of a single osteon. Level 6: light micrograph of femur. Level 7: whole bovine bone (scale:10cm).(Figure taken from Weiner *et al.*[2])

1.1.1.1 Composition of Bone: the major components

Bone is a composite of material that consists of mineral phase (43% of the volume), organic matrix (32% of volume) and water (25% of volume).[4] The organic matrix of bone mainly consists of type I collagen (90%) with small amounts of non-collagenous proteins

like osteopontin, osteocalcin, osteonectin, bone sialoprotein, fibrillin-1 and 2. The mineral phase of bone contains primarily calcium and phosphate with small amounts of carbonate and some impurities (sodium, magnesium, potassium, citrate, fluoride, etc). The mineral phase is actually an analogue of the naturally occurring geological mineral hydroxyapatite (HA), $Ca_{10}(PO_4)_6(OH)_2$. The mature crystals are plate-shaped.[5] The mineral cystal nucleates within the discrete spaces of collagen fibrils. The average lengths and widths of the mineral plates are 50 x 25 nm, with 2-3 nm thickness.[6] A schematic drawing of a probable arrangement of mineral particles with respect to the collagen molecules is shown in Figure 1.3

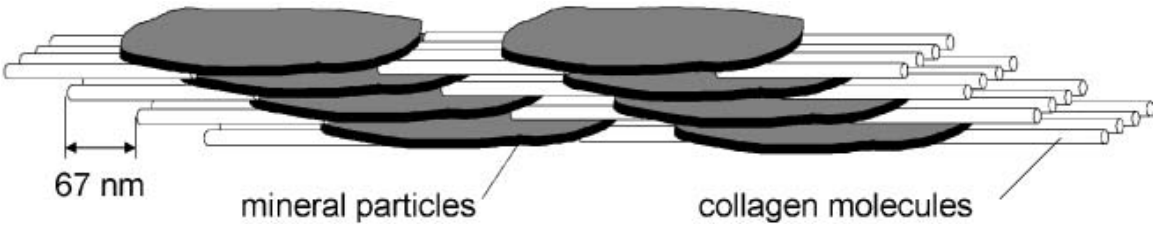

Figure 1.3 Illustration of the mineral-collagen composite structure. Mineral particles are believed to be nucleated at sites which are in register with the 67 nm period of the axial stagger of collagen molecules. (Figure taken from Fratzl *et al.*[7])

1.1.1.2 Fibril arrays

Mineralized collagen fibrils form bundles or arrays aligned along their length.[2] However, these bundles are not discrete and fibers from one bundle may fuse with a neighboring bundle. The diversity in the organizational pattern of fibril arrays is shown in Figure 1.2, Level 4. Parallel-fibered bone is typically found in the bovid bone and laid down very rapidly. Woven bone is when the fibrils are loosely packed and poorly oriented and hence, the matrix and the mineral are disorganized. Woven bone is common in the

skeleton of human embryo and during development it is replaced by other bone types (lamellar). Woven bone is also formed very rapidly which is why its structure is very disordered. Lamellar bone has a plywood-like pattern characterized by sets of parallel fibrils present in discrete layers, with different fibril orientation in each layer [2]. The lamellar bone is the most common bone type in humans with its rotated plywood-like structure.

1.1.1.3 Osteons

When the mineralized collagen fibers form into planar arrangements, it is called lamellae (3-7 μm thick).[3] Osteon or Harvesian systems contain a lamellae wrapped in concentric layers around a central canal (Figure 1.1 and 1.2). The structure of an osteon in cross-section is onion-like (with multiple layers of lamellae) and in longitudinal section it is cylindirical.[2]

1.1.1.4 Whole bone: Cortical versus Cancellous Bone

There are two types of bone at the macrostructural level; cortical and cancellous. Cortical bone is the solid, dense part of the bone which forms the outer wall of all bones and is mainly responsible for the supportive and protective function of the skeleton. Trabecular or cancellous bone is spongy and makes up the bulk of the interior of most bones. The microstructure of cortical bone is composed of regular, cylindrically shaped lamellae.

Whereas, the microstructure of cancellous bone is composed of irregular, sinuous convolutions of lamellae

1.2 BONE CELLS AND THEIR FUNCTIONS

Bone is a living tissue that undergoes matrix formation and resorption throughout its life span. Bone includes two major categories of cellular elements, the osteoblasts and osteoclasts. The structural development and continual remodeling of bone are controlled by the coordinated activities of these cells.

1.2.1 OSTEOCLASTS

An osteo-clast (Greek words for "bone" and "broken") is a type of bone cell that removes bone tissue by dissolving the bone's mineralized matrix. This process is known as bone resorption. An osteoclast is a large cell that is characterized by multiple nuclei (up to 100μm in diameter and containing 4-20 nuclei) and a cytoplasm with a homogenous, "foamy" appearance. At a site of active bone resorption, the osteoclast forms a specialized cell membrane, the "ruffled border" (sealing zone), which touches the bone surface.[8] The attachment of the cell to the matrix is performed by integrin receptors, which bind to specific arginine-glycine-aspartic acid (RGD) sequences in the matrix.[1] Osteoclastic resorption takes place by the acidification and dissolution of hydroxyapatite crystals and bone matrix within the sealing zone. After the resorption cycle, the osteoclasts undergoes apoptosis (death of cell).[9] This is characterized by the loss of ruffled border, detachment from bone surface and condensation of the nuclear chromatin (Figure 1.4).

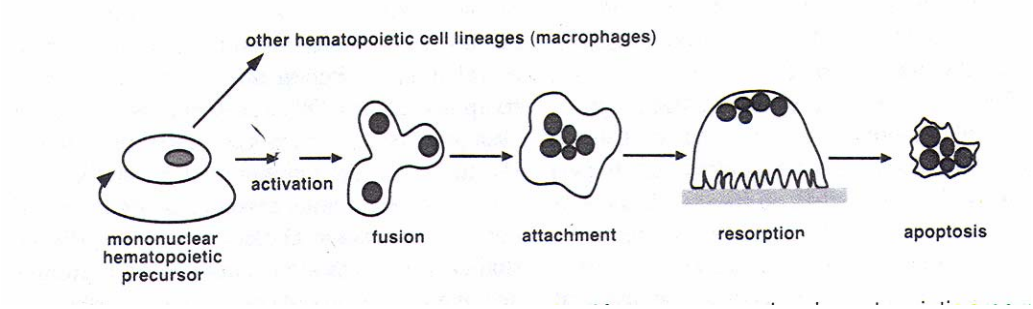

Figure 1.4 Life cycle of osteoclast. Mononuclear hematopoietic precursor fuses with other precursors to form osteoclast cells that attaches to the bone surface and initiates resorption. After bone resorption, osteoclast undergoes apoptosis. (Figure is taken from Sims *et al.*[1])

1.2.2 OSTEOBLASTS

Osteoblasts are the specialized cells responsible for bone formation. They are always found in clusters of cuboidal cells (100-400 cells) along the bone surface. Osteoblasts produce all the components of the bone matrix. Bone formation occurs by production, maturation and mineralization of the osteoid (unmineralized) matrix. The initial stage of bone formation is the rapid deposition of the collagen, without mineralization. The second stage is an increase in mineralization rate until it reaches the rate of collagen synthesis. At this stage the cells also begin to produce alkaline phosphatase and then matrix gla protein. At the final stage the mineralization continues as the rate of collagen synthesis decreases and the wave of alkaline phosphatase production is followed by osteocalcin and osteopontin production.[10,11] At the end of the matrix secretion period, osteoblast maturation takes place and around 15% of the mature osteoblasts become encapsulated in the new bone matrix and differentiate into osteocytes and the rest remain

on the bone surface becoming lining cells (Figure 1.5). Although the activitiy of osteoblasts decreases significantly once it has differentiated into osteocytes though, these cells still produce matrix proteins. It is likely that osteocytes respond to straining of bone and this influences bone remodeling by signaling and recruiting osteoclasts.[12]

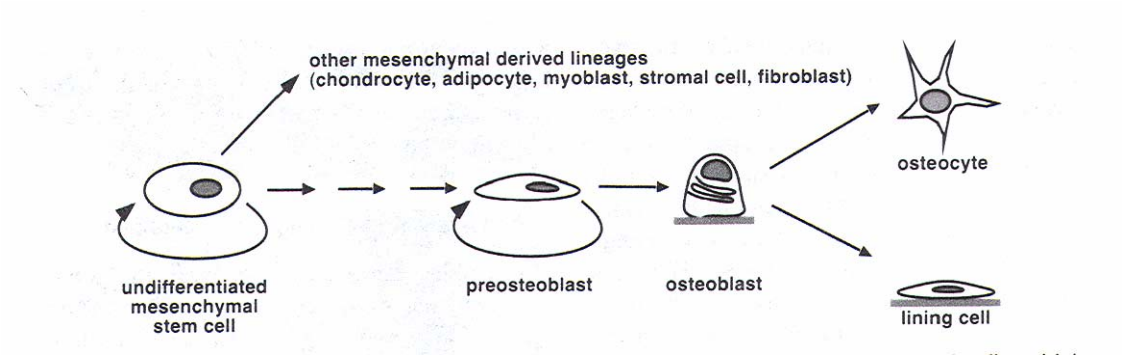

Figure 1.5 Osteoblasts proliferate and differentiate from undifferentiate mesenchymal cells. After bone formation, the mature osteoblasts can no longer proliferate but differentiated into an osteocyte embedded in the bone matrix or set into a lining cell on the bone surface. (Figure is taken from Sims *et al*.[1])

1.2.3 BONE REMODELING

Bone formation and resorption (bone remodeling) are coordinated events by which the old bone is replaced by new bone. It consists of a sequence of events which starts with osteoclast activation. This is followed by the resorption and eventually by increased attraction, proliferation and differentiation of osteoblasts, which then lay down new bone and repair the resorption defects caused by osteoclasts (Figure 1.6). The complete remodeling cycle for a bone takes about 3 months in humans.

Until maturity, during growth, the volume of bone that is formed exceeds the volume of bone that is resorbed (bone modeling). So, modeling is the deposition of bone onto

surfaces without necessarily being preceded by resorption.[13,14] Longitudinal growth of long bones at the metaphysis and diaphysis are examples of bone modeling .[15] However, on reaching maturity coupling between the resorption and formation takes place maintaining the bones mass. This is followed by an uncoupling in old age when the rate of bone resorption to bone formation increases. Rapid remodeling is associated with bone loss and an increase in fracture risk.[16] The reduced bone mineral density (BMD) is the main cause of the most common bone diseases, namely osteopenia/osteoporosis which is characterized by the microarchitectural deterioration of bone tissue and an increase in fracture risk. Current treatments for osteoporosis and osteopenia focus on either increasing osteoblastic activity or reducing osteoclastic activity. In both cases there is a close link between bone cell activity and the presence of non-collagenous bone matrix proteins. Research has indicated that the non-collageous proteins have a role in bone turnover regulation and contribute to the structural integrity of bone.[17]

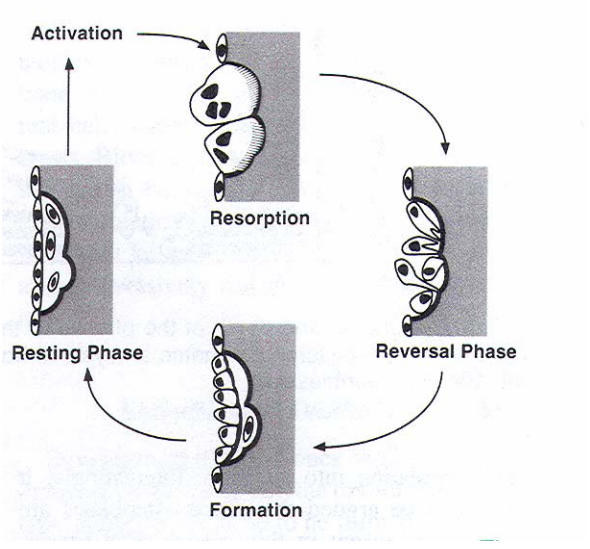

Figure 1.6 Sequence of events involved in bone remodeling. Activation-resorption-formation (ARF) sequence of cellular events. (Figure is taken from Sims *et al*. [1])

1.3 NON-COLLAGENOUS BONE MATRIX PROTEINS

The unmineralized osteoid consists of about 95% collagen and 5% noncollagenous proteins based on dry weight.[18] Non-collagenous proteins have been studied by many researchers in terms of their possible roles in binding to the bone mineral and in the regulation of mineral deposition.[19] Osteocalcin, osteopontin, osteonectin, bone sialoprotein fibrillin 1 and 2 are among the most abundant non-collagenous proteins of bone matrix. These proteins are synthesized by osteoblasts and have been identified in the mineralized matrix.[20] Mineral crystal form in the gap region of collagen fibers, but it is well known that collagen has a very poor ability to initiate the mineralization process, therefore, it was suggested that non-collagenous proteins may act as nucleators or that they may control the arrangement of other matrix protein that are nucleators. Moreover, it was suggested that they regulate the growth and proliferation of mineral crystals.[19-21] Roach *et al.* [20] used single and double immuno-histochemistry during mineralization and bone resorption to investigate the roles of four major non-collagenous proteins. The results suggested that osteopontin and bone sialoprotein were important for the initiation of mineralization and bone sialoprotein probably acts as a crystal nucleator. Osteocalcin and osteonectin slowed down the crystal growth, thus preventing excessive mineralization. Moreover, osteocalcin recruited the osteoclast precursors to resorption sites and facilitated their differentiation to osteoclasts. The attachment of osteoclasts to the matrix was facilitated by both osteopontin and bone sialoprotein.

During the past decade there has been an increase in research focused on the noncollagenous proteins due to the availability of genetically altered mice which allows

investigators to study the consequences of the deletion or knockout of these proteins. Table 1.1 shows the mineral analyses of transgenic and knock-out animals and what has revealed the functions of bone matrix proteins in the mineralization process.[18]

Table 1.1: Mineral analysis of transgenic and knock-out mice reveal the functions of bone matrix proteins[18]

Protein	Postulated Function	Modification	Observed Effect
Collagen (type I)	Mineralization template	Transgenic	Brittle bones Smaller crystals
Collagen (type X)	Mineralization regulator	Transgenic	Altered pattern of mineral deposition
		Knockout	No effect
Osteocalcin	Osteoclast recruiter	Knockout	Thickened bones, smaller crystals
Biglycan	Nucleator/regulator	Knockout	Fewer, but larger crystals, thinner bones
Osteopontin	Inhibitor	Knockout	Larger crystals
Bone sialoprotein	Nucleator	Knockout	No reported phenotype or mineral defect
Osteonectin	Inhibitor	Knockout	Corneal defect, mineral not studied
Alkaline phosphatase	Increases local [Pi]	Knockout-bone specific enzyme only	Hypophosphatasia/ poorly mineralized bones
Matrix gla-protein	Inhibitor	Knockout	Cartilage and blood vessel calcification

In summary, the investigators have proposed that the unique mix of non-collagenous proteins gives bone its characteristic properties, for instance its ability to mineralize compared to other tissues. However, the role of these proteins on bone mechanical and chemical properties are unknown at the nano-scale. The primary aim of this thesis is to provide new insight into how three non-collageous proteins, namely osteopontin (OPN), osteocalcin (OC) and Fibrillin2 (Fbn2), affect the nanomechanics and chemistry of bone tissue. This investigation is essential to the successful development of new treatments for osteopenia/osteoporosis that may involve control of noncollagenous protein activity. The research has particular relevance to the avoidance of undesirable side effects due to new

treatments.

2 CHARACTERIZATION TECHNIQUES

To gain a full understanding of the mechanical, chemical and structural effects of the non-collagenous bone matrix proteins osteopontin, osteocalcin and fibrillin-2 on bone, it is essential to use a range of characterization techniques, as described in this chapter.

2.1 MECHANICAL CHARACTERIZATION

Bone is a nonlinear, viscoelastic, anisotropic, and heterogeneous material and therefore can be complex to analyse mechanically. The fact that bone has the inherent ability to adapt continually to metabolic and environmental changes *in vivo*, provides even more complexity, making an understanding of the specifics of bone mechanics difficult.[22] This thesis describes an investigatation into the mechanical properties of bones from knock-out small animals via nanoindentation.

2.1.1 HARDNESS TESTING

Indentation is the most commonly used method to measure hardness, which is one of the fundamental mechanical properties of materials. The technique originated from the Mohs' hardness scale in which materials are ranked according to what they can scratch and, in turn, be scratched by. Vickers, Brinell, Knoop and Rockwell tests were all established by modifying the basic method of indenting one material with the other. In conventional indentation tests, a hard tip (frequently diamond) is pressed into the sample with known load. Upon the removal of load, the area of contact is calculated from direct measurements of the dimensions of the residual impression left in the sample surface

with an optical microscope. The hardness is then defined as maximum force divided by this residual area. Besides hardness, indentation techniques can also be used to calculate elastic modulus (often called Young's modulus), fracture toughness for brittle materials and viscoelastic properties.[22]

The basic idea of "nanoindentation" arose from the need to test very small volumes (such as thin films, biomaterials, coatings, etc). Typically, a very sharp tip is used so the contact area and, therefore, the volume of the material tested can be very small (less than a micrometer cubed). Most indentation techniques use electron or light microscopy for the residual area measurement. However, due to the very small impression formed by nanoindentation, the contact area measurement becomes impossible with light microscopy and very difficult with electron microscopy.[23] To solve this problem, depth-sensing indentation, which is also known by names such as instrumented indentation testing, continuous-recording indentation, ultra-low-load indentation and nanoindentation, was developed as a new form of mechanical testing that significantly expands the capabilities of traditional hardness testing.[24] This technique allows the continuous measurement of force and displacement as a function of time while the indentation is being made. Thus, the recorded indentation load-displacement data can be analysed to determine mechanical properties even if the indentation is on the sub-micron scale and cannot be imaged. One of the great advantages of the nanoindentation technique is its ability to probe a surface and map its properties with a spatial resolution better than 1 μm.[23-25]

2.1.2 NANOINDENTATION

Nanoindentation is widely used to probe the mechanical response of materials from metals and ceramics to polymeric materials and biological tissues.[25] Many of the microstructural features of interest in bone are only a few microns or less across; the nanoindentation technique offers a way to examine local variations in mechanical properties associated with these small structural features.[26]

The construction of most nanoindentation systems can be generalized as shown schematically in Figure 2.1.

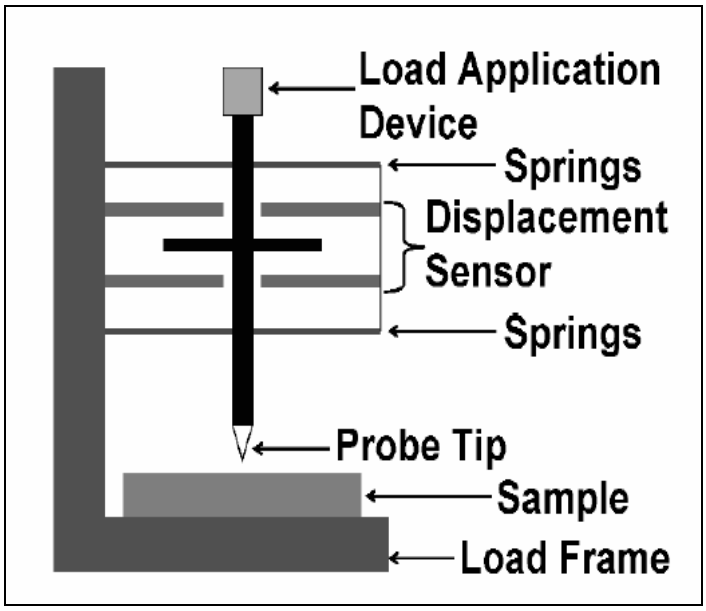

Figure 2.1 Schematic illustration of an instrumented indentation system (Figure taken from Vanladingham M.R.[25])

Force is applied using electromagnetic or electrostatic actuation, and a capacitive sensor is typically used to measure displacement. In contrast to traditional hardness testers, this

system allows the application of a specific force and the recording of the force - displacement history. Force, P, and displacement, h, are controlled and measured simultaneously, and continuously, over a complete loading cycle.[25] The most widely used test method for force - controlled indentation is to apply a constant loading rate. This is the simplest use of the method. For a displacement controlled experiment a constant displacement rate is required. And, since the instruments are force controlled, feedback is used for these cases. For viscoelastic materials, such as bone, characterization of the time - dependent response can also be done by application of the standard "quasi-static" test method. Investigators have used indentation creep tests and indentation stress relaxation tests for such purposes.[27] Further details on these tests and their applications to bone mechanics are given under section 2.1.3.

2.1.2.1 Analyzing Load-Displacement Data

Nanoindentation testing uses analysis of the load-displacement curves to extract the elastic modulus and hardness of the material. The fitting the load-displacement curves provides a way to calculate hardness and elastic modulus, but also gives information on non-linear events such as phase transformations, cracking and delamination of films.[23] Examples of load-displacement curves for different materials' responses and properties is shown in Figure 2.2.

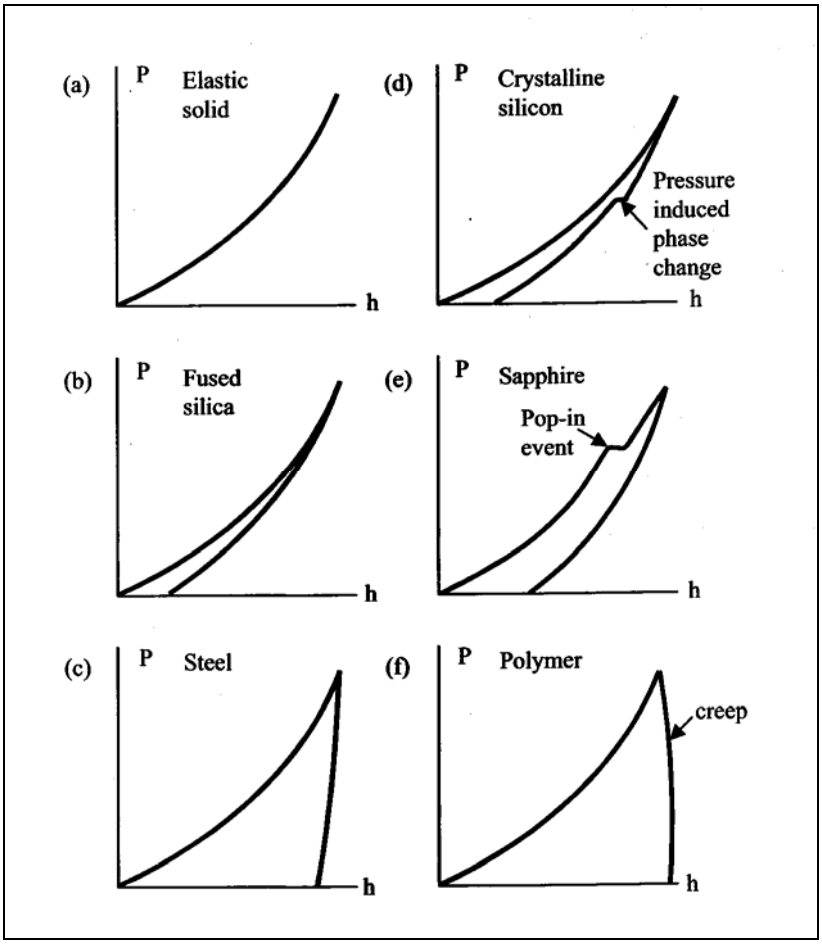

Figure 2.2 Load-displacement curves for; (a) Elastic Solid; (b) Fused Silica without cracking (limited ductility); (c) ductile solid; (d) crystalline solid; (e) brittle solid with cracking during loading; and (f) polymer exhibiting creep

The most common method for analyzing nanoindentation load-displacement data is that of Oliver and Pharr[28] which expands on ideas developed by Doerner and Nix[29] which in turn is based on Loubet *et al.,*[30] but is not constrained by the assumption of a flat punch that is used in the early methods. Oliver and Pharr's method calculates hardness and elastic modulus by analyzing the indentation load-displacement data obtained during one cycle of loading and unloading. The original method published in 1992 was intended for

the applications using sharp, geometrically self-similar indenters like Berkovich triangular pyramids, however in a more recent publication it was shown that the method could also be applied to a variety of axisymmetric indenter geometries including the sphere.[31]

A schematic illustration of the cross- section of an elastic-plastic indentation is shown in Figure 2.3. As the indentation takes place, the indenter produces an impression that conforms to the shape of the indenter. Contact depth is respresented by h_c and the width of the contact is $2a$. As the indenter is withdrawn, the elastic portion of the displacement is recovered which allows one to separate elastic properties from plastic. The residual depth after unloading is defined by h_f. Thus, the contact depth $h_c = h - h_f$, where h is the maximum depth under P_{max} (maximum load)

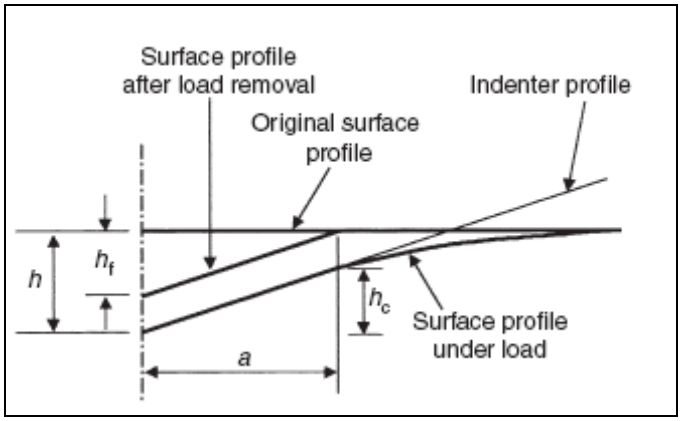

Figure 2.3 Shematic Illustration of s section through an axisymmetric indentation from Oliver and Pharr (1992)

A typical load-displacement (P-h) curve obtained with a Berkovich indenter is shown in Figure 2.4 along with several important parameters used in the Olive-Pharr's analysis.

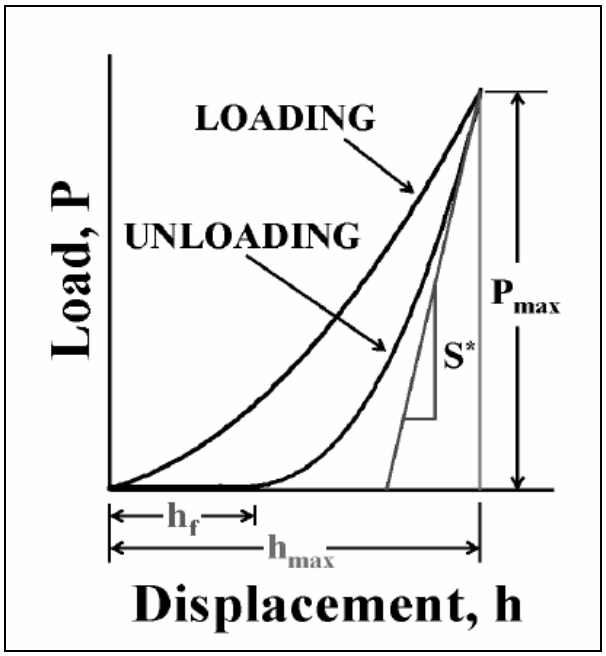

Figure 2.4 Typical force-displacement curve for nanoindentation after Oliver and Pharr (1992).

The following equations are used to find the bone's elastic modulus, E_s, and hardness, H from the load displacement curve.

$$E_r = \frac{\sqrt{\pi}}{2}\frac{S^*}{\sqrt{A_c}} \qquad (1)$$

$$E_s = \frac{1-\nu_s^2}{\frac{1}{E_r}-\frac{1-\nu_i^2}{E_i}} \qquad (2)$$

$$H = \frac{P_{\max}}{A_c} \qquad (3)$$

where, H is the hardness, E_i is the elastic modulus of the indenter, E_r is the reduced elastic modulus, S*, the measured contact stiffness, which is the slope of the tangent line to the unloading curve at maximum loading point P_{max} and A_c the contact area. v_i and v_s are Poisson's ratio for the indenter and sample, respectively.

It should be noted that this analysis assumes the unloading behavior of the material is characterized by elastic recovery only and it is the elastic nature of the unloading curve that facilitates the analysis. Consequently, this method can not be applied to materials exhibiting reversible plasticity during unloading or substantial viscoelastic deformation.

2.1.2.1.1 Determining the contact area

In order to calculate the hardness (Eq 3) and elastic modulus (Eq 1) a precise measurement of the contact area, A_c, and the contact stiffness, S*, is required. The unloading portion of the load-displacement data is fitted to the power law relation of Eq 4.

$$P = \alpha(h - h_f)^m \qquad (4)$$

α is an experimentally determined fitting parameter, m is a curve fitting parameter ranging from 1 to 2 and h_f is the final residual indentation depth after complete unloading. Contact stiffness is calculated by differentiating equation (4) at the maximum depth of penetration, h_{max}:

$$S = \left(\frac{dP}{dh}\right)_{h=h_{\max}} = \alpha m\left(h_{\max} - h_f\right)^{m-1} \qquad (5)$$

The next step is to determine the contact depth h_c (see Figure 2.3). For elastic contact, h_c is less than the total depth of penetration (h_{max}). Contact depth is given as:

$$h_c = h - \varepsilon \frac{P}{S^*} \qquad (6)$$

ε is a constant that depends on the indenter geometry. For spherical indenters ε is 0.75, conical indenters 0.72 and 0.75 for Berkovich.

Finally, the contact area is calculated by evaluation of the experimentally determined indenter area function *A=f(d)* at the contact depth h_c; which is:

$$A = f(h_c) \qquad (7)$$

The indenter area function relates the cross sectional area of the indenter to the distance from its tip. An experimental procedure using a standard sample is used to determine the area function (calibration of tip area function).

2.1.2.1.1.1 Tip area function calibration

The area function is determined by making a series of indentations in a material of known elastic modulus. Indentations should be made at depths covering the whole range of interest (usually from as low as possible to as large as possible).Upon obtaining the load displacement data, equations 5 and 6 are applied to calculate the contact stiffness and contact depths. In most cases fused quartz is used for calibration, it has an elastic modulus of 72 GPa and a Poisson's ratio of 0.17. The diamond indenter that is typically

used has *E= 1141 GPa and v = 0.07*. From these quantities the contact areas are calculated as:

$$A = \frac{\pi}{4}\left(\frac{S}{E_r}\right)^2 \qquad (8)$$

After a series of indents the computed area as a function of contact depth is plotted and curve fitting is employed using the following polynomial equation.

$$A = C_0 h_c^2 + C_1 h_c + C_2 h_c^{1/2} + C_3 h_c^{1/4} + C_4 h_c^{1/8} + C_5 h_c^{1/16} + \ldots \qquad (9)$$

C_0 for an ideal Berkovich tip is 24.5, while for a cube corner tip is 2.598.

2.1.2.2 Measuring Viscoelasticity

One application of nanoindentation to the measurement of time-dependent properties utilizes indentation creep tests[25,27] and indentation stress relaxation tests. In an indentation creep test the force is held constant and displacement or strain is examined.[27,32] For the stress relaxation tests the displacement is held constant while the gradual decrease in force is recorded. However, there are some instrumental limitations for these tests regarding the application of the force and displacement. There is often overshooting or undershooting and also it may not be effective in measuring small areas.[33] All these limitations affect the quality of the results, particularly for the shorter

time data. Therefore, quasi-static techniques developed for elastic plastic materials are generally not adequate for the characterization of viscoelastic materials. To overcome this problem, researchers have been using dynamic mechanical analysis techniques. One of these is nanoDMA^{TM} which provides information on the nanoscale viscoelasticity of the sample [Hysitron Inc., MN]. This force modulation method uses an AC oscillation in addition to the DC load, introducing the possibility of measuring viscoleastic properties during nanoindentation testing. A typical model of the dynamic indentation system is represented in Figure 2.5.

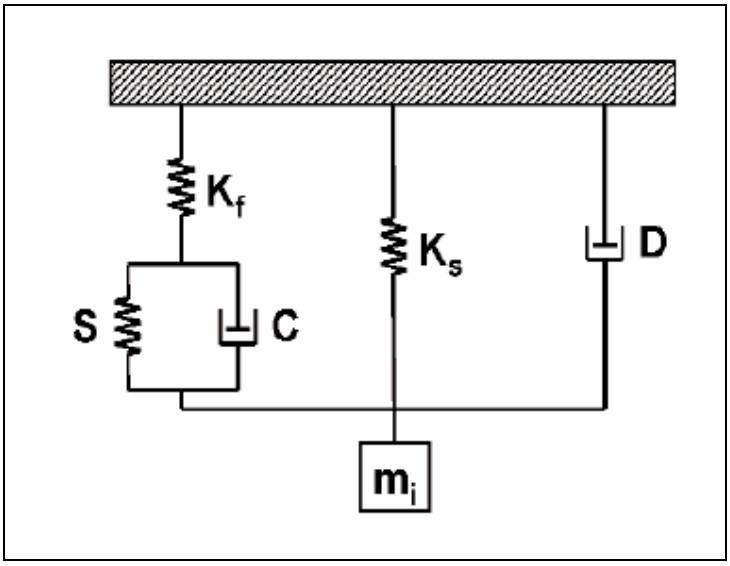

Figure 2.5 Schematic illustration of a dynamic model for an instrumented indentation system. (Figure from Vanlandingham M.R. [25])

In Figure 2.5, K_f represents the load-frame stiffness, K_s represents the stiffness of the springs, D and m_i represent the damping characteristics and mass, respectively, of the

instrument, *S* and *C* represent the storage and loss components, respectively, of the mechanical impedance related to the tip-sample contact.[25]

This technique is useful for characterizing elastic modulus as a function of depth as well as measuring viscoelastic properties. Recording the displacement response to the AC force oscillation, enables quantitative studies of dynamic mechanical properties such as the storage modulus, loss modulus and loss tangent to be found for viscoelastic materials.

The most recent development in nanomechanical characterization techniques combines dynamic mechanical analysis (nanoDMA^{TM}) and Scanning Probe Microscopy (SPM) and is called Modulus Mapping (Hysitron Inc. MN). Dynamic Testing provides the capability to oscillate the indenter tip with small forces while monitoring the resultant displacement and phase lag of the material response. SPM imaging allows the indenter to be rastered across the material surface and is typically used to produce a topographic image of the material surface. The modulus mapping technique employs these techniques simultaneously allowing a dynamic test to be performed at each point on a region of the sample's surface. An advantage of this technique is that not only can it be used to map the stiffness contrast, but also to map the complex elastic modulus quantitatively for both storage and loss components.

The commercial implementation of this modulus mapping technique closely followed the work of Asif *et al.*[34] They reported the development of this force modulation technique using a capacitive load displacement transducer capable of indenting and imaging. They showed that the stiffness sensitivity of the instrument is less than 0.1 N/m and it is

possible to detect long-range surface forces. This work was followed by a study where they used a fiber-epoxy composite to demonstrate an imaging technique that is used to map the tip-sample mechanical response quantitatively.[35]

Most recently by the use of this technique G. Balooch *et al.*[33] were able to measure the widths of the dentin- enamel junction (DEJ) and the peritubular-intertubular dentin junction (PIJ) in teeth. In addition, local variations of elastic modulus within the intertubular dentin and enamel were also reported. All tests were conducted without causing plastic deformation to the material with an increased spatial resolution when compared with the previous discrete nanoindentation experiments.

2.1.3 NANOINDENTATION MEASUREMENTS ON BONE

Improved preventive and healing treatments for skeletal diseases such as osteoporosis will benefit from a better understanding of the nanostructural mechanical properties of bone; these are influenced by cell-mediated adaptation processes. Nanoindentation, has the ability to probe a surface and map its properties on a spatially-resolved basis with a resolution of better than 1 μm. Consequently, it has been widely used to measure the mechanical properties of cortical and trabecular bone lamellae. After the initial nanoindentation studies proved to be effective for bone applications, the focus of nanoindentation studies has been to find the biological and physiological factors affecting the bone mechanics, such as diseases, aging and genetic modifications.

2.1.3.1 Osteoporosis

There have been many studies conducted on either human bone or animal models to examine the changes in bone due to aging. This helps us to understand age related bone loss and osteoporosis.[36-38] Most of these studies have been conducted with conventional mechanical tests and compositional analysis techniques. To date, very few researchers have used the nanoindentation technique, so the subject still remains an attractive area for research.

Rho *et al.*[39] were among the first that used force-controlled nanoindentation to examine the elastic modulus and hardness of human femoral bone of various ages. Although they did not find any difference associated with the age, they reported a clear difference between the stiffness and hardness of secondary osteonal and interstitial bone, the latter being stiffer.

Besides the human models,[39-43] it has been popular for researchers to use animal models (most often mouse) to investigate the mechanical effects of osteoporosis. Mouse bones are popular due to the large availability of transgenic strains. Nanoindentation has become an effective, even vital technique for mouse models due to its applicability to small samples. While animal models of bone loss cannot be directly compared to that which occurs in humans, they may still serve as useful tools.[32,44,45]

Silva et al. (2001), (2004) used senescence accelerated mouse as a model of senile osteoporosis (SAMP6 and SAMR1 control). They conducted nanoindentation tests and whole-bone bending tests to measure the elastic modulus and hardness of cortical bone

from mice of two different genotypes and then compared the results obtained from both tests. One conclusion they arrived at was that, the mouse model used for osteoporosis, mimics the changes that occur with aging in humans.[32,44] Elastic modulus was increased by an average of 8% in SAMP6 versus SAMR1 and the hardness was increased by 11%. Also, significant changes in material properties within each strain were noted from 4 to 12 months, and the mechanical properties increased with age. Jamsa *et al.*[46] also used an animal model to examine the osteoporosis. The objective of their study was to measure bone tissue properties by nanoindentation in long bones of rat osteoporotic mutations. Despite their hypothesis that the osteoporotic rat bone would be weaker they did not find any significant differences in the elastic modulus or hardness of bone from the two groups. These findings may indicate that the bone geometry and macroscopic structure are most important in predicting bone mechanical competence in osteoporosis. Hengsberger *et al.*[40] were the first ones to use a combined atomic force microscope and nanoindentation to study the mechanical properties of an osteoporotic human femur. With this new combination technique they were able to select the location of the indentations within a few tenths of ängstrom resolution and to quantify the sample's topography, and hence the quality of the sample preparation.

2.1.3.2 Limitations / Alternative approaches: Accuracy of Nanoindentation for determining bone elastic modulus at the microscale

2.1.3.2.1 Effects of Physiological Conditions

Most Nanoindentation work has focused on dried bone because of experimental complications associated with testing in a liquid environment and keeping specimens wet during testing. However, it is documented by several authors that mechanical properties of bone show substantial changes with dehydration.[40,47,48] It was reported that in general drying increases the elastic modulus, decreases toughness and reduces the strain to fracture. After the application of a series of tests human bone under both dry and physiological (wet) conditions it was concluded that drying increases the elastic modulus by 9.7% for interstitial lamella and 15.4 % for osteons. Similarly the hardness was found to increase by 12.2% for interstitial lamella and 17.6 for osteons.[48]

2.1.3.2.2 Nanoindentation vs. Bending Test

When compared with other mechanical testing methods, nanoindentation presents different results. Silva et. al (2004)[32] obtained a significantly different elastic modulus using nanoindentation and whole-bone bending test. This was explained by several factors: first, unlike the bending test, nanoindentation provides a measure of elastic modulus of the solid phase with no influence of porosity; second the loading rates and testing locations are different for each test.

2.1.3.2.3 Effects of Anisotropy of Bone

Bone is an anisotropic material, and its mechanical properties are determined by its composition as well as its microstructure. However, it should be noted that the measurement methods described for nanoindentation by Oliver and Pharr[28] were derived under the assumption that the material is homogeneous and isotropic in its mechanical

properties. The anisotropy was investigated by several authors and it was suggested that for anisotropic materials, the indentation modulus in a specific direction is a composite quantity that depends on all of the elastic constants.[41,43,49] It was also suggested the elastic modulus derived from the nanoindentation method is an average of the anisotropic elastic constants biased toward the modulus in the direction of testing.

2.1.3.2.4 Effects of Viscoelasticity of Bone

Bone is a natural composite material consisting primarily of three phases: mineral, organic and water. The mineral phase is essentially composed of hydroxyapatite crystals that are very defective and relatively brittle. The mineral is largely responsible for the elastic properties of bone. The organic phase consists of collagen and collagen fibrils in addition to other proteins such as osteopontin, osteocalcin and fibrillin. The organic play an important role in determining the viscoelastic properties of the bone due to its polymeric molecular structure. A better understanding of the viscoelastic behavior of bone could help to further elucidate the mechanisms by which osteoporosis leads to fractures.

Although nanoindentation has been used to investigate the microscale and nanoscale properties of bone as discussed above, the effects of time-dependent plasticity and viscoelastic properties on nanoindentation measurements have not been defined.[3,50,51]

Quasi-static Nanoindentation measurements are based on an assumption of fully elastic recovery without consideration of viscoelasticity and time-dependent plasticity.

Therefore, load-time functions should be designed carefully when nanoindentation testing is applied to bone material.

Fan *et. al*[27] investigated how different load-functions affect the nanoindentation elastic modulus to determine the time-dependent plasticity and viscoelasticity of human cortical bone. They used three load-time sequences with different indentation rates, different hold time at maximum load and different load/unload cycles. They concluded that the effects of time-dependent plasticity can be diminished by multiple loading-unloading cycles and a long hold period at maximum load.

2.1.4 DYNAMIC MECHANICAL ANALYSIS OF BONE

2.1.4.1 Static load vs. dynamic load

The majority of researchers to date have focused on the elastic behavior of bone in connection with changes in the bone mineral density. Until recently most of the bone mechanics studies have been performed under pseudo-static experimental conditions (nanoindentation). Although understanding static mechanical properties is beneficial as discussed previously, it is also very important to understand the viscoelastic behavior of bone under dynamic loading conditions.

Dynamic Mechanical Analysis (DMA) is a powerful technique frequently used in material science to characterize the viscoelastic behavior of materials.

The first study utilizing the standard Dynamic Mechanical Analyzer on bone was conducted by Yamashita *et. al.*[52] to measure the loss tangent and storage modulus. They

evaluated the effects of various test parameters, such as stress levels, test duration, temperature and scan rate to establish a reliable technique for using DMA in bone research. Later, in another study of Yamashita *et. al.*[53] the changes in viscoelastic properties of bone as a function of the amount of thermally denatured collagen were tested.

For further investigations in this area the recently developed techniques of nanoDMA™ and Modulus Mapping™ have advantages. Compared with conventional DMA techniques the new methods provide a nanoscale analog, providing the ability to characterize the mechanical properties of small volumes of viscoelastic materials.

2.2 CHEMICAL CHARACTERIZATION

The mechanical properties of bone depend in part on the chemical and structural aspects of its mineral phase. At least two different characteristics of the mineral component affect the bone's mechanical properties: the degree of mineralization (mineral: collagen ratio) and the degree of crystallinity of the mineral (grain size, length scale of structural continuity within a grain). Vibrational spectroscopy techniques can be applied to get a detailed insight into the mineral phase of bone.

2.2.1 RAMAN SPECTROSCOPY

2.2.1.1.1 Raman scattering

When an electromagnetic wave encounters a molecule, or passes through a lattice scattering occurs (Figure 2.6). When light encounters a molecule or atom, most photons

are elastically scattered (Rayleigh scattering). On the other hand, a small proportion of the photons are scattered inelastically (Raman scattering) where the energy and hence the frequency of the incident light shifts due to the vibrational energy that is gained or lost in the molecule.[54]

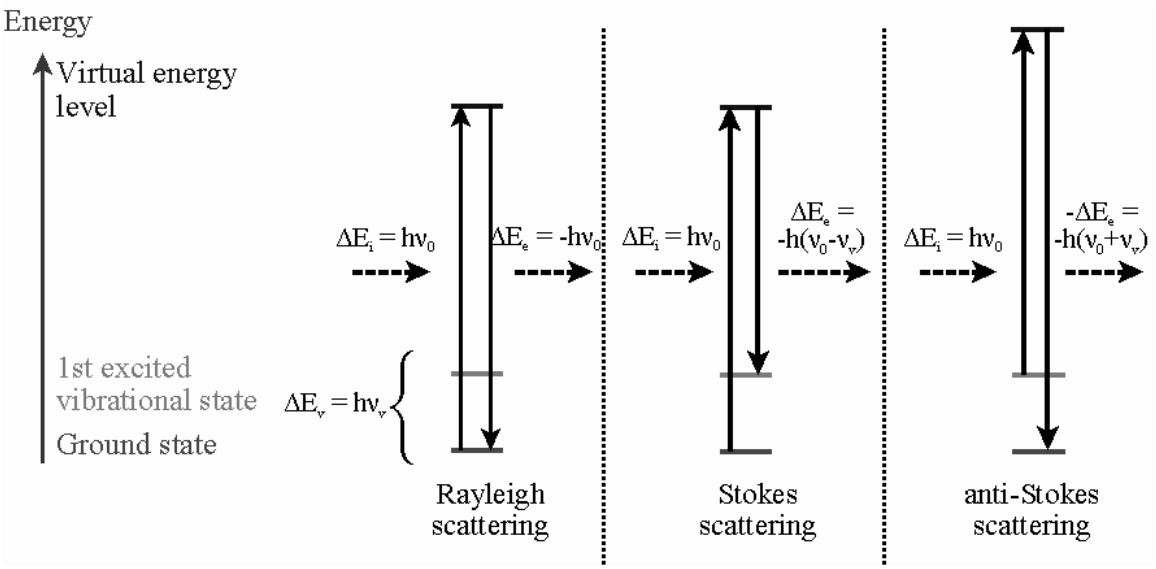

Figure 2.6 Schematic representation of Raman scattering and Rayleigh scattering.

Rayleigh scattering does not involve any energy change, consequently the light returns to the same energy state. The Raman scattering process from the ground vibrational state leads to absorption of energy by the molecule and its promotion to a higher energy state. This is called Stokes scattering. However, some molecules may be present in an excited state. Scattering from these states to the ground state is called anti-Stokes which is a very weak scattering and involves transfer of energy to the scattered photon.

Raman scattering occurs with a change in vibrational, rotational or electronic energy of a molecule and is presented as the Stokes spectrum. This is given as a shift in energy from the energy of the laser beam and is obtained by subtracting the scattered energy from the laser energy.

2.2.2 RAMAN SPECTROSCOPY ON BONE

Raman Spectroscopy is a non-destructive way of analyzing the molecular structure of the mineral components of bone at the microscopic level. With this technique, the laser beam is focused to 1 μm in diameter with the help of an optical microscope, thereby providing micrometer-scale resolution. Raman spectroscopy gives information about covalent and ionic bonds in general and, thus, can characterize both the organic and inorganic component of bone. It provides quantitative information on the changes in the mineral and matrix compositon as well as the nature and amounts of substituents in the mineral. Most importantly, very little sample preparation is required for Raman analysis of bone. In order to reduce the fluorescence background, different sample preparation techniques (i.e. bleaching with hydrogen peroxide) have been proposed by researchers.[55,56] However, recently it has been suggested that even mild treatments may modify the biological content of bone tissue samples.[57] Raman spectroscopy was also found to exhibit little interference from water which makes it very advantageous in the study of biological specimens.

Given the above advantages of Raman Spectroscopy, it has recently gained importance as a method to study the compositional changes of bone due to aging, diseases and mechanical deformation.

2.2.2.1 Analysis of the Raman spectra

The Raman spectrum of bone is quite complex (Figure 2.7), so researchers have mainly focused on specific bands including the phosphate ν_1 band at ~957- 960 cm^{-1}, carbonate ν_1 band at 1070 cm^{-1}, and the bands associated with collagen (amide III at ~1220-1280 cm^{-1}, CH_2 wag at ~1450 cm^{-1}, amide I at ~1600-1700 cm^{-1}).[58-60]

Summary of the Raman band assignments for bone is given in Table 2.1.[61]

Table 2.1 Raman band assignments

Raman Band Assignment	**Raman Shift (cm^{-1})**
PO_4^{3-} ν_2	422-454
PO_4^{3-} ν_4	578-617
Hydroxyproline, ν (C-C)	855
Hydroxyproline, ν (C-N)	876
$CO_3^{2-}\nu_2$	860-890
PO_4^{3-} ν_1	857-962
Proline, ν(C-N)	921
H PO_4^{3-} ν_3	1003-1005
Phenylalanine	1004

PO_4^{3-} ν_3	1006-1055
$CO_3^{2-}\nu_1$ /PO_4^{3-} ν_3	1065-1071
Amide III	1243-1320
$\delta(CH_2)$ wag	1447-1452
Amide II	1540-1580
Amide I	1595-1700
ν (CH_2) stretching	2840-2986
ν(O-H) stretching	3572-3575

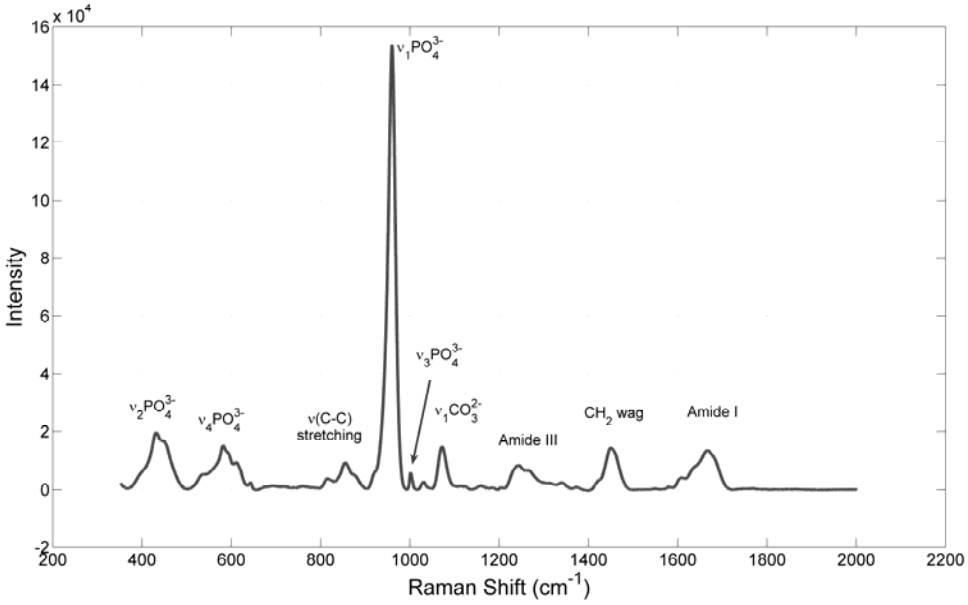

Figure 2.7 Typical raman spectra of cortical mouse bone femora

Analysis of the various Raman bands of bone provides the following information on the mineral and organic components of bone [57,61-66]

1. Ratio of the areas or intensities of peaks for ν_1 PO_4^{3-} (Phosphate) at around 960 cm^{-1} to amide I vibration at around 1660 cm^{-1} provides information on the mineral to organic matrix ratio and mineralization.

2. Bandwidth of the ν_1 PO_4^{3-} (Phosphate) at around 960 cm^{-1} (peak width at half maximum intensity) is related to the mineral crystallinity. An increase in the mineral crystallinity is indicative of an increase in mineral size and/or decrease in the non-stoichiometric substitutions.

3. Peak at 1071cm^{-1} correlates to the substitution of the PO_4^{3-} functional group by CO_3^{2-} (type B carbonate substitution). Whereas, type A substitution of carbonate, OH^- substitution, exhibits a peak at 878 cm^{-1}. The substitution of carbonate ions for OH^- (type A carbonate) and PO_4^{3-} (type B carbonate) could be quantified by phosphate to carbonate ratio. Researchers have indicated that the carbonate substitutions create vacancies and distortions that may change the shape of the crystal lattice.[67]

4. Carbonate (CO_3^{2-}) to amide I intensity ratio also indicates the carbonate amount and mineral:organic ratio in the hydroxyapatite lattice.

5. The positions of the Amide I band at around 1660 cm^{-1} and Amide III band at around 1250cm^{-1} are indicators of protein conformation because of the amide moiety's role in collagen cross-linking and bonding. It has been reported that structural changes induced by an applied load cause shifts in bands especially in the amide I and amide III bands.[58,68]

2.2.2.2 Applications of Raman spectroscopy on bone studies - Literature review

2.2.2.2.1 Biocompability of implants

Raman Spectroscopy has been recently found to have applications in the field of bone and bone implant compatibility. Penel *et al.*[63] have conducted micro-Raman spectroscopy on synthetic apatitic compounds. Specifically, they have compared the spectra from synthetic apatite with biological calcium phosphate (enamel, dentine and bone). In another study conducted by Penel *et al.*[57], intravital Raman microspectroscopy was used on the rabbit calvaria implanted with hydroxyapatite. This was the first study to observe Raman spectra of bone and calcium phosphate biomaterials at different times, *in situ* within the same animal.

2.2.2.2.2 Effects of Aging

Changes in the mineralization and the crystal structure of bone due to aging have been one of the most popular areas of research using the Raman spectroscopy on biomaterials. Freeman *et al.* (2001)[59] demonstrated the use of Raman spectroscopic analysis for studying structural and compositional changes in mouse bone that occurred with aging. With this technique they were able to detect the increase in the degree of crystallinity of bioapatite in mouse bone induced by bone aging. Akkus *et al.*[66] also studied the effects of aging, but they tested and compared the different regions of human compact bone. From the Raman spectra, they have quantified the degree of mineralization, mineral crystallinity and type B carbonate substitution for different age groups. Ager *et al.*[69] conducted Deep UV Raman spectroscopy to investigate the correlation of the spectral

changes in amide I with age (human cortical bone used). This technique was shown to avoid the problem of the fluorescence background which usually exists for visible and near–IR excitation. It has been proven that the amide I band resonance can be enhanced with UV excitation.

Raman spectroscopy has also been used along with mechanical testing techniques to study the effects of aging on the mechanical properties (fracture susceptibility, toughness, elastic modulus etc.) of the cortical bones from rat[65] and human[68].

2.2.2.2.3 Imaging

Recently, it has been suggested that Raman spectroscopy, as a point spectrum, would give very little information about the bone as a whole since bone does not have a homogeneous structure. However, Raman spectra that is collected over a two-dimensional area would give spatially relevant image information. As described by Carden *et al.*[58]a Raman imaging system uses a line-shaped laser beam focused onto the specimen. A 2-dimensional image is acquired by moving the specimen in 1 micron steps while obtaining a new line of spectra at each new position. Therefore, an image data set consists of a matrix of Raman spectrum points. Multivariate analysis is used for the analysis of the raw image data to provide the display of spectra of individual components and maps of the components' spatial locations.[70] In summary, Raman imaging provides high definition chemical state images which enable the analysis of small local variations in bone composition.[61,70,71]

2.2.2.2.4 Mechanical Deformation

In the past few years, given the advances in Raman Imaging, combined systems of Raman Spectroscopy and mechanical testing have been applied to study the effects of loading on the microstructure and mineralization of bone tissue. Morris *et al.*[70] have examined the mechanism of fracture in mouse bones. From the Raman Imaging they observed the changes in mineral around the fracture area which may indicate a phase transformation at the fracture zone. Subsequently, Carden *et al.*[58] have used a cylindrical indenter to examine how mechanical deformation affects bovine cortical bone structure. Raman spectroscopy and Raman imaging around the deformed area indicated changes in the amide I and amide III bands. The shifts in those bands attributed to the rupture of the collagen cross links due to the shear forces applied during indentation. More recently, Callender *et al.*[60] have developed a dynamic mechanical testing system that allows Raman spectral analysis during loading and unloading of bone tissue. The set-up was operated on the stage of a Raman microprobe. Changes in mineral bands were observed as a series of loads were applied to bone alternately in tension and compression.

In conclusion, Raman spectra can provide quantification of changes in bone mineral properties that can be compared with bone mechanical properties to further understand the structure-function relation of bone.

3 CONCLUSIONS

The effects of aging and non-collagenous proteins, osteopontin (OPN), osteocalcin (OC) and fibrillin-2 (Fbn2) on the bone mechanical and chemical properties of mouse bones were investigated at the nano-scale and micro-scale. Nanoindentation and Raman Microspectroscopy tests were conducted across the cortical cross-sections of femora from mutant and wild-type mice.

The study investigating the effects of OPN and aging, revealed that mechanical properties of bones from < 12 weeks old OPN-/- mice are significantly lower than for OPN+/+ mice. This suggests OPN may have a role in the earliest stages of bone formation. In terms of the chemical properties; mineralization and crystallinity of bones from OPN-/- mice (<12 weeks) were slightly lower than OPN+/+ mice, however, this difference was not of any significance. Bones from OPN-/- mice older than 12 weeks had significantly more mineral and larger crystal size compared to OPN+/+. The mechanical properties of the bones from OPN-/- mice showed very little variation with aging while mineralization, crystallinity and type-B carbonate substitution all increased. Hardness and elastic modulus dropped significantly for OPN+/+ bones between 12 weeks and 50 weeks, but there was an inverse correlation between the mechanical and chemical properties of the bones with aging in OPN+/+ mice. Intra-bone variations showed that the distribution of mechanical properties in the mice older than 50 weeks were more homogenous across the cortical thickness. Both aging and OPN deficiency have been found to alter the collagen properties.

The second part of this thesis involved the effects of OC and Fbn2 deficiency on the bones properties. Increases in the mechanical properties typically correlated with increases in the crystallinity of the bones from *OC-/-* mice when compared to *OC+/+* mice. On the other hand, mechanical properties decreased substantially in the absence of Fbn2, while the crystallinity increased; however, the mechanical properties were also related to carbonate substitution in the apatite phase. This appeared to have a greater effect on hardness than elastic modulus. The effects of mutations that remove OC and Fbn2 on bone mechanical and chemical properties were not uniform across the width of femoral cortical bones. The most significant difference between the genotypes was generally observed in the mid-cortical sections.

In summary, this thesis work has demonstrated that the non-collagenous proteins OPN, OC and Fbn2 are vital in determining the mechanical and chemical properties of bones at the nano-scale. In the future, new clinical approaches for the treatment of bone diseases such as osteopenia, osteoporosis and conditions such as Marfan's syndrome and congenital contractural arachnodactyly (CCA) may involve control of non-collagenous protein activity. This might be achieved for instance with antibodies that target the proteins or gene therapy that enables cells to express the protein. In each case knowledge of how the proteins affect the nanomechanics and chemistry of bone is essential to the successful development of these treatments and the avoidance of undesirable side-effects.

4 REFERENCES

1. Sims N, Baron R. Bone Cells and Their Function. In: Canalis E, editor. Skeletal Growth Factors. Philadelphia: Lippincott Williams and Wilkins; 2000. p 1-16.

2. Weiner S, Wagner HD. The material bone: Structure mechanical function relations. Annual Review of Materials Science 1998;28:271-298.

3. Rho JY, Kuhn-Spearing L, Zioupos P. Mechanical properties and the hierarchical structure of bone. Medical Engineering & Physics 1998;20(2):92-102.

4. Nyman JS, Reyes M, Wang XD. Effect of ultrastructural changes on the toughness of bone. Micron 2005;36(7-8):566-582.

5. Traub W, Arad T, Weiner S, Ziv V. Bone structure: Angstroms to millimeters. Abstracts of Papers of the American Chemical Society 1996;212:172-INOR.

6. Ziv V, Weiner S. Bone Crystal Sizes - a Comparison of Transmission Electron-Microscopic and X-Ray-Diffraction Line-Width Broadening Techniques. Connective Tissue Research 1994;30(3):165-175.

7. Fratzl P, Gupta HS, Paschalis EP, Roschger P. Structure and mechanical quality of the collagen-mineral nano-composite in bone. Journal of Materials Chemistry 2004;14(14):2115-2123.

8. Vaananen HK, Zhao H, Mulari M, Halleen JM. The cell biology of osteoclast function. Journal of Cell Science 2000;113(3):377-381.

9. Kameda T, Ishikawa H, Tsutsui T. Detection and Characterization of Apoptosis in Osteoclasts in-Vitro. Biochemical and Biophysical Research Communications 1995;207(2):753-760.

10. Jee WSS. Integrated Bone Tissue Physiology: Anatomy and Physiology. In: Stephen CC, editor. Bone Mechanics Handbook. Boca Raton: CRC Press LLC; 2001. p 1-20.

11. Stein G, Lian J. Molecular mechanisms mediating proliferation/differentiation interrelationships during progressive development of osteoblast phenotype. Endocr Rev 1993;14:424-442.

12. Lanyon L. Osteocytes, strain detection, bone modeling and remodeling. Calcified Tissue International 1993;53(1):S102-S107.

13. Seeman E. Bone quality. Osteoporosis International 2003;14:S3-S7.

14. Seeman E, Delmas PD. Mechanisms of disease - Bone quality - The material and structural basis of bone strength and fragility. New England Journal of Medicine 2006;354(21):2250-2261.

15. Sommerfeldt DW, Rubin CT. Biology of bone and how it orchestrates the form and function of the skeleton. European Spine Journal 2001;10:S86-S95.

16. Mundy GR. Bone Remodeling. Bone Remodeling and Its Disorders. London: Martin Dunitz; 1999. p 1-11.

17. Kaartinen MT, Pirhonen A, LinnalaKankkunen A, Maenpaa PH. Transglutaminase-catalyzed cross-linking of osteopontin is inhibited by osteocalcin. Journal of Biological Chemistry 1997;272(36):22736-22741.

18. Boskey AL. Bone Mineralization. In: Cowin SC, editor. Bone Mechanics Handbook. Boca Raton: CRC Press LLC; 2001. p 5-1 5-21.

19. Romberg RW, Werness PG, Riggs BL, Mann KG. Inhibition of hydroxyapatite crystal growth by bone-specific and other calcium-binding proteins. Biochemistry 1986;25(5):1176-1180.

20. Roach HI. Why Does Bone-Matrix Contain Noncollagenous Proteins - the Possible Roles of Osteocalcin, Osteonectin, Osteopontin and Bone Sialoprotein in Bone Mineralization and Resorption. Cell Biology International 1994;18(6):617-628.

21. Boskey A. Bone mineral crystal size. Osteoporosis International 2003;14:S16-S20.

22. An YH, Barfield WR, Draughn RA. Basic Concepts of Mechanical Property Measurement and Bone Biomechanics. In: An YH, Draughn RA, editors. Mechanical Testing of Bone and the Bone-Implant Interface. Boca Raton: CRC Press LLC; 2000. p 23-39.

23. Fischer-Cripps AC. Nanoindentation. NY: Springer Verlag; 2002. p 224.

24. Hay J, Pharr GM. Instrumented Indentation Testing. ASM International 2000:232-243.

25. VanLandingham MR. Review of instrumented indentation. Journal of Research of the National Institute of Standards and Technology 2003;108(4):249-265.

26. Rho JY, Pharr GM. Nanoindentation Testing of Bone. In: An YH, Draughn RA, editors. Mechanical Testing of Bone and the Bone-Implant Interface. Boca Rotan: CRC Press LLC; 2000. p 257-270.

27. Fan ZF, Rho JY. Effects of viscoelasticity and time-dependent plasticity on nanoindentation measurements of human cortical bone. Journal of Biomedical Materials Research Part A 2003;67A(1):208-214.

28. Oliver WC, Pharr GM. An improved technique for determining hardness and elastic modulus using load and displacement sensing indentation experiments. Journal of Materials Research 1992;7:1564-1583.

29. Doerner MF, Nix WD. A method for interpreting the data from depth-sensing indentation instruments Journal of Materials Research 1986;1(4):601-609.

30. Loubet JL, Georges JM, Marchesini O, Meille G. Vickers Indentation Curves of Magnesium Oxide Journal of Tribology 1984;106(1):43.

31. Oliver WC, Pharr GM. Measurement of hardness and elastic modulus by instrumented indentation: Advances in understanding and refinements to methodology. Journal of Materials Research 2004;19(1):3-20.

32. Silva MJ, Brodt MD, Fan ZF, Rho JY. Nanoindentation and whole-bone bending estimates of material properties in bones from the senescence accelerated mouse SAMP6. Journal of Biomechanics 2004;37(11):1639-1646.

33. Balooch G, Marshall GW, Marshall SJ, Warren OL, Asif SAS, Balooch M. Evaluation of a new modulus mapping technique to investigate microstructural features of human teeth. Journal of Biomechanics 2004;37(8):1223-1232.

34. Asif SAS, Wahl KJ, Colton RJ. Nanoindentation and contact stiffness measurement using force modulation with a capacitive load-displacement transducer. Review of Scientific Instruments 1999;70(5):2408-2413.

35. Asif SAS, Wahl KJ, Colton RJ, Warren OL. Quantitative imaging of nanoscale mechanical properties using hybrid nanoindentation and force modulation. Journal of Applied Physics 2001;90(3):1192-1200.

36. Ferguson VL, Ayers RA, Bateman TA, Simske SJ. Bone development and age-related bone loss in male C57BL/6J mice. Bone 2003;33(3):387-398.

37. Wang X, Shen X, Li X, Agrawal CM. Age-related changes in the collagen network and toughness of bone (vol 31, pg 1, 2002). Bone 2003;32(1):107-107.

38. Boskey A. Variations in bone mineral properties with age and disease. Journal of Musculoskel Neuron Ineract 2002;2(6):532-534.

39. Rho JY, Zioupos P, Currey JD, Pharr GM. Microstructural elasticity and regional heterogeneity in human femoral bone of various ages examined by nano-indentation. Journal of Biomechanics 2002;35(2):189-198.

40. Hengsberger S, Kulik A, Zysset P. A combined atomic force microscopy and nanoindentation technique to investigate the elastic properties of bone structural units. European Cells and Materials Journal 2001;1:12-17.

41. Fan Z, Swadener JG, Rho JY, Roy ME, Pharr GM. Anisotropic properties of human tibial cortical bone as measured by nanoindentation. Journal of Orthopaedic Research 2002;20(4):806-810.

42. Zysset PK, Guo XE, Hoffler CE, Moore KE, Goldstein SA. Elastic modulus and hardness of cortical and trabecular bone lamellae measured by nanoindentation in the human femur. Journal of Biomechanics 1999;32(10):1005-1012.

43. Rho JY, Tsui TY, Pharr GM. Elastic properties of human cortical and trabecular lamellar bone measured by nanoindentation. Biomaterials 1997;18(20):1325-1330.

44. Silva MJ, Brodt MD, Ettner SL. Long bones from the senescence accelerated mouse SAMP6 have increased size but reduced whole-bone strength and resistance to fracture. Journal of Bone and Mineral Research 2002;17(9):1597-1603.

45. Chen Q, Rho JY, Fan Z, Laulederkind SJF, Raghow R. Congenital lack of COX-2 affects mechanical and geometric properties of bone in mice. Calcified Tissue International 2003;73(4):387-392.

46. Jamsa T, Rho JY, Fan ZF, MacKay CA, Marks SC, Tuukkanen J. Mechanical properties in long bones of rat osteopetrotic mutations. Journal of Biomechanics 2002;35(2):161-165.

47. Hengsberger S, Kulik A, Zysset P. Nanoindentation discriminates the elastic properties of individual human bone lamellae under dry and physiological conditions. Bone 2002;30(1):178-184.

48. Rho JY, Pharr GM. Effects of drying on the mechanical properties of bovine femur measured by nanoindentation. Journal of Materials Science-Materials in Medicine 1999;10(8):485-488.

49. Roy ME, Rho JY, Tsui TY, Evans ND, Pharr GM. Mechanical and morphological variation of the human lumbar vertebral cortical and trabecular bone. Journal of Biomedical Materials Research 1999;44(2):191-197.

50. Keller TS, M.A.K. L. Tensile and Compression Testing of Bone. In: An YH, Draughn RA, editors. Mechanical Testing of Bone and the Bone-Implant Interface. Boca Raton: CRC Press LLC; 2000. p 175-200.

51. Sasaki N. Viscoelastic Properties of Bone and Testing Methods. In: An YH, Bradley A, editors. Mechanical Testing of Bone and the Bone-Implant Interface. Boca Raton: CRC Press LLC; 2000. p 329-347.

52. Yamashita J, Furman BR, Rawls HR, Wang XD, Agrawal CM. The use of dynamic mechanical analysis to assess the viscoelastic properties of human cortical bone. Journal of Biomedical Materials Research 2001;58(1):47-53.

53. Yamashita J, Li XO, Furman BR, Rawls HR, Wang XD, Agrawal CM. Collagen and bone viscoelasticity: A dynamic mechanical analysis. Journal of Biomedical Materials Research 2002;63(1):31-36.

54. Smith E, Dent G. Introduction, Basic Theory and Principles. Modern Raman Spectroscopy- A Practical Approach: John Wiley & Sons Ltd; 2005. p 1-9.

55. Freeman JJ, Silva MJ. Separation of the Raman spectral signatures of bioapatite and collagen in compact mouse bone bleached with hydrogen peroxide. Applied Spectroscopy 2002;56(6):770-775.

56. Penel G, Leroy G, Bres E. New preparation method of bone samples for Raman microspectrometry. Applied Spectroscopy 1998;52(2):312-313.

57. Penel G, Delfosse C, Descamps M, Leroy G. Composition of bone and apatitic biomaterials as revealed by intravital Raman microspectroscopy. Bone 2005;36(5):893-901.

58. Carden A, Rajachar RM, Morris MD, Kohn DH. Ultrastructural changes accompanying the mechanical deformation of bone tissue: A Raman imaging study. Calcified Tissue International 2003;72(2):166-175.

59. Freeman JJ, Wopenka B, Silva MJ, Pasteris JD. Raman spectroscopic detection of changes in bioapatite in mouse femora as a function of age and in vitro fluoride treatment. Calcified Tissue International 2001;68(3):156-162.

60. Callender AF, Finney WF, Morris MD, Sahar ND, Kohn DH, Kozloff KM, Goldstein SA. Dynamic mechanical testing system for Raman microscopy of bone tissue specimens. Vibrational Spectroscopy 2005;38(1-2):101-105.

61. Morris MD, Finney WF. Recent developments in Raman and infrared spectroscopy and imaging of bone tissue. Spectroscopy-an International Journal 2004;18(2):155-159.

62. Michael DM, Finney WF. Recent developments in Raman and infrared spectrocopy and imaging of bone tissue. Spectroscopy 2004;18(2):155-159.

63. Penel G, Cau E, Delfosse C, Rey C, Hardouin P, Jeanfils J, Delecourt C, Lemaitre J, Leroy G. Raman microspectrometry studies of calcified tissues and related

biomaterials. Raman studies of calcium phosphate biomaterials. Dental and Medical Problems 2003;40(1):37-43.

64. McCreadie BR, Morris MD, Chen T-c, Sudhaker Rao D, Finney WF, Widjaja E, Goldstein SA. Bone tissue compositional differences in women with and without osteoporotic fracture. Bone;In Press, Corrected Proof.

65. Akkus O, Adar F, Schaffler MB. Age-related changes in physicochemical properties of mineral crystals are related to impaired mechanical function of cortical bone. Bone 2004;34(3):443-453.

66. Akkus O, Polyakova-Akkus A, Adar F, Schaffler MB. Aging of microstructural compartments in human compact bone. Journal of Bone and Mineral Research 2003;18(6):1012-1019.

67. Penel G, Leroy G, Rey C, Bres E. MicroRaman spectral study of the PO4 and CO3 vibrational modes in synthetic and biological apatites. Calcified Tissue International 1998;63(6):475-481.

68. Nalla RK, Kruzic JJ, Kinney JH, Balooch M, Ager JW, Ritchie RO. Role of microstructure in the aging-related deterioration of the toughness of human cortical bone. Materials Science & Engineering C-Biomimetic and Supramolecular Systems 2006;26(8):1251-1260.

69. Ager JW, Nalla RK, Breeden KL, Ritchie RO. Deep-ultraviolet Raman spectroscopy study of the effect of aging on human cortical bone. Journal of Biomedical Optics 2005;10(3).

70. Morris MD, Carden A, Rajachar RM, Kohn DH. Effects of applied load on bone tissue as observed by Raman spectroscopy. Proceedings of SPIE 2002;4614:47-54.

71. Carden A, Morris MD. Application of vibrational spectroscopy to the study of mineralized tissues (review). Journal of Biomedical Optics 2000;5(3):259-268.

APPENDIX I – FIVE PUBLICATION FORMING BASIS OF THESIS

Effects of Osteopontin Deficiency and Aging on Nanomechanics of Mouse Bone

N. Beril Kavukcuoglu[a], David T. Denhardt[b], Nejat Guzelsu[c,d], Adrian B. Mann[a,d]

[a] *Department of Materials Science and Engineering, Rutgers University, NJ 08854, USA*

[b] *Department of Cell Biology and Neuroscience, Rutgers University, NJ 08854, USA*

[c] *Department of Osteosciences/Biomechanics, UMDNJ-SOM, NJ 08084., USA*

[d] *Department of Biomedical Engineering, Rutgers University, NJ 08854, USA*

Abstract

Osteoporosis is a bone disease characterized by low bone mass and deterioration of the tissue leading to increased fragility. Osteopontin (OPN), a non-collageneous bone matrix protein, has been shown to play an important role in osteoporosis, bone resorption and mineralization. However, OPN's role in bone mechanical properties on the submicron scale has not been studied in any detail. In this study, nanoindentation techniques were utilized to investigate how OPN and aging affect bone mechanical properties. Hardness and elastic modulus were calculated and compared between the OPN-deficient mice (OPN-/-) and their age and sex-matched wild-type (OPN+/+) controls. The results show that the mechanical properties of the young OPN-/- bones (age<12 weeks) are significantly lower than for the young OPN+/+ bones. This finding was confirmed by additional microindentation testing. Biochemical analysis using micro-Raman spectroscopy indicated more mineral content in young OPN+/+ bones. Mature (age=12-50 weeks) and old (age>50 weeks) bones did not show any significant differences in mechanical properties with genotype. In addition, OPN+/+ bones showed decreasing mechanical properties between young and mature age groups. By contrast, OPN-/- bones showed no significant change in mechanical properties with aging.

Keywords: Bone; Osteopontin; Osteoporosis; Nanoindentation; Micro-Raman

Introduction

Bone is a living tissue that undergoes matrix formation and resorption throughout its life span [1]. Osteoclasts are the specialized cells that resorb bone while osteoblasts are responsible for the production of bone matrix. However, the activity level of these cells, and hence the rates of bone formation and resorption, vary during the life cycle of mammals. In humans, sometime after the fifth decade, bone resorption exceeds bone formation and uncoupling takes place causing a reduction in the skeletal strength and an increase in fracture risk with time. The loss of bone mass is commonly called osteoporosis. Osteoporosis is characterized by low bone mass, microarchitectural deterioration of bone tissue, enhanced bone fragility, and, consequently, an increased risk of fracture [2].

Since osteoporotic patients suffer from an increase in the ratio of osteoclastic bone resorption to osteoblastic bone formation, treatments for osteoporosis focus on either increasing osteoblast activity or reducing osteoclast activity. Osteoclastic bone resorption involves the attachment of osteoclasts to bone and the formation of a sealing zone. Once the sealing zone is formed, osteoclasts secrete hydrogen ions into the zone, creating an acidic environment, which causes dissolution of the bone mineral. Simultaneously, matrix metalloproteases are produced that degrade the bone's organic components particularly the collagen matrix [3].

As well as collagen, bone contains several other proteins including osteopontin (OPN), which is a phosphorylated glycoprotein produced by both osteoblasts and osteoclasts.

OPN is also known to occur in many other tissues, cells and biological fluids [4]. However, because of its abundance in bone and its possible role in bone resorption, it has drawn the interest of many investigators studying its effect on bone mineral density and mineral crystal size [3-11]. It has been observed that OPN is highly enriched at the sites where osteoclasts are attached to the underlying mineral surface. The $\alpha_v\beta_3$ integrin of the osteoclast is also highly enriched in the sealing zone region of the membrane. Moreover, the $\alpha_v\beta_3$ receptor of osteoclasts recognizes a common tripeptide sequence RGD (Arg-Gly- Asp) which has been shown to be crucial for specific binding and which is present in the bone matrix protein osteopontin. Thus, it is known that osteopontin binds and potentially forms a tight attachment at the sealing zones of osteoclasts, and hence it is believed to be important in facilitating local bone resorption [5,6,7]. Several studies have shown the importance of OPN in bone resorption, remodeling, mineralization and osteoporosis [3, 9-11]. However, how OPN deficiency affects the bone's mechanical properties on the submicron scale has not been studied in any detail.

In recent years, nanoindentation based techniques have been used extensively to examine bone mechanical properties [12-24]. Knowledge of the nanomechanics of bone is a vital component of research on OPN and bone mineralization. The ultimate aim is to find new clinical approaches that are efficacious in the treatment of osteoporosis and other bone diseases. Before these treatments can be developed it is essential that the effects of OPN deficiency on the nanoscale mechanical properties of bone are identified.

The primary objective of the study reported here was to utilize nanoindentation to investigate the contribution of OPN to the hardness (H) and elastic modulus (E) of bones

from OPN-/- and OPN +/+ mice. Microindentation was also used as an alternative technique to verify the changes observed with nanoindentation. Raman microspectroscopy has been used to study the biochemical effects of OPN on bone. Mechanical changes were then compared to the changes in mineral to organic matrix ratio as determined by comparing the Raman bands of the two phases. Given the importance of OPN in bone remodeling and osteoporosis the study also examined mice from several different age groups so that the combined effects of aging and OPN deficiency on nanoscale mechanical properties could be identified.

Materials and Methods

Mice with a targeted disruption of the OPN gene were developed as described in Rittling et. al [25,26]. The mice used in this study were inbred lines of essentially isogenic SW129 mice. The research was approved by the Rutgers Animal Care and Facilities Committee and NIH guidelines for the care and use of laboratory animals (NIH Publication #85-23 Rev. 1985) have been observed. Bones from male mice aged between 3 weeks and 77 weeks from both OPN-/- and OPN+/+ genotype were used during the nanoindentation experiments. For parts of the study these were split into three age groups (<12 weeks, 12-50 weeks and >50 weeks) to provide statistically significant data. For microindentation and Raman analyses mice aged between 3 and 5 weeks were used. This age was chosen as the nanoindentation data showed the largest dependence on genotype for young mice. All mice were sacrificed by CO_2 suffocation. The left femur from the mice for each age group and genotype were excised and cleaned of soft tissue. The bones were then prepared in the manner outlined by Roy et. al. [18]. Briefly, this involved dehydration in graded alcohol solutions (70-100%) and mounting in a low temperature

cure epoxy (SPI supplies, West Chester,PA). Dehydration can affect the mechanical properties of bone [21,22], however, this study was focused on comparing OPN-/- and OPN+/+ bones so the absolute values for mechanical properties are less important than the relative values. After mounting, the included femora were sectioned transversely at a point just below the hip joint using a diamond wafering saw. The surfaces were ground with silicon carbide paper of decreasing grit size (400, 600 and then 1200 particles per inch) followed by polishing with diamond paste down to ½ then ¼ μm grit size. After the polishing all specimens were cleaned ultrasonically to remove surface debris.

Mechanical testing

Nanoindentation is now well established as a standard tool for characterizing the mechanics of materials at small length scales. It has the ability to probe a surface and map its properties with a resolution substantially smaller than 1μm. Since many of the microstructural features of interest in bone are on this same scale, the technique offers a way of examining how changes in the biochemistry of the bone affect local mechanical properties [12]. Most nanoindentation studies of bone have focused on identifying how biological and physiological factors, diseases and aging affect the bone's mechanics [13-22,27]. Besides human models [14-17,27], it has been popular for researchers to use animal models (most often mouse) to investigate the mechanical effects of osteoporosis. Mouse bones are popular due to the availability of numerous transgenic strains. Given the small dimensions of mouse bones nanoindentation is the most effective, even vital, technique for examining mouse bone mechanical properties [19,23,28]. While small animal models of bone are not directly comparable to humans, they do serve as important

tools in identifying how specific mutations affect the properties of bone.

In this study, nanoindentation tests were performed using a Triboindenter™ (Hysitron Inc., MN) in load control mode. All samples were tested in the ambient environment. Prior to testing the bones, fused silica was used to calibrate the indenter tip area using the standard procedure [29]. The tip was nominally a diamond Berkovich pyramid and the loading direction was parallel to the long axis of the femur. For each bone a grid pattern of approximately 300 indents were performed across the radial sections in the cortical bone (see Fig. 1). For each indent a maximum load of 1000 μN was applied with a 2 second hold time at peak load. The distance between indents was 2.5 μm and 10 μm in the x- and y-directions, respectively. The Oliver-Pharr method [29] was used to determine the mechanical properties. The following equations were used to find the bone's elastic modulus, E and hardness, H:

$$E_r = \frac{\sqrt{\pi}}{2}\frac{S}{\sqrt{A_c}} \qquad \mathrm{E} = \frac{1-\nu_s^2}{\frac{1}{E_r} - \frac{1-\nu_i^2}{E_i}} \qquad \mathrm{H} = \frac{P_{\max}}{A_c}$$

where, E_r is the reduced elastic modulus, S is the measured contact stiffness, $P_{\max}$ is the maximum load and A_c is the contact area. ν_i and ν_s are Poisson's ratio for the indenter and sample, respectively. The values for the diamond indenter tip are E_i = 1140 GPa, ν_i = 0.07 and the Poisson's ratio for the bone was taken to be ν_s = 0.3. The contact area, A_c, was determined by analysis of the load-depth curve and calibrating the tip on a standard material (fused quartz).

Microindentation

A Leco DM-400FT Hardness tester was used to measure the micro-mechanical properties of the included and fine polished bones from 4 weeks old OPN-/- and OPN+/+ mice. Ten grams of load with a diamond cube-corner tip was used to perform microindents around the radial axis of each femur giving approximately 25 indents for each bone (see Fig. 1). The areas of the individual indents were than measured optically to obtain and compare the micro-hardness of the genotypes.

Raman spectroscopy

Raman microspectroscopy is a non-destructive testing technique that has the advantages of micron-scale spatial resolution and minimal sample preparation. Recently, it has gained in importance as a method to study the compositional changes of bone due to aging, diseases and mechanical deformation [30-35]. The Raman spectrum of bone is quite complex, so researchers have mainly focused on specific bands including the phosphate ν_1 band at ~957- 960 cm^{-1}, carbonate ν_1 band at 1070 cm^{-1}, and the bands associated with collagen (amide III at ~1220-1280 cm^{-1}, CH_2 wag at ~1450 cm^{-1}, amide I at ~1600-1700 cm^{-1}) [32,34].

A Renishaw inVia Raman microscope was used for this study. Included mice femora aged between 3 and 5 weeks from OPN-/- and OPN+/+ were subjected to the Raman analysis. A line of approximately 14 measurements over the spectral range of 350-2000 cm^{-1} were conducted on the radial axis of each specimen (see Fig. 1). The 785 nm laser beam that was used was focused on each point of interest using a Leica DMLM, 50X/0.75 NA objective providing an approximately 2 μm spot size. In order to reduce

the signal to noise ratio, 18 seconds of exposure time and 3 accumulations were performed for each measurement.

The Wire 2 software of Renishaw was used to remove sample background using cubic spline interpolation and for each peak Gaussian-Lorentzian curve fitting was performed. The phosphate ν_1 (~958 cm^{-1}) to amide I (~1667cm^{-1}) peak height ratios were calculated for each spectra to assess differences in the ratio of mineral to organic matrix [30] of the OPN-/- and OPN+/+ mice bones.

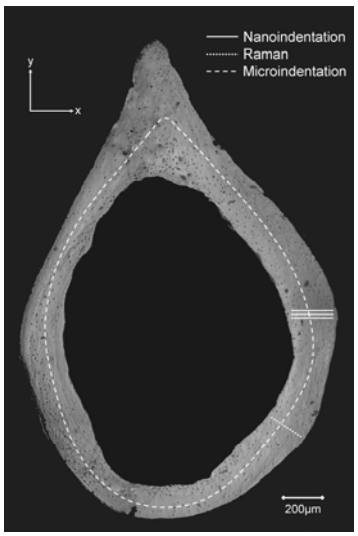

Fig 1 Optical image (Leica, 5X) of a mouse femur's radial section. The white marks represent the nanoindentation, microindentation and raman test locations.

1

Statistical Analysis

The nanoindents across the radial axis of each OPN-/- and OPN+/+ cortical femur from mice aged between 3 and 77 weeks were examined to give the intra- and inter-bone variations for each genotype and age. The average values for each combination of genotype and age were also calculated. The variation in the mechanical properties with

osteopontin deficiency, aging and location across the cortical thickness (periosteal, mid-cortical and endosteal) were analyzed. To gain statistically significant data for each genotype and age group the bones were divided into young (≤12 weeks old, n = 16), mature (12-50 weeks, n = 13) and old (≥50 weeks old, n = 17). One-way analysis of variance (ANOVA) was utilized to compare the mechanical properties (H and E) measured for OPN -/- and OPN +/+ control mice ($\alpha = 0.05$). A linear regression analysis tool was used to analyze the effect of aging and intra-bone variations on mechanical properties for both genotypes. ANOVA was also employed to determine the correlation between the individual age groups and mechanical properties for OPN+/+ and OPN-/- mice. Raman and microindentation analyses were conducted on bones from the young age group and the calculated mineralization and H values were averaged for OPN-/- and OPN+/+ bones. Only bones from young mice were examined with these techniques because nanoindentation showed no statistically significant difference in older groups. All statistical tests were performed using 95% minimum level of confidence.

Results

OPN-/- versus OPN+/+

Mean values and the standard errors for H and E of both genotypes were calculated. The results were plotted as bar charts to show the variation of H and E for OPN+/+ and OPN -/- mice for different age groups (Figures 2 & 3). ANOVA analyses comparing the H and E data from both OPN-/- and OPN +/+ revealed no statistically significant difference with genotype for mature and old age groups ($F < F_{critical}$ and $P > 0.05$). However, for the young age group the mechanical properties of OPN-/- mice were significantly lower than

those of the wild-type controls ($F > F_{critical}$ and $P < 0.05$). The mean H values for young OPN-/- and OPN+/+ mice were 1.52 ± 0.05 GPa and 2.64 ± 0.07 GPa, respectively. Similarly, the mean E for young OPN-/- mice was 30.84 ± 0.66 GPa, but 45 ± 0.98 GPa for OPN+/+ mice.

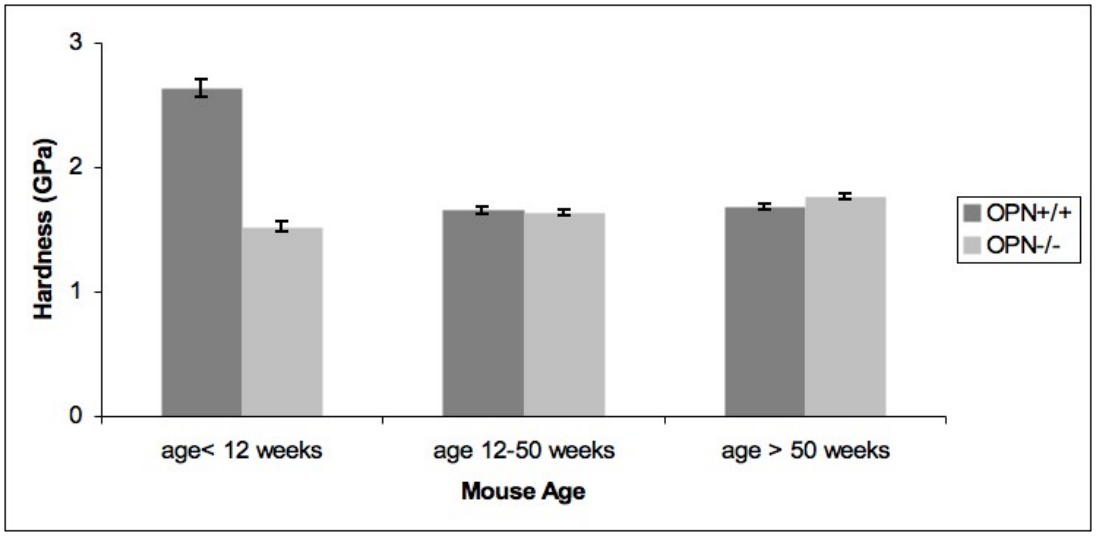

Fig 2 Change in mean hardness (H) as a function of age groups for femora from OPN+/+ and OPN-/- mice. The age groups were divided into young (≤12 weeks old), mature (12-50 weeks) and old (≥50 weeks old). The error bars are standard statistical errors.

Microindentation

Microindentation tests were conducted on the femora of 4 week old mice to confirm the differences observed in H by nanoindentation. The average micro-hardness was calculated as 0.82 ± 0.02 GPa for OPN-/- and 0.92 ± 0.02 GPa for OPN+/+ mice femora. ANOVA confirmed that these were statistically significant differences, hence, the microindentation data agreed with the nanoindentation data in young mouse bones. Note that the H obtained by microindentation is lower than that obtained by nanoindentation due to differences in the contact geometry.

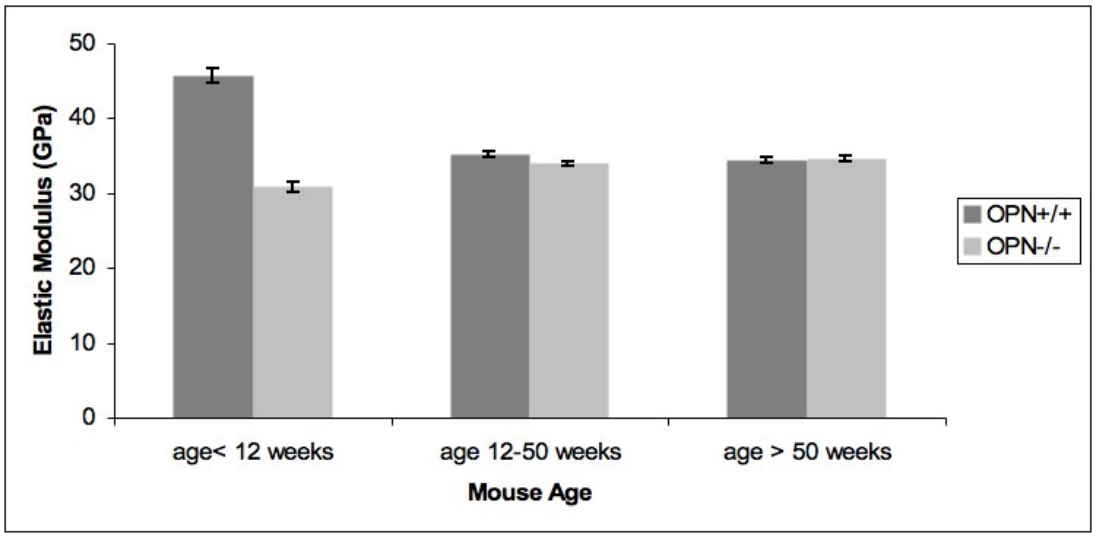

Fig. 3. Change in mean elastic modulus (E) as a function of age groups for femora from OPN+/+ and OPN-/- mice. The age groups were divided into young (≤12 weeks old), mature (12-50 weeks) and old (≥50 weeks old). The error bars are standard statistical errors.

Raman Spectroscopy

Raman analysis was performed only on the bones from the young age group of OPN-/- and OPN+/+ mice to compare the mechanical changes observed in nanoindentation and microindentation with the compositional changes. The height ratios of the phosphate ν_1 band at ~958 cm^{-1} and the amide I band at ~1667cm^{-1} at each measurement point were calculated. The average ratio of the mineral to organic matrix peaks for young OPN-/- and OPN+/+ mice bones were found to be 12.28 ± 0.4 and 13.41 ± 0.51, respectively. ANOVA showed that these differences were statistically significant. An example spectrum from the young OPN-/- and OPN+/+ mice femur is shown in Figure 4. It was observed that the peaks associated with the bone's mineral component phosphate (PO_4^{3-} ν_1 at ~ 958 cm^{-1}, PO_4^{3-} ν_2 at 422-454cm^{-1}, PO_4^{3-} ν_3 at 1006-1055 cm^{-1} and PO_4^{3-} ν_4 at

578-517 cm^{-1}) had lower intensities for OPN-/- mouse femur.

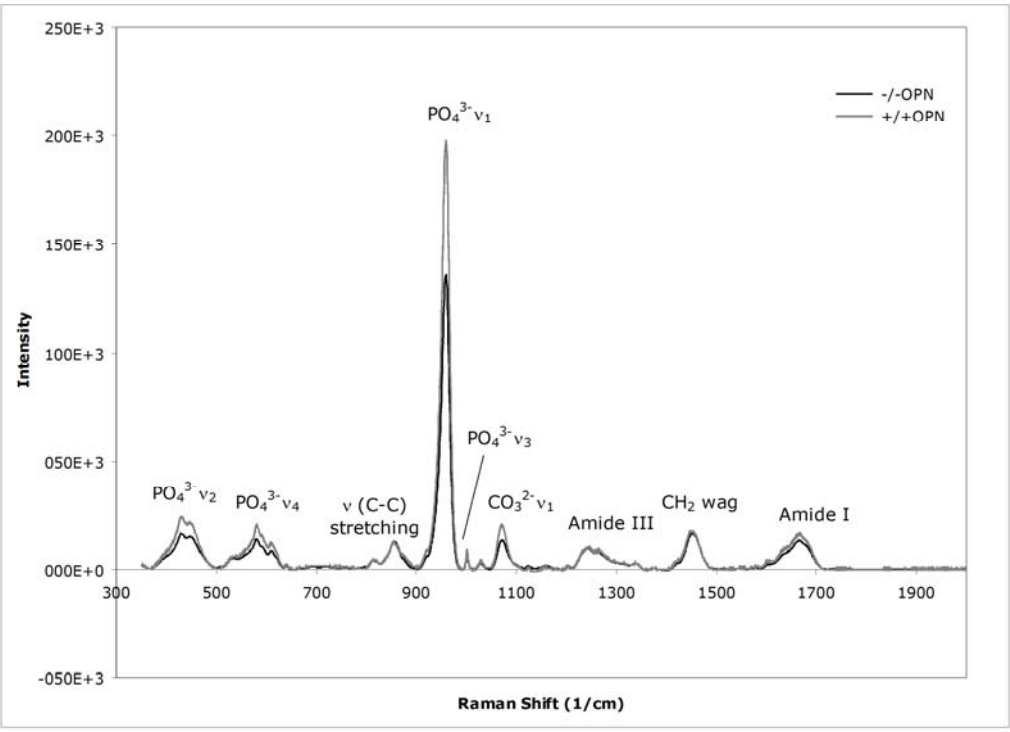

Fig. 4. Raman spectra for femora bones from 4 week-old OPN+/+ and OPN-/- mice after the baseline subtraction. The spectra are averaged over 14 measurements that traverse between the outer periosteal and inner endosteal regions of the femur's cortical bone.

A summary of results of the mechanical and biochemical tests conducted on the young mice bones are shown in Table I.

TABLE I
Summary of nanoindentation results for bones from young mice (<12-week-old), microindentation for bones from 4-week-old mice, and micro-Raman for bones from 3-5 week-old mice. ANOVA confirmed that the differences between OPN-/- and OPN+/+ mice bones are statistically significant.

Property of bones	OPN-/-	OPN+/+
Elastic Modulus	30.84 ± 0.66 GPa	45.75 ± 0.98 GPa
Nanohardness	1.52 ± 0.05 GPa	2.64 ± 0.07 GPa
Microhardness	0.82 ± 0.02 GPa	0.92 ± 0.02 GPa
Raman mineral:organic peak ratio	12.28 ± 0.4	13.41 ± 0.51

Age

Linear regression analyses showed that for bones from OPN+/+ mice H decreased significantly from 2.64 ± 0.07 GPa for mice <12 weeks-old to 1.69 ± 0.03 GPa for mice >50 weeks-old mice ($P < 0.05$). On the other hand, for the OPN-/- mice, there was an increase in bone H from 1.52 ± 0.05 GPa to 1.76 ± 0.02 GPa when going from <12 weeks-old to >50 weeks-old mice (Fig.2). ANOVA analysis indicated that this increase was statistically of low significance ($P = 0.06$). Elastic modulus followed a similar trend as H, that is, the E for the OPN+/+ mice bones decreased significantly from 45.75 ± 0.98 GPa to 34.38 ± 0.38 GPa when going from <12 weeks-old to >50 weeks-old mice ($P<0.05$). E showed no significant difference with age for the OPN-/- mice bone ($P=0.33$) although there was an increase in the average value from 30.84 ± 0.66 GPa for mice <12 weeks-old to 34.61 ± 0.35 GPa for mice >50 weeks-old (see Fig. 3).

Cortical bone location (Intra-bone variations)

Nanoindents across the radial axis of each OPN +/+ femur and OPN -/- femur from matching age groups (between 3 and 77 weeks) were examined. Figures 5 and 6 show the H and E distributions for typical young and old mouse bones from both genotypes. It was observed that the mechanical properties (H and E) were highest at the mid-cortical and lowest at the periosteal part of the femur from young OPN+/+ mice. Whereas, for OPN-/-, both H and E were lower and more homogeneously distributed throughout the endosteal and periosteal part. For bones from the older mice the mechanical properties were uniform between the outer periosteal and inner endosteal parts of both genotypes.

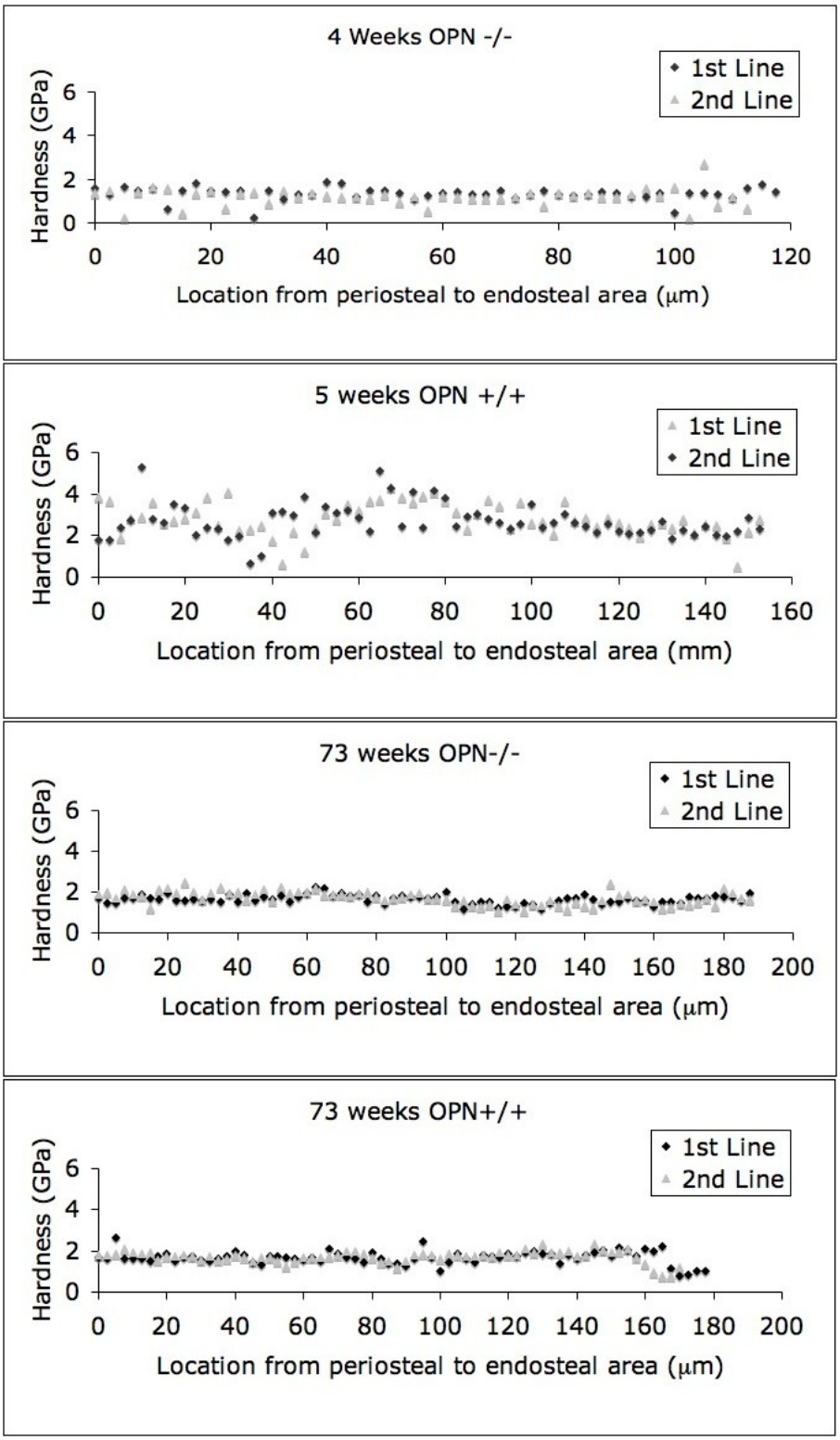

Fig. 5. Intra-bone variations in hardness (H) for typical femora from young and old mice. The data is taken along a line traversing the radial section of the cortical bone. Each figure shows the data from two lines of indents.

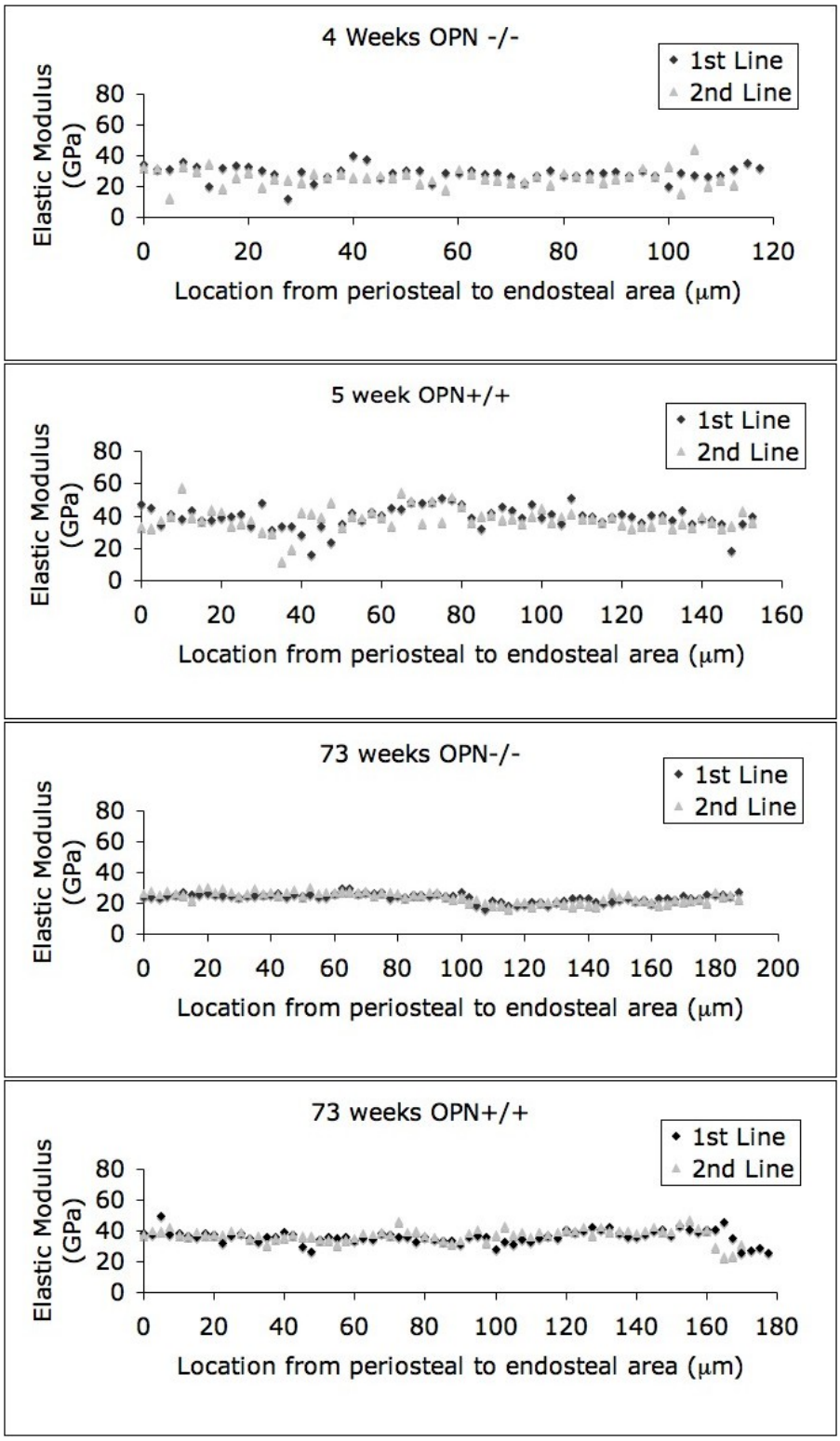

Fig. 6. Intra-bone variations in elastic modulus (E) for typical femora from young and old mice. The data is taken along a line traversing the radial section of the cortical bone. Each figure shows the data from two lines of indents.

Discussion

The primary objective of this study was to examine the effects of OPN on the mechanical properties of mice bone on the sub-micron scale. Nanoindentation tests were performed on bones from young, mature and old OPN-/- and OPN+/+ mice.

The most important finding is that the mechanical properties (E and H) of bones from young OPN-/- mice are significantly lower than their OPN+/+ control (Figs. 2,3). This finding was confirmed by additional testing using microindentation to evaluate H and correlated with the biochemical differences observed by Raman microspectroscopy. Raman spectra of bones from young mice showed that the ratio of mineral to organic matrix was decreased in the absence of OPN (Fig. 4). These results support previous research indicating a role for OPN in the earliest stages of bone formation, mineralization and osteoblast activity [36,37]. The previous studies have indicated that OPN probably acts as a trigger in the early differentiation of osteoblasts as well as playing an important role in promoting osteoclastic activities [6,36,38]. On the other hand, some studies have indicated that bones from mature OPN-/- mice (12 weeks-old and 16 weeks-old) have more mineral content and increased crystal size compared to their background matched OPN+/+ controls [10,11], but the current study does not show an equivalent difference in mechanical properties with genotype for bones in this age range. More recently, Duvall *et al.* has revealed that OPN-/- mouse bones (10 weeks old) showed increased whole bone mechanical properties (elastic modulus, maximum stress and failure stress) and decreased ductility relative to OPN+/+ control bones [39]. Current study, however, is focused on the sub-micron scale measurements, therefore direct comparison of the results between the current study and the study conducted by Duvall *et al.* is not possible.

In this study we have also examined and compared the effects of aging on nanomechanical properties of bones from both OPN +/+ and OPN-/- mice. There have been several previous studies examining the effects of aging and osteoporosis on the mechanical properties of normal bones (containing OPN) from various mammalian species. However, this earlier research has given some contradictory results with some nanoindentation studies showing no significant change in E with increasing age [27,40,41] while others, at the microscale, show a significant decrease in bone toughness and E [30,42-44]. These contradictory results are probably due to differences in the microscale structure which do not affect nanoindentation results. In fact correcting for the effective volume fraction in microscale studies (that is accounting for the pores in bone) the mechanical properties at the nano- and micro-scale are found to be similar [45].

The nanoindentation results presented in this paper for the effects of aging on H and E show a significant difference between the two genotypes. Specifically, bones from OPN-/- mice have been found to show very little variation in H and E with age, but bones from OPN+/+ mice show significant differences in H and E between the young and mature mice. That is, H and E are relatively high for bones from young mice (<12 weeks-old), but lower for older mice (>12 weeks-old) though they remain essentially constant with age for mice >12 weeks-old (Figs. 2, 3). The decrease in the mechanical properties of bone with age for OPN+/+ mice could be attributed to a decrease in the degree of bone mineralization [44,46-48] and deterioration of the mechanical integrity of the collagen network with increasing age [42]. Interestingly, when compared with other studies on mouse bone mechanical properties the current study reveals significantly higher H and E values for young OPN+/+ mice [23,44]. This could be a feature of the particular mouse

strain examined in the current study. Recent results for three inbred mouse strains indicate that there are differences in the material properties of both cortical and cancellous bone that depend upon strain [28]. So it is possible that the 129 background mouse bones in the current study might have unusually high mechanical properties.

The current study has found that bones from OPN-/- mice show only a small increase of low statistical significance in H and E with age. This suggests that for the OPN-/- genotype the degree of mineralization remains fairly constant throughout the life of the mice. However, the current study has only examined bones from male mice up to 77 weeks-old. It is possible that the mechanical properties of bones from female mice and/or mice >77 weeks-old would show a greater change in H and E.

The local variations of mechanical properties across the radial axis of OPN-/- and OPN +/+ cortical mice bone with increasing age (Fig. 5,6) have also been examined and compared. The results indicate that there are large, abrupt variations in mechanical properties across the radial section of cortical femur bone from young OPN+/+ mice. However, the mechanical variations for the young OPN-/- mouse bones were found to be more uniform. For older mouse bone the mechanical properties were uniformly low across the radial axis for both genotypes.

In conclusion, the results of this study indicate that the mechanical properties of bones from young mice show a strong dependence on the presence or absence of OPN. Specifically, the H and E of bones from OPN-/- mice are much lower than their background matched OPN+/+ equivalents. Further to this, the H and E of bones from OPN-/- mice show very little change with the age of the mouse, but the H and E of bones

from OPN+/+ mice diminish substantially with the age of the mouse. The H, E and mineral to organic matrix ratio for young (age ≤12 weeks) OPN-/- mouse bones were all found to be less than those of their OPN+/+ controls. However, for mature and old mice the mechanical properties for both genotypes were similar. Intra-bone analysis showed that aging is also associated with a decrease in the variation of H and E across the axis of the cortical bone of the femur. That is, the mechanical properties are more homogeneous in old bones (≥50 weeks). Collectively, the results indicate that OPN plays an important role in the very earliest stages of bone formation and mineralization.

REFERENCES

1. Sandy C, Marks Jr, and Donna CH. The structure and development of Bone. In: Bilezikian JP, Raisz LG, Rodan GA, editors. Principles of Bone Biology. California: Academic Press; 1996. p 3-13

2. Ammann P, Rizzoli R, 2003. Bone strength and its determinants. Osteoporos Int 2003;14:13-18

3. Yoshitake H, Rittling SR, Denhardt DT and Noda M. Osteopontin-deficient mice are resistant to ovariectomy-induced bone resorption. Proc Natl Acad Sci 1999;96:8156-8160

4. Noda M, Denhardt DT. Osteopontin. Principles of Bone Biology 2002;1:239-250

5. Ross FP, Chappel J, Alvarez JI, Sander D, Buttler WT, Farach-Carson MC, Mintz KA, Robey PG, Teitelbaum SL, Cheresh DA. Interactions between the bone matrix proteins osteopontin and bone sialoprotein and the osteoclast integrin αvβ3 potentiate bone resorption. J Biol Chem 1993;268:9901-9907

6. Uemura T, Nemoto A, Kiu Y, Kojima H, Dong J, Yabe T, Yoshikawa T, Ohgushi H, Ushida T, Tateishi T. Osteopontin involvement in bone remodeling and its effects on in vivo osteogenic potential of bone marrow-derived osteoblasts/porous hydroxyapatite constructs. Mater Sci Eng C 2001;17: 33-36

7. Reinholt FP, Hultenby K, Oldberg A, Heingard D. Osteopontin – a possible anchor of osteoclasts to bone. Proc Natl Acad Sci 1990;87:4473-4475

8. Boskey AL, Merasca M, Ullrich W, Doty SB, Buttler XT, Prince CW. Osteopontin-hydroxyapatite interactions in vitro: inhibition of hydroxyapatite formation and growth in a gelatin-gel. Bone Miner 1993;22:147-59

9. Ishijima M, Rittling SR, Yamashite T, Tsuji K, Kurosawa H, Nifuji A, Denhardt DT Noda M. Enhancement of osteoclastic bone resorption and suppression of osteoblastic bone formation in response to reduced mechanical stress do not occur in the absence of osteopontin. J Exp Med 2001;193:399-404

10. Boskey AL, Spevak L, Pashalis E, Doty SB, Mckee MD. Osteopontin deficiency increases mineral content and mineral crystallinity in mouse bone. Calcif Tissue Int 2002; 71:145-154

11. Shapses SA, Cifuentes M, Spevak L, Chowdhury H, Brittingham J, Boskey AL, Denhadt DT. Osteopontin facilitates bone resorption, decreasing bone mineral crystallinity and content during calcium deficiency. Calcif Tissue Int 2003; 73:86-92

12. Rho JY, Pharr GM. Nanoindentation Testing of Bone. In: An YH, Draughn RA, editors. Mechanical Testing of Bone and the Bone-Implant Interface. Florida: CRC Press LLC; 2000. p 257-269

13. Roy M, Rho JY, Tsui TY, Pharr GM. Variations of Young's modulus and hardness in human lumbar vertebrae measured by nanoindentation. Adv Bioeng 1996;BED-33:385-386

14. Hengsberger S, Kulik A, Zysset PH. A combined atomic force microscopy and nanoindentation technique to investigate the elastic properties of bone structural units. Eur Cells Mater 2001;1:12-17

15. Fan Z, Swadener JG, Rho JY, Roy ME, Pharr GM. Anisotropic properties of human tibial cortical bone as measured by nanoindentation. J Orthop Res 2002;20:806-810

16. Zysset PK, Guo E, Hoffler EC, Moore KK, Goldstein SA. Elastic modulus and hardness of cortical and trabecular bone lamellae measured by nanoindentation in the human femur. J Biomech 1999;32:1005-1012

17. Rho JY, Tsui TY, Pharr GM. Elastic properties of human cortical and trabecular bone measured by nanoindentation. Biomaterials 1997;18:1325-1330

18. Roy ME, Rho JY, Tsui TY, Evans ND, Phar GM. Mechanical and morphological variation of the human lumbar vertebral cortical and trabecular bone. J Biomed Mater Res 1998; 44: 191-197

19. Chen Q, Rho JY, Fan Z, Laulederkind JF, Raghow R. Congenital lack of COX-2 affects mechanical and geometric properties of bone in mice. Calcif Tissue Int 2003;73:387-392.

20. Jamsa T, Rho JY, Fan Z, MacKay CA, Marks SC, Tuukkanen J. Mechanical properties in long bones of rat osteopetrotic mutations. J Biomech 2002;35:161-165

21. Hengsberger S, Kulik A, Zysset PH. Nanoindentation discriminates the elastic properties of individual human bone lamellae under dry and physiological conditions. Bone 2002;30:178-184

22. Rho JY, Pharr GM. Effects of drying on the mechanical properties of bovine femur measured by nanoindentation. Mater Sci Mater Med 199;10:485-488

23. Silva MJ, Brodt MD, Fan Z, Rho JY. Nanoindentation and whole-bone bending estimates of mineral properties in bones from the senescence accelerated mouse SAMP6. J Biomech 2004; 37:1639-1646.

24. Ge J, Wang X, Cui F. Microstructural characteristics and nanomechanical properties across the thickness of the wild-type zebrafish skeletal bone. Mater Sci Eng C 2005; article in press

25. Rittling SR, Matsumoto HN, McKee MD, Nanci A, An XR, Novick KE, Kowalski AJ, Noda M, Denhardt DT. Mice lacking osteopontin show normal development and bone structure but display altered osteoclast formation in vitro. J Bone Min Res 1998; 13:1101-1111.

26. Soriano P, Montgomery C, Geske R, Bradley A. Targeted disruption of the c-src proto-oncogene leads to osteopetrosis in mice. Cell 1991; 64:693-702.

27. Rho JY, Ziopos P, Currey JD, Pharr GM. Microstructural elasticity and regional heterogeneity in human femoral bone of various ages examined by nano-indentation. J Biomech 2002;35:189-198

28. Akhter MP, Fan Z, Rho JY. Bone intrinsic material properties in three inbred mouse strains. Calcif Tissue Int 2004;75:416-420

29. Oliver WC, Pharr GM. An improved technique for determining hardness and elastic modulus using load and displacement sensing indentation experiments. J. Mater. Res 1992; 7:1564-1583

30. Akkus O, Adar F, Schaffler MB. Age-related changes in physicochemical properties of mineral crystals are related to impaired mechanical function of cortical bone. Bone 2004;34:443-453

31. Carden A, Morris MD. Application of vibrational spectroscopy to the study of mineralized tissues (rewiev). J Biomed Optics 2000;5:259-268

32. Carden A, Rajachar RM, Morris MD, Kohn DH. Ultrastructural changes accompanying the mechanical deformation of bone tissue: a raman imaging study. Calcif Tissue Int 2003; 72:166-175

33. Freeman JJ, Wopenka B, Silva MJ, Pasteris JD. Raman spectroscopic detection of changes in bioapatitein mouse femora as a function of age and in vitro fluoride treatment. Calcif Tissue Int 2001;68:156-162

34. Callender AF, Finney WF, Morris MD, Sahar ND, Kohn DH, Kozloff KM, Goldstein SA. Dynamic mechanical testing system for raman microscopy of bone tissue specimens. Vibrational Spectroscopy 2005: in press

35. Morris MD, Finney W. Recent developments in Raman and infrared spectroscopy and imaging of bone tissue. Spectroscopy 2004;18:155-159

36. Uemura T, Liu Y, Nemoto A, Yabe T, Ushida T, Miyamoto H, Tateishi T. The role of sialoproteins in recognition of bone surface by osteoblasts via integrin. Mater Sci Eng C 1997;4:303-309

37. Kasugai S, Nagata T, Sodek J. Temporal studies on the tissue compartmentalization of bone sialoprotein (BSP), osteopontin (OPN), and SPARC protein during bone formation in vitro. J Cell Biol 1992;152:467-477

38. Chen J, Singh K, Mukherjee BB, Sodek J. Developmental expression of osteopontin (OPN) mRNA in rat tissue, evidence for a role for OPN in bone formation and resorption. Matrix 1993;13:113-23

39. Duvall CL, Taylor WR, Guldberg RE. Osteopontin deficient mice display reduced vascular response and altered bone properties during fracture healing. ASME Bioengineering Conference Summer 2005; Vail, Colorado

40. Hoffler CE, Moore KE, Kozloff K, Zysset PK, Brown MB, Goldstein SA. Heterogeneity of bone lamellar-level elastic moduli. Bone 2000; 26(6):603–609

41. Hoffler CE, Moore KE, Kozloff K, Zysset PK, Goldstein SA. Age, gender and bone lamellae elastic moduli. J Orthop Res 2000;18:432-437

42. Wang X, Shen X, Li X, Agrawal CM. Age-related changes in the collagen network and toughness of bone. Bone 2002; 31:1-7

43. Nalla RK, Kruzic JJ, Kinney JH, Balooch M, Ager III JW, Ritchie RO. Role of microstructure in the aging-related deterioration of the toughness of human cortical bone. Mater Sci Eng C;2005:Article in press

44. Ferguson VL, Ayers RA, Bateman TA, Simske SJ. Bone development and age-related bone loss in male C57BL/6J mice. Bone 2003;33:387-398

45. Hengsberger S, Enstroem J, Peyrin F, Zysset PH. How is the indentation modulus of bone tissue related to its macroscopic elastic response? A validation study. J Biomech 2003;36:1503-1509

46. Roschger P, Grabner BM, Rinnerhaler S, Tesch W, Kneissek M, Gupta HS, Berzlanovich A, Klaushofer K, Fratzl P. Structural development of the mineralized tissue in human L4 vertabral body. J Struct Biol 2001;136:126-130

47. Roschger P, Fratz P, Eschberger J, Klaushofer K. Validation of quantitative backscattered electron imaging for the measurement of mineral density distribution in human bone biopsies. Bone 1998;23:319-326

48. Goldman HM, Bromage TG, Boyde A, Thomas CD, Clement JG. Intrapopulation variability in mineralization density at the human femoral mid-shaft. J Anat 2003; 203: 243-255

Raman Microspectroscopic Analysis of Age Related Changes in Osteopontin Deficient Mouse Bones

N. Beril Kavukcuoglu[a], David T. Denhardt[b], Adrian B. Mann[a,c]

[a] *Department of Materials Science and Engineering, Rutgers University, NJ 08854, USA*

[b] *Department of Cell Biology and Neuroscience, Rutgers University, NJ 08854, USA*

[c] *Department of Biomedical Engineering, Rutgers University, NJ 08854, USA*

Abstract

Osteopontin (OPN), a non-collagenous bone matrix protein, binds to the $\alpha_v\beta_3$ integrin of osteoclasts via the RGD sequence and is believed to play an important role in bone resorption and bone remodeling. Raman Micro-spectroscopy has been used to investigate and compare the chemical properties of bones from OPN deficient (OPN-/-) and wild-type (OPN+/+) mice. The mineral:organic matrix ratio, mineral crystallinity and type-B collagen substitution were measured. The results showed no statistically significant difference in the bones from OPN-/- and OPN+/+ mice less than 12 weeks of age. However, the mineral:organic ratio and mineral crystallinity from >50 week OPN-/- bones were significantly higher than for OPN+/+ bones. Mineralization, crystallinity and type-B carbonate substitution increased significantly for both genotypes with aging. In addition, both OPN deficiency and aging appeared to alter the collagen (organic) structure.

Introduction

Osteopontin (OPN) is one of the most abundant non-collageneous bone matrix proteins; it is both highly phosphorylated and glycosylated [Denhardt and Noda 1998]. OPN has been reported to be localized in the cell-matrix and at matrix-matrix interfaces with high concentrations of OPN being found in the cement lines and lamina limitans.[1,2]

OPN possesses an arginine-glycine-aspartate (RGD) sequence which binds to the $\alpha_v\beta_3$ integrin of bone resorbing cells, osteoclasts. Moreover, it has been demonstrated that OPN possibly mediates the binding of osteoclasts to bone at clear zones where osteoclasts secrete hydrogen ions creating an acidic environment; this leads to dissolution of the bone mineral.[2-5] Patrick Ross *et al.* have reported a decreased ability of osteoclasts to bind and resorb bone when the interactions between the $\alpha_v\beta_3$ integrin and OPN are interrupted.[1] It has been shown by many researchers that OPN plays an important role in bone resorption.[1,5,6] Further to this, it has been found that OPN binds to hydroxyapatite crystals[7] and inhibits the formation and growth of the crystals. Similarly, it inhibits calcium phosphate growth in the mineralized tissue.[8,9] A number of researchers have shown that osteoblasts, bone formation cells, also express OPN early in bone development suggesting a role for this protein as a trigger in early differentiation of osteoblasts and initial bone formation.[10-13] In addition, the mechanical properties of bones from OPN-/- mice (age <12 weeks) was shown to be significantly diminished compared to OPN+/+ mice.[14] Therefore, OPN may have a role in regulation of both bone formation and bone remodeling.[12,15] Studies by Rittling *et al.* on mice lacking OPN revealed that OPN was not necessary for normal mouse development (2-4 month old mice were

used).[16] However, bones from OPN-/- (osteopontin deficient) mice exhibited higher mineralization and crystallinity than OPN+/+ (wild-type) mice.[17] Morever, it has been found that OPN-/- mice are more resistant to ovariectomy induced bone loss (4-6 month old mice used) suggesting that OPN is important in the development of osteoporosis.[5] It has also been found that OPN is required for unloading induced bone loss.[4,6,15] A recent study of bone nano-mechanics has shown that bones from OPN-/- mice <12 weeks of age had lower mechanical properties than OPN+/+ mice at the nano-scale.[14] However, after 12 weeks of age, the mechanical properties did not show any significant difference between the genotypes. This indicates that the role of OPN on bone properties is very age dependent.

Raman Spectroscopy is a non-destructive way of analyzing the molecular structure of the mineral and organic components of bone at the microscopic level. It uses a laser beam focused with micrometer resolution using an optical microscope. The incident laser beam is scattered elastically and inelastically by the sample. The inelastic scattering gives the Raman spectra which provides information about covalent and ionic bonds and, thus, can characterize both the organic and inorganic components of bone. It provides quantitative data on the changes in the mineral and matrix compositon as well as the nature and amounts of substituents in the mineral. Most importantly, very little sample preparation is required for Raman analysis of bone when compared to IR spectroscopy. A potential issue with Raman spectroscopy is fluorescence, but different sample preparation techniques (i.e. bleaching with hydrogen peroxide) have been proposed by researchers to reduce the fluorescence background.[18,19] Recently it has been suggested that even mild treatments may modify the biological content of bone tissue samples.[20] Therefore, bone

samples of variable thickness, without any treatments should be used. Raman spectroscopy was also found to exhibit little interference from water which makes it very advantageous in the study of biological specimens. Given the advantages of Raman spectroscopy, it is not surprising that it has recently gained importance as a method to study the compositional changes of bone due to aging, diseases and mechanical deformation.

In the current study the mineralization, crystallinity and collagen structure of bones from background and age-matched OPN-/- and OPN+/+ mice were investigated using Raman microspectroscopy. In addition, aging related changes in the bone properties of OPN-/- mice bones were compared to those in OPN+/+ mice bones. Consequently, this study reveals the combined effects of aging and OPN deficiency on bone mineralization and, hence, provides an insight into OPN's role in bone remodeling and osteoporosis.

Materials and Methods

Sample Preparation

This study used the inbred lines of isogenic SW129 mice with a targeted disruption of the OPN gene as described in Rittling *et al*.[16,21] The research was approved by the Rutgers Animal Care and Facilities Committee, and NIH guidelines for the care and use of laboratory animals (NIH Publication #85-23 Rev. 1985) were observed. Bones from male mice aged between 3 weeks and 77 weeks from both OPN-/- and OPN+/+ genotypes were used. It should be noted that these are a sub-set of the bones used in an earlier study of bone mechanical properties[14] plus a number of new samples. Although Raman studies do not essentially require any kind of sample preparation,[22] the bones in

this study had also been used for nanoindentation testings which required sample preparation in a manner outlined by Roy *et al.*[23] and summarized below.

All mice were sacrificed by CO_2 suffocation. The left femur from the mice of each age group and genotype were excised and cleaned of soft tissue. The bones were then dehydrated in graded alcohol solutions (70-100%) and mounted in a low temperature cure epoxy (SPI supplies, West Chester,PA). Embedding samples into epoxy does not have an effect the Raman data as discussed by Carden *et al*.[24] After mounting, the included femora were sectioned transversely at a point just below the hip joint using a diamond wafering saw. The surfaces were ground with silicon carbide paper of decreasing grit size (400, 600 and then 1200 particles per inch) followed by polishing with diamond paste down to ½ then ¼ μm grit size. After the polishing all specimens were cleaned ultrasonically to remove surface debris.

Raman Microspectroscopy

A Renishaw inVia™ Raman microscope was used for this study with 785 nm wavelength laser and a grating of 1200 1/mm. The laser was focused on each point of interest with a Leica DMLM, 50X/0.75 NA objective providing an approximately 2 μm spot size. A line of approximately 14 measurements were conducted on the radial axis of each specimen. All spectral acquisitions were performed in the 350-2000cm^{-1} range. Signal to noise ratio and fluorescence background were minimized by employing 18 seconds of exposure time and 3 times of accumulation at each measurement point.

The Wire 2 software of Renishaw was used to remove sample background using cubic spline interpolation at each acquisition. A single spectrum for each sample was obtained

by averaging the 14 acquisitions per sample using a custom-written Matlab code (The Mathworks Inc., Natick, MA, USA). Each spectrum was then exported to Wire 2 software and the peaks were analyzed after performing Gaussian-Lorentzian curve fitting. A typical Raman spectrum from a mouse bone is shown in Fig. 1(a). The intensities of the following peaks were measured after curve fitting: phosphate ν_1 at ~958 cm^{-1} (PO_4^{3-} symmetric stretching band), carbonate ν_1 at ~1071 cm^{-1} (CO_3^{2-} symmetric stretching band), CH_2 wag at ~1450cm^{-1} (C-H bending band), amide I at ~1667cm^{-1} (C=O stretching band) and amide III at ~1243cm^{-1} (in-phase combination of the N-H bending and C-N stretching). The width (full width at half maximum, FWHM) of phosphate ν_1 at around 958 cm^{-1} was measured. Degree of mineralization for each sample was calculated by taking the ratios of the intensities of PO_4^{3-} ν_1 to amide I and PO_4^{3-} ν_1 to CH_2 wag. An increase in these ratios indicates a more mineralized matrix.[25-29] In bone, two types of carbonate substitutions have been reported:[28,30] if the CO_3^{2-} ion substitutes for OH^- ion, it is called type-A carbonate substitution; if it is PO_4^{3-} that is substituted it is called type-B carbonate substitution. In the present study the type-B carbonate substitution was quantified by the peak intensity ratios of CO_3^{2-} (~1071 cm^{-1}) to PO_4^{3-} ν_1 (~958cm^{-1}).[25,26] Type-A substitution could not be quantified because the vibrational signal for this substitution (~1108 cm^{-1}) was very weak and could not be observed by Raman. This study has also calculated and compared the ratio of intensities for CO_3^{2-} ν_1 to amide I, which has been reported elsewhere as carbonate substitution normalized per protein[31] and is correlated with the mineral component of bone.[32] In addition, the bandwidth of PO_4^{3-} ν_1 (~958 cm^{-1}) peak was calculated to assess the crystallinity of each sample. It has been reported by a number of researchers that as the mineral crystallinity increases (larger

crystals and/or more atomic ordering), the bandwidth of PO_4^{3-} ν_1 decreases.[25,28,30] In the current study, changes in the peak positions were also analyzed by normalizing each spectrum with respect to the strongest band (PO_4^{3-} ν_1 at ~958cm^{-1}) to gain information on the compositional changes caused by deficiency of OPN and/or aging. The positional changes in the bands were related to the changes in the degree of the crystallinity[33-35] or to the structural changes in the proteins.[24,27,36] Several studies, using either Raman[27,29,36] or FTIR[31,37,38] spectrometry, have studied the organic bone matrix by investigating the amide I and amide III peaks.[39,40] Raman studies have attributed the changes in the organic peaks to the alterations in collagen structure and crosslinking upon loading[27]or aging.[29,36] For the IR studies the relative percent area ratio of two sub-bands of Amide I, ~1660cm^{-1} and ~1686cm^{-1}, was related to the collagen cross-links and collagen maturity of the bone matrix.[31,37,38] However, the peak at ~1690cm^{-1} is not resonance enhanced in the Raman spectrum, so researchers[29,36] normalized the Raman spectra at different ages with respect to the height of CH_2 wag and analyzed the changes in area under the amide I peak at ~1660cm^{-1}. In the current study, the changes in the position and the area under the Amide I and Amide III peaks were investigated and compared between the genotypes and age groups. A custom-written Matlab program was used for the normalization and comparison studies.

Statistical Analysis

Samples were divided into three age groups; I (<12 weeks old, n=8), II (12-50 weeks, n=7) and III (>50 weeks, n=9) to provide statistically comparable data. Kruskal-Wallis analysis, a non-parametric alternative to one-way analysis of variance test, was utilized to

measure the significance of the differences in the calculated ratios between OPN-/- and OPN+/+ mice from the same age groups. The mean values of peak ratios for each combination of genotype and age were also calculated. The Kruskal-Wallis test was also used to test the significance of the effects of aging on the peak ratios for both OPN-/- and OPN+/+. All tests used 95% minimum level of confidence and $p \leq 0.05$ was considered significant while $0.05<p<0.1$ was accepted as marginally significant.

Results

Effects of OPN on Bone Mineral Parameters

Average Raman spectra for the bones from OPN-/- and OPN+/+ mice were normalized with the phosphate peak at ~958cm^{-1} and the peak positions and intensities were compared between age groups (Fig.1). OPN-/- bones younger than 12 weeks exhibited higher Amide I peak (~1667cm^{-1}), and similar Amide III (~1243cm^{-1}), carbonate (~1071 cm^{-1}) and CH_2 wag (~1450cm^{-1}) peak intensities compared to OPN+/+. However, for ages older than 50 weeks, the raman spectra of the bone's organic matrix (Amide I, III and CH_2) were lower in the bones from OPN-/- mice compared to OPN+/+ mice. There was not any statistically significant shift observed in the peak positions of phosphate, amide I and III, carbonate and CH_2.

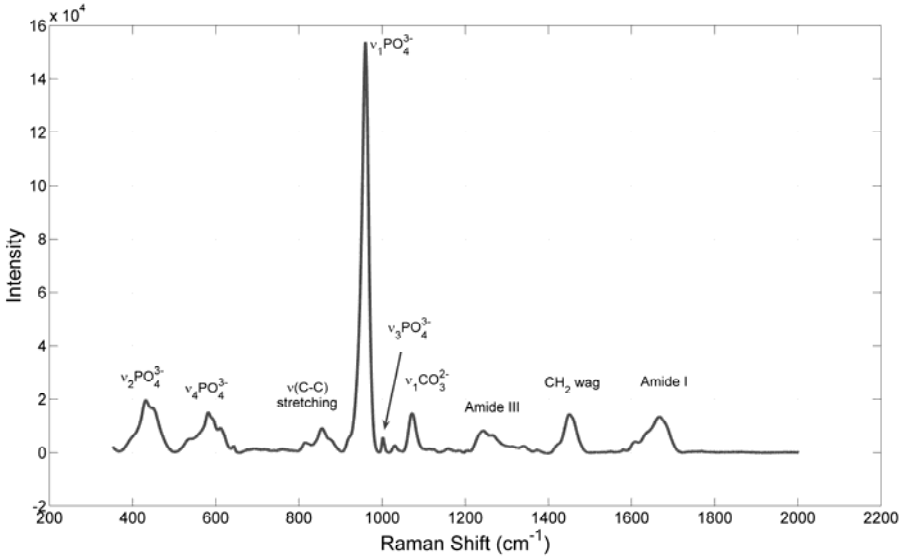
x 10^4
Intensity
Raman Shift (cm^-1)
ν1PO4 3-
ν3PO4 3-
ν1CO3 2-
ν2PO4 3-
ν4PO4 3-
ν(C-C) stretching
Amide III
CH2 wag
Amide I

(a)

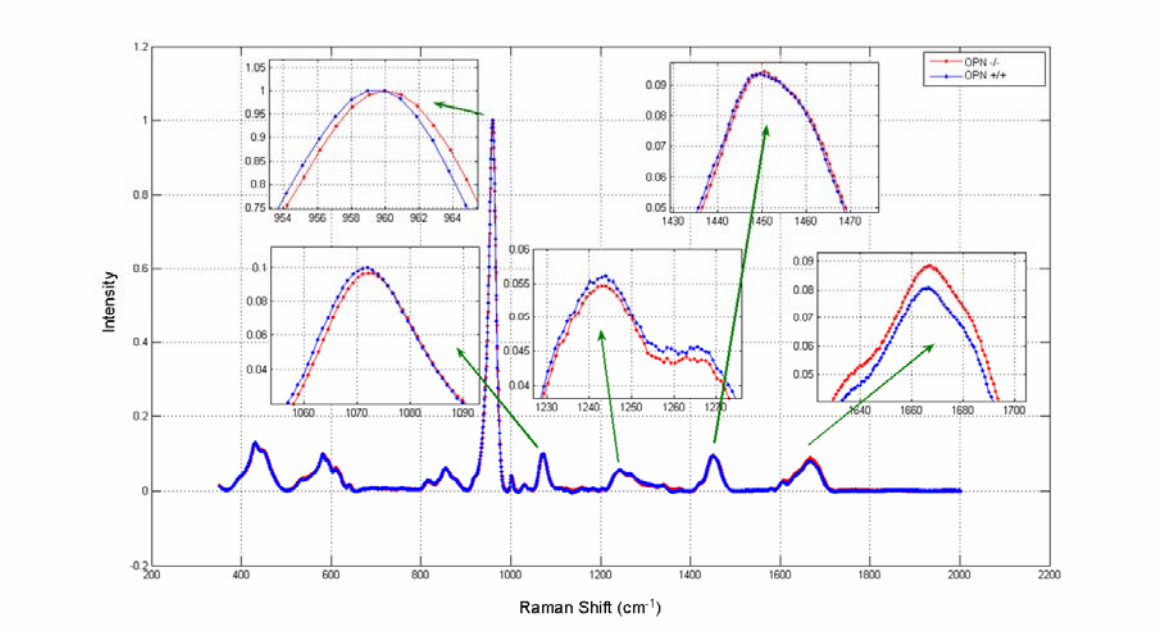
OPN -/-
OPN +/+
Intensity
Raman Shift (cm-1)

(b)

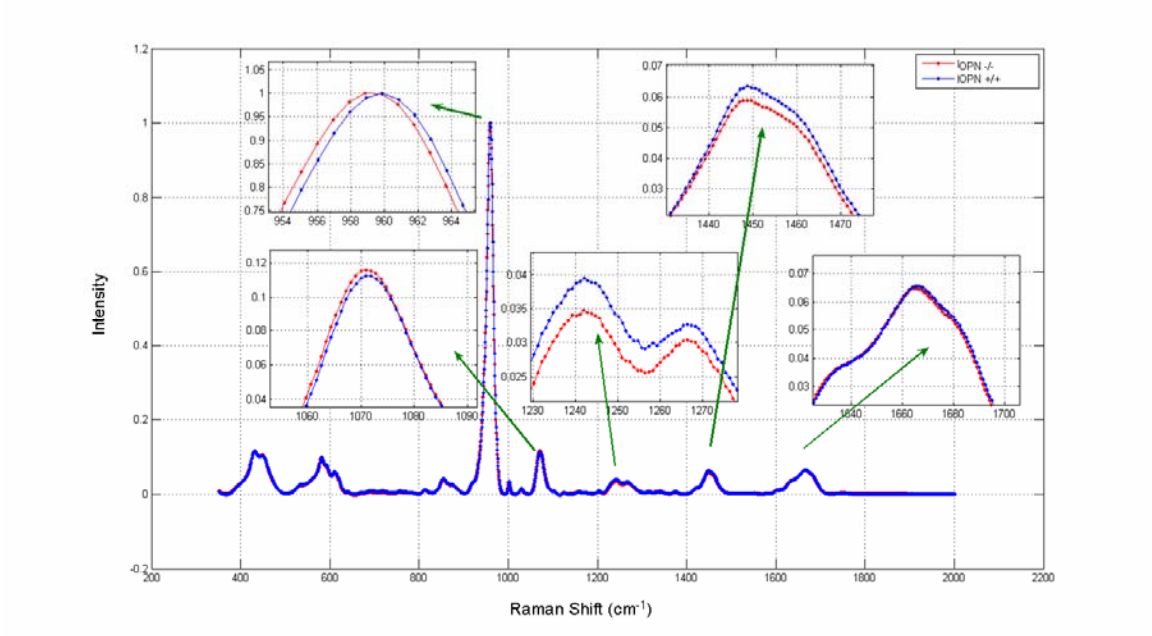

(c)

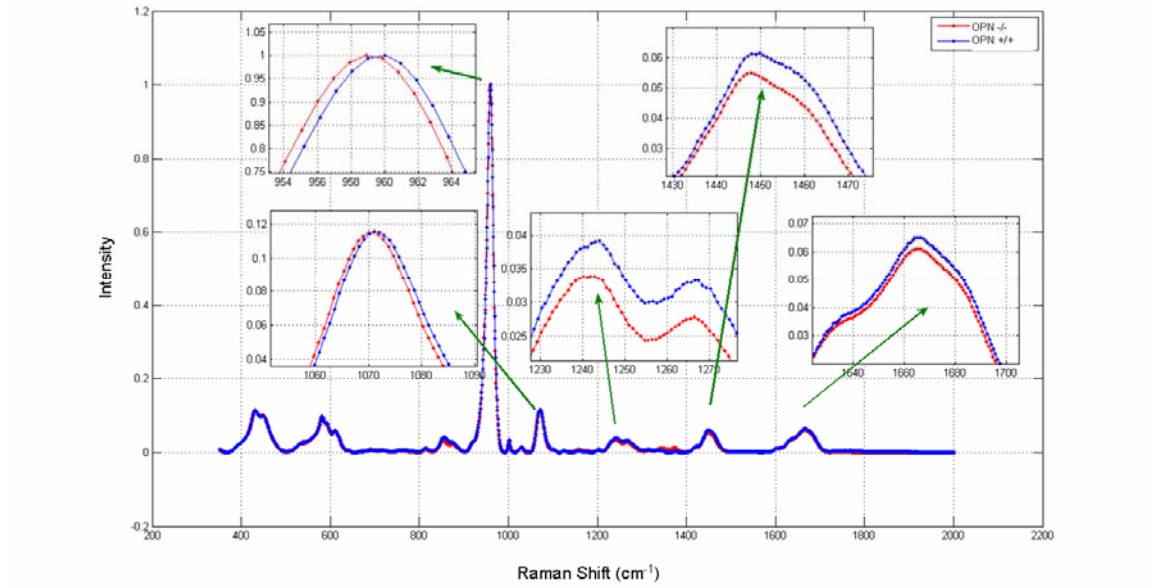

(d)

Fig. 1 (a) Typical Raman spectra of mice bone. Raman Spectra of the bones from OPN-/- and OPN+/+ mice of (b) age <12 weeks, (c) age 12-50 weeks and (d) age>50 weeks. Raman data were averaged for all samples and the spectrum was normalized with the intensity of phosphate peak at ~958cm^{-1}

Average intensities of phosphate ν_1 to amide I ratio, type-B carbonate to amide I ratio, type-B carbonate to phosphate ν_1 ratio and FWHM of phosphate ν_1 are plotted at each age group for OPN-/- and OPN+/+ mice bones (Fig. 2).

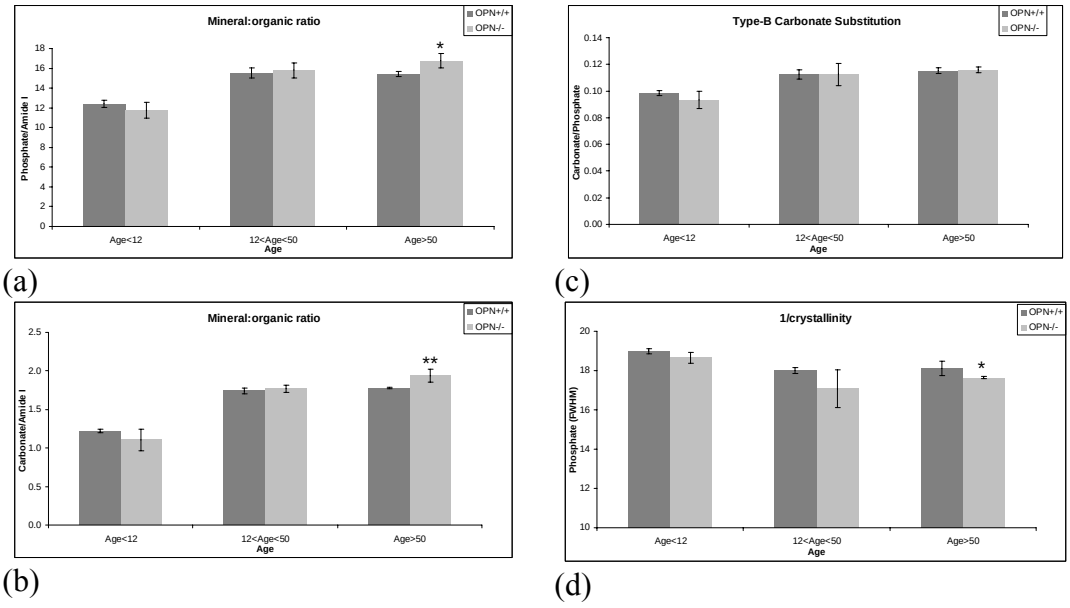

Fig. 2 Bar charts of the average peak ratios for (a,b) mineral:organic ratio, (c) type-B carbonate substitution and (d) inverse crystallinity of the bones from OPN-/- and OPN+/+ mice * indicates a marginally significant difference ($0.05<p<0.1$) and ** indicates a statistically significant difference ($p\leq0.05$) when comparing genotypes

The mineral to organic matrix ratio, ν_1 PO_4^{3-}/amide I, was lower in the bones from OPN-/- mice than OPN+/+ mice (group I, age<12 weeks). However, the difference was not statistically significant ($p>0.05$). Bones from OPN-/- mice (age>50 weeks) showed higher ν_1 PO_4^{3-}/amide I ($p=0.071$) compared to OPN+/+ bones. ν_1 PO_4^{3-}/CH_2, also a

mineral:organic ratio, exhibited higher values in the bones from OPN-/- mice (data not shown). Type-B carbonate substitution (type B-CO_3^{2-}/ν_1 PO_4^{3-}) did not show any statistically significant difference between genotypes. Type B-CO_3^{2-}/ amide I ratio and crystallinity (inverse ν_1 PO_4^{3-} FWHM) was significantly higher in the bones from OPN-/- mice ($p=0.039$, $p=0.071$ respectively) compared to OPN+/+ mice at ages older than 50 weeks.

Effects of OPN on Bone Organic Matrix

The effects of OPN deficiency on the Raman spectra of the organic bone matrix (amide I, amide III and CH_2) were analyzed. The average spectra of each age-matched genotype were normalized with the intensity of the CH_2 wag at ~1450cm^{-1}. Fig. 3 shows details of the difference with genotype between the Raman spectra of bones from mice aged between 12 and 50 weeks. Spectra from other age groups displayed similar shifts of amide band intensities (data not shown). The area under the Amide I peak (~1667cm^{-1}) of the bones from OPN-/- mice was slightly higher than OPN+/+ bones at all ages while the area under Amide III (~1243cm^{-1}) peak was lower. There was no statistically significant shift observed in any of the peak positions.

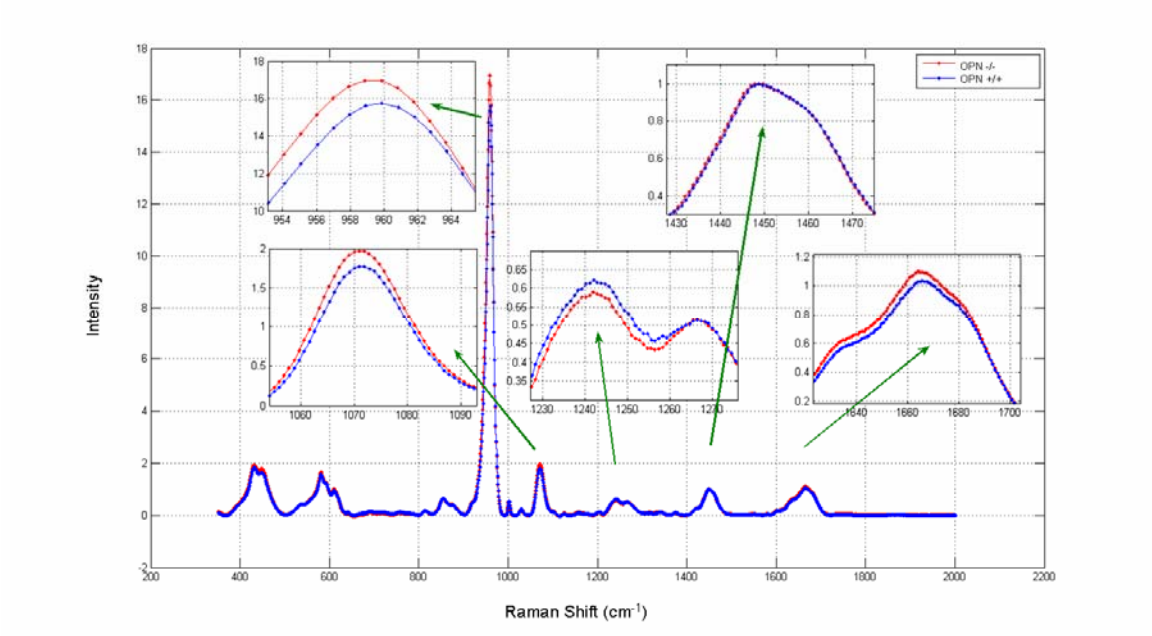

Fig. 3 Raman Spectra of the bones from OPN-/- and OPN+/+ mice (age 12-50 weeks). Raman data were averaged for all samples and the spectrum was normalized with the intensity of CH_2 wag at ~1450cm^{-1}

Effects of Aging on Bone Mineral Parameters

The average Raman spectra of the bones from OPN-/- mice and OPN+/+ mice were analyzed (Fig. 4) and compared between the age groups. Both genotypes displayed a significant decrease in the intensities of amide I, amide III and CH_2 wag peaks and an increase in the carbonate peak with aging. There was no statistically significant shift observed in the peak positions of phosphate, amide I and III, carbonate and CH_2.

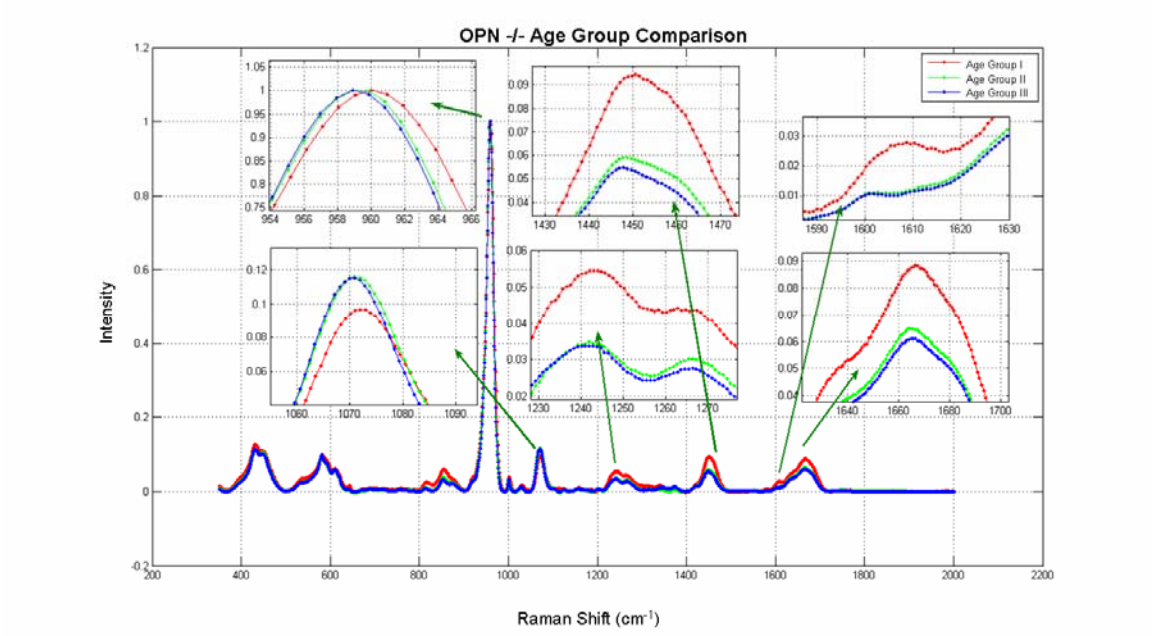

(a)

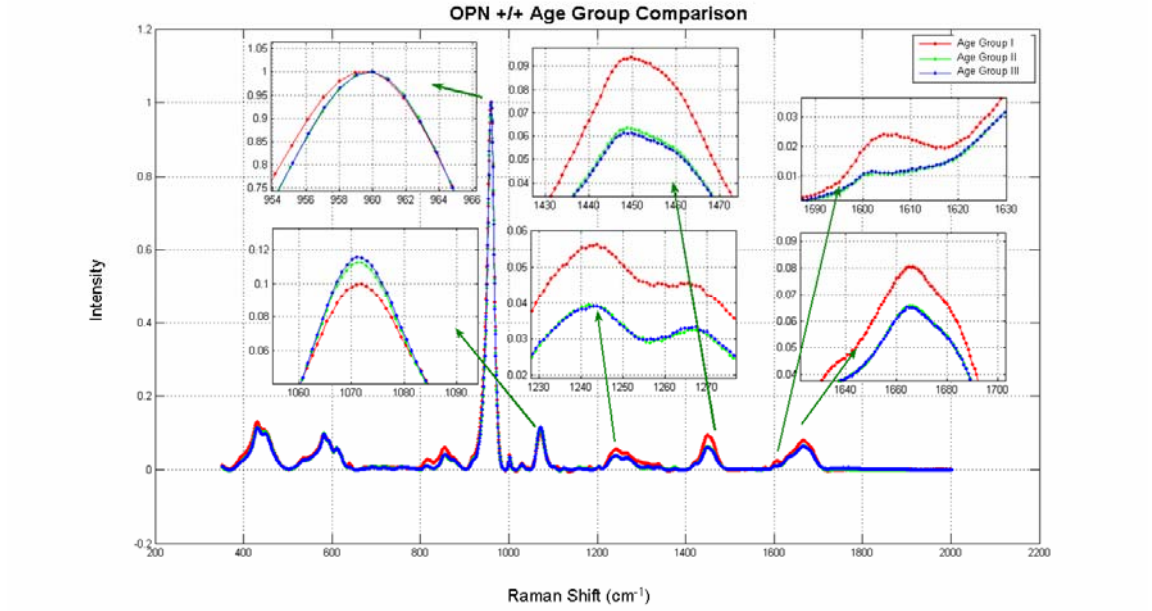

(b)

Fig. 4 Raman spectra of the bones from (a) OPN-/- mice of age I, II and III, (b) OPN+/+mice age I, II and III. Raman data for each age group were averaged and the spectrum normalized with respect to the intensity of the phosphate peak at ~958cm^{-1}

Mean values of the peak ratios of the bones from each age group and genotype combination were calculated (Table 1).

The peak ratios associated with bone mineralization; ν_1 PO_4^{3-}/amide I, and ν_1 PO_4^{3-} /CH_2(data not shown) all increased substantially in the bones of OPN-/- mice ($p=0.01$) and OPN+/+ mice ($p=0.03$) between ages<12 weeks and >50 weeks. Similarly, type-B carbonate substitution, and carbonate to amide ratio increased significantly for both genotypes ($p<0.05$). The band width of ν_1 PO_4^{3-} (FWHM) peak decreased significantly for OPN-/- bones, but the decrease was less significant in the bones from OPN+/+ mice ($P = 0.08$).

Table 1 Bone parameters of OPN-/- and OPN+/+ mice. Ratios are the peak height ratios calculated after curve fitting. Data represented as mean (Standard Error). * indicates the full width at half maximum intensity.

Raman Peak Ratios	**OPN-/-**			**OPN+/+**		
	<12 weeks	**12-50 weeks**	**>50 weeks**	**<12 weeks**	**12-50 weeks**	**>50 weeks**
PO_4^{3-} /amide I	11.75 (0.78)	15.81 (0.77)	16.76 (0.74)	12.43 (0.35)	15.52 (0.52)	15.42 (0.26)
CO_3^{2-}/ν_1 PO_4^{3-}	0.093 (0.006)	0.113 (0.008)	0.116 (0.002)	0.098 (0.002)	0.112 (0.003)	0.115 (0.002)
CO_3^{2-} /amide I	1.11 (0.14)	1.77 (0.05)	1.94 (0.08)	1.22 (0.02)	1.74 (0.036)	1.78 (0.01)
PO_4^{3-} width*	18.66 (0.28)	17.07 (0.95)	17.64 (0.06)	19 (0.13)	17.99 (0.15)	18.11 (0.37)

Effects of Aging on Bone Organic Matrix

The effects of aging on the organic bone matrix were analyzed by normalizing the average spectra of bones from each genotype with the intensity of CH_2 wag at ~1450cm^{-1} (Fig. 5). The area under the Amide I peak (~1667cm^{-1}) increased between the age groups I and II and stayed relatively constant afterwards. On the other hand, the area under the shoulder at ~1605cm^{-1} did decrease with aging. Amide III (~1243cm^{-1}) peak did not show a significant change with aging. There was not any statistically significant shift observed in the peak positions of amide I and amide III. The positions and the intensities of the phosphate ν_1 at ~958 cm^{-1} and carbonate ν_1 at ~1071 cm^{-1} peaks increased for both genotypes with the age of the mouse.

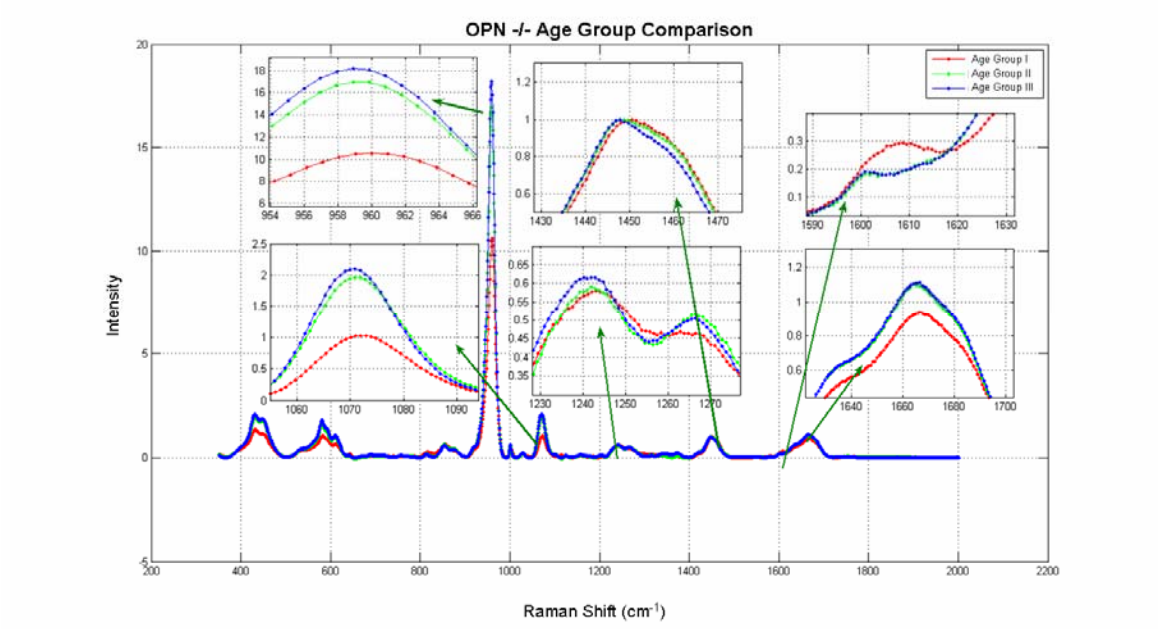

(a)

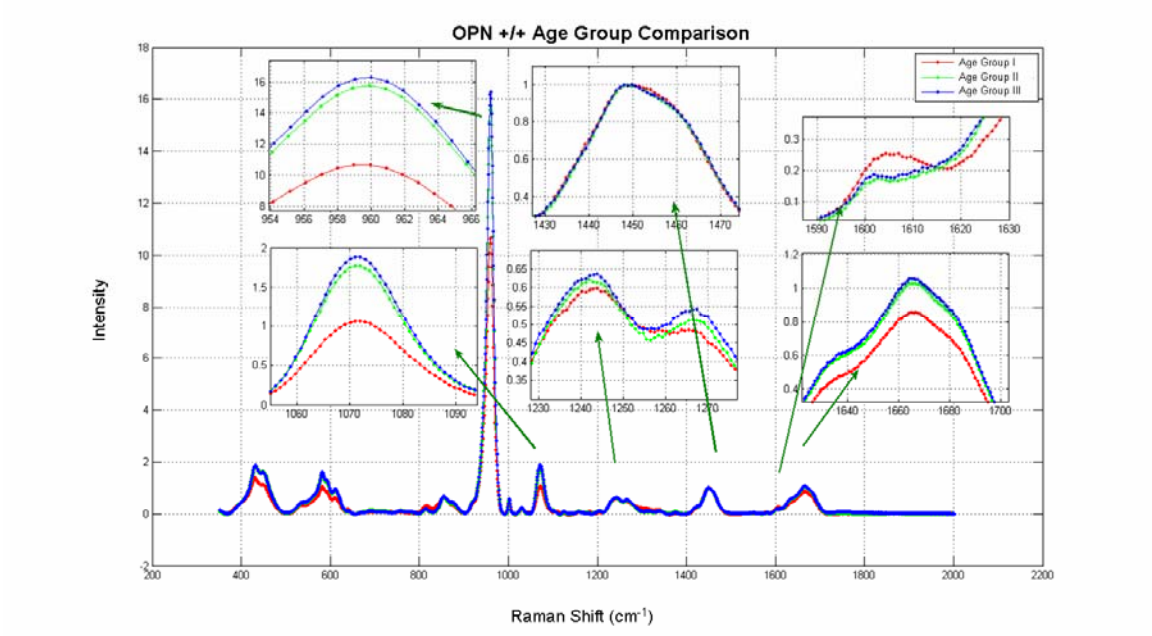

(b)

Fig. 5 Raman spectra of the bones from (a) OPN-/- mice of age I,II and III, (b) OPN+/+ mice of age I,II and III. Raman data of each age group were averaged and the spectrum was normalized with the intensity of CH_2 wag at ~1450cm^{-1}

Discussion

In the current study, Raman micro-spectroscopy has shown that mineralization and crystallinity (mineral to organic matrix ratio) is altered both in the presence of OPN and due to aging. OPN-/- bones from age<12 weeks old mice had less mineralization compared to their age matched control group (OPN+/+), however, this difference was not statistically significant (Fig.1 and 2). In the previous study conducted on the same set of bones, lower mechanical properties (hardness, H and elastic modulus, E) in OPN-/- mice bones were observed at ages younger than 12 weeks.[14] Collectively, both studies confirm other research demonstrating OPN's possible role in the very early stages of bone

formation, mineralization and osteoblast activity.[7,41] Similarly, an earlier study conducted on OPN-/- mice (2-4 months), by Rittling *et al.* had revealed no histologically detectable phenotype in the mineralized tissue in the deficiency of OPN. Moreover, they observed an increase in the formation of osteoclast-like cells in the co-cultures with OPN-/- calvariar osteoblasts suggesting an inhibitory effect of OPN on osteoclast differentiation.[16]

At ages >50 weeks, bones from OPN-/- mice became more mineralized compared to OPN+/+ mice (Fig. 1 and 2). Similarly, crystallinity (inverse Phosphate FWHM) of the bones from OPN-/- mice was larger than OPN+/+ mice bones (age >50 weeks). Crystallinity is reported to be related to an increase in the mineral crystal size, maturity and atomic ordering.[26,28,42] This agrees with several studies that have shown the importance of OPN in the regulation of bone crystal size, mineralization, remodeling, resorption, and osteoporosis.[5,6,17,43] A previous FTIR study demonstrated that the bones from mature OPN-/- mice had increased mineral content, crystallinity (crystal size) and collagen maturity.[17] A more recent study by Duval *et al.* reported that the bones from OPN-/- mice were more brittle compared to OPN+/+ bones which could be correlated to a more mineralized matrix of the OPN-/- bones[44] (even in 10 weeks old mice). OPN deficiency did not affect the type-B carbonate substitution, however, the amount of carbonate normalized per protein displayed higher values in the bones from OPN-/- mice compared to OPN+/+ mice (age >50 weeks). This also indicates a more mineralized matrix in OPN-/- mice bone.

Average Raman spectra normalized with CH_2 peak of the bones from age matched OPN-/- mice displayed slightly higher Amide I intensity than OPN+/+ bones (Fig.3). However,

unlike the Amide I band, the intensity of the Amide III band (~1243cm^{-1}- 1265cm^{-1}) of OPN+/+ bones was higher than that of the OPN-/- bone. A previous Raman study has attributed the spectroscopic shifts in amide I and III bands to the altered collagen cross-links formed upon mechanical loading.[27] Boskey *et al.* have shown an increase in collagen maturity for OPN-/- bones using FTIR spectroscopy.[17] Collectively, the results presented in this study may indicate a change in collagen structure and cross-linking due to the deficiency of OPN.

Aging affected the bone mineral and organic properties for both OPN-/- and OPN+/+ mice (Fig.4 and Fig. 5). Mineralization, crystallinity and type-B carbonate substitution of bones from both genotypes increased significantly with aging. However, this was more pronounced and significant in the bones from OPN-/- mice. Previous studies that have used Raman or IR spectroscopy to investigate the chemical properties of bones from aging human[29,36] or small animals[31,33,37,45,46] correlated the age related mineral and collagen changes to the decreased mechanical properties of bones at the macro-scale. Mineral:organic matrix ratio, crystallinity and carbonate substitution were shown to increase with age and correlate with deterioration of tissue-level mechanical properties.[26] However, in our previous study we reported that the hardness (H) and elastic modulus (E) of bones from OPN-/- mice displayed a very small increase with aging at the nano-scale, while H and E of the OPN+/+ mice bones decreased significantly after 12 weeks of age and remained fairly constant afterwards.[14] This inverse relation between the mechanical properties and mineralization could either be specific to this particular strain of mice or due to the deterioration of the mechanical integrity of the collagen network with increasing age as indicated by Wang *et al.*[47] Previous studies have correlated the age

related increase in the collagen conformation to the decrease in fracture toughness.[29,36] The results of this current study have shown that the relative intensity of the Amide I band increased significantly after 12 weeks of age for both genotypes(Fig.5). As discussed above, this may indicate an alteration in the collagen cross-linking or collagen maturity. Another observation in this study was the age related change in the shoulder at ~1605cm^{-1} corresponding to an amino acid side chain[39,40,48] (most probably an aromatic group). This peak was shifted slightly to a lower wavelength at ~1601cm^{-1} and decreased in intensity. The shift in the peak position may indicate a conformational change in the side chain proteins.[24]

Amide I and III bands are actually a composite of several bands, hence they are resolvable into several maxima and shoulders. The changes in these maximas or shoulders could be attributed to alterations in interfibril cross-links. However, this is a complex problem and the present study is based only on spectroscopic observations. Thus, a definite conclusion regarding changes in cross-linking cannot be made based on these results.

In the current study no statistically significant shift in the peak positions in the normalized spectra were seen when comparing different genotypes and age groups (Fig 1 and Fig 4). This means that although there were some significant compositional changes due to deficiency of OPN and due to aging, this did not significantly affect the bonding energies within the mineral/organic.[42]

In conclusion, changes in the mineralization, crystallinity (crystal size and maturity) and the organic properties of bones with OPN deficiency and aging have been observed.

Specifically, in the bones from mice age>50 weeks, the mineral properties (crystallinity and mineral:organic ratio) were higher in OPN deficient mouse bones. In addition, aging caused an increase in bone mineralization, crystallinity, type-B carbonate substitution, and alterations in collagen structure in the bones from both OPN-/- and OPN+/+ mice. This increase was found to be most pronounced and significant in the absence of OPN. Collectively the results indicate that OPN affects the chemistry and structure of both the mineral and organic phases of bone. This could be either a direct result of the chemical and biochemical interactions of OPN with the mineral and organic phases, or an indirect effect resulting from changes in the rate of bone remodeling due to OPN deficiency.

References

1. Ross FP, Chappel J, Alvarez JI, Sander D, Butler WT, Farach-Carson MC, Mintz KA, Robey PG, Teitelbaum SL, Cheresh DA. Interactions between the bone matrix proteins osteopontin and bone sialoprotein and the osteoclast integrin alpha v beta 3 potentiate bone resorption. Journal of Biological Chemistry 1993;268(13):9901-9907.

2. Denhardt DT, Noda M. Osteopontin expression and function: Role in bone remodeling. Journal of Cellular Biochemistry 1998:92-+.

3. Reinholt FP, Hultenby K, Oldberg A, Heinegard D. Osteopontin-A Possible Anchor of Osteoclast to Bone. Volume 87; 1990. p 4473-4475.

4. Ishijima M, Ezura Y, Tsuji K, Rittling SR, Kurosawa H, Denhardt DT, Emi M, Nifuji A, Noda M. Osteopontin is associated with nuclear factor kappa B gene expression during tail-suspension-induced bone loss. Experimental Cell Research 2006;312(16):3075-3083.

5. Yoshitake H, Rittling SR, Denhardt DT, Noda M. Osteopontin-deficient mice are resistant to ovariectomy-induced bone resorption. Proceedings of the National Academy of Sciences of the United States of America 1999;96(14):8156-8160.

6. Ishijima M, Rittling SR, Yamashita T, Tsuji K, Kurosawa H, Nifuji A, Denhardt DT, Noda M. Enhancement of osteoclastic bone resorption and suppression of osteoblastic bone formation in response to reduced mechanical stress do not occur in the absence of osteopontin. Journal of Experimental Medicine 2001;193(3):399-404.

7. Kasugai S, Nagata T, Sodek J. Temporal studies on the tissue compartmentalization of bone sialoprotein (BSP), osteopontin (OPN), and SPARC protein during bone formation in vitro. Journal of Cellular Physiology 1992;152(3):467-477.

8. Boskey AL, Maresca M, Ullrich W, Doty SB, Butler WT, Prince CW. Osteopontin-hydroxyapatite interactions in vitro: inhibition of hydroxyapatite formation and growth in a gelatin-gel. Bone and Mineral 1993;22(2):147-159

9. Boskey AL. Osteopontin and related phosphorylated sialoproteins: effects on mineralization. Annals of New York Academy of Sciences 1995(760):249-256.

10. Chen J, Singh K, Mukherjee BB, Sodek J. Developmental expression of osteopontin (OPN) mRNA in rat tissues: evidence for a role for OPN in bone formation and resorption. Matrix 1993;13(2):113-123.

11. Dodds RA, Connor JR, James IE, Rykaczewski EL, Appelbaum E, Dul E, Gowen M. Human Osteoclasts, Not Osteoblasts, Deposit Osteopontin onto Resorption

Surfaces - an in-Vitro and Ex-Vivo Study of Remodeling Bone. Journal of Bone and Mineral Research 1995;10(11):1666-1680.

12. Uemura T, Nemoto A, Liu YK, Kojima H, Dong J, Yabe T, Yoshikawa T, Ohgushi H, Ushida T, Tateishi T. Osteopontin involvement in bone remodeling and its effects on in vivo osteogenic potential of bone marrow-derived osteoblasts/porous hydroxyapatite constructs. Materials Science & Engineering C-Biomimetic and Supramolecular Systems 2001;17(1-2):33-36.

13. Denhardt DT, Noda M, O'Regan AW, Pavlin D, Berman JS. Osteopontin as a means to cope with environmental insults: regulation of inflammation, tissue remodeling, and cell survival. Journal of Clinical Investigation 2001;107(9):1055-1061.

14. Kavukcuoglu NB, Denhardt DT, Guzelsu N, Mann AB. Effects of Osteopontin Deficiency and Aging on Nanomechanics of Mouse Bone. Journal of Biomedical Materials Research 2006:In Press.

15. Noda M, Denhardt DT. Osteopontin. In: Bilezikian JP, Raisz LG, Rodan GA, editors. Principles of Bone Biology, Second Edition: Academic Press; 2002. p 239-250.

16. Rittling SR, Matsumoto HN, McKee MD, Nanci A, An XR, Novick KE, Kowalski AJ, Noda M, Denhardt DT. Mice lacking osteopontin show normal development and bone structure but display altered osteoclast formation in vitro. Journal of Bone and Mineral Research 1998;13(7):1101-1111.

17. Boskey AL, Spevak L, Paschalis E, Doty SB, McKee MD. Osteopontin deficiency increases mineral content and mineral crystallinity in mouse bone. Calcified Tissue International 2002;71(2):145-154.

18. Freeman JJ, Silva MJ. Separation of the Raman spectral signatures of bioapatite and collagen in compact mouse bone bleached with hydrogen peroxide. Applied Spectroscopy 2002;56(6):770-775.

19. Penel G, Leroy G, Bres E. New preparation method of bone samples for Raman microspectrometry. Applied Spectroscopy 1998;52(2):312-313.

20. Penel G, Delfosse C, Descamps M, Leroy G. Composition of bone and apatitic biomaterials as revealed by intravital Raman microspectroscopy. Bone 2005;36(5):893-901.

21. Soriano P, Montgomery C, Geske R, Bradley A. Targeted disruption of the c-src proto-oncogene leads to osteopetrosis in mice. Cell 1991;64:693-702.

22. Morris MD, Finney WF. Recent developments in Raman and infrared spectroscopy and imaging of bone tissue. Spectroscopy-an International Journal 2004;18(2):155-159.

23. Roy ME, Rho JY, Tsui TY, Evans ND, Pharr GM. Mechanical and morphological variation of the human lumbar vertebral cortical and trabecular bone. Journal of Biomedical Materials Research 1999;44(2):191-197.

24. Carden A, Morris MD. Application of vibrational spectroscopy to the study of mineralized tissues (review). Journal of Biomedical Optics 2000;5(3):259-268.

25. Akkus O, Polyakova-Akkus A, Adar F, Schaffler MB. Aging of microstructural compartments in human compact bone. Journal of Bone and Mineral Research 2003;18(6):1012-1019.

26. Akkus O, Adar F, Schaffler MB. Age-related changes in physicochemical properties of mineral crystals are related to impaired mechanical function of cortical bone. Bone 2004;34(3):443-453.

27. Carden A, Rajachar RM, Morris MD, Kohn DH. Ultrastructural changes accompanying the mechanical deformation of bone tissue: A Raman imaging study. Calcified Tissue International 2003;72(2):166-175.

28. Yerramshetty JS, Lind C, Akkus O. The compositional and physicochemical homogeneity of male femoral cortex increases after the sixth decade. Bone;In Press, Corrected Proof.

29. Nalla RK, Kruzic JJ, Kinney JH, Balooch M, Ager JW, Ritchie RO. Role of microstructure in the aging-related deterioration of the toughness of human cortical bone. Materials Science & Engineering C-Biomimetic and Supramolecular Systems 2006;26(8):1251-1260.

30. Penel G, Leroy G, Rey C, Bres E. MicroRaman spectral study of the PO4 and CO3 vibrational modes in synthetic and biological apatites. Calcified Tissue International 1998;63(6):475-481.

31. Boskey AL, Goldberg M, Kulkarni A, Gomez S. Infrared imaging microscopy of bone: Illustrations from a mouse model of Fabry disease. Biochimica Et Biophysica Acta-Biomembranes 2006;1758(7):942-947.

32. Boskey AL, DiCarlo E, Paschalis E, West P, Mendelsohn R. Comparison of mineral quality and quantity in iliac crest biopsies from high- and low-turnover osteoporosis: an FT-IR microspectroscopic investigation. Osteoporosis International 2005;16(12):2031-2038.

33. Freeman JJ, Wopenka B, Silva MJ, Pasteris JD. Raman spectroscopic detection of changes in bioapatite in mouse femora as a function of age and in vitro fluoride treatment. Calcified Tissue International 2001;68(3):156-162.

34. Morris MD, Carden A, Rajachar RM, Kohn DH. Effects of applied load on bone tissue as observed by Raman spectroscopy. Proceedings of SPIE 2002;4614:47-54.

35. Crane NJ, Popescu V, Morris MD, Steenhuis P, Ignelzi JMA. Raman spectroscopic evidence for octacalcium phosphate and other transient mineral species deposited during intramembranous mineralization. Bone 2006;39(3):434-442.

36. Ager JW, Nalla RK, Breeden KL, Ritchie RO. Deep-ultraviolet Raman spectroscopy study of the effect of aging on human cortical bone. Journal of Biomedical Optics 2005;10(3).

37. Paschalis EP, Verdelis K, Doty SB, Boskey AL, Mendelsohn R, Yamauchi M. Spectroscopic characterization of collagen cross-links in bone. Journal of Bone and Mineral Research 2001;16(10):1821-1828.

38. Busa B, Miller LM, Rubin CT, Qin YX, Judex S. Rapid establishment of chemical and mechanical properties during lamellar bone formation. Calcified Tissue International 2005;77(6):386-394.

39. Barth A, Zscherp C. What vibrations tell us about proteins. Quarterly Reviews of Biophysics 2002;35(4):369-430.

40. Zhu F, Isaacs NW, Hecht L, Barron LD. Raman Optical Activity: A Tool for Protein Structure Analysis. Structure 2005;13(10):1409-1419.

41. Uemura T, Liu YK, Feng Y, Nemoto A, Yabe T, Ushida T, Miyamoto H, Tateishi T. The role of sialoproteins in recognition of bone surface by osteoblasts via integrin. Materials Science & Engineering C-Biomimetic Materials Sensors and Systems 1997;4(4):303-309.

42. Pasteris JD, Wopenka B, Freeman JJ, Rogers K, Valsami-Jones E, van der Houwen JAM, Silva MJ. Lack of OH in nanocrystalline apatite as a function of degree of atomic order: implications for bone and biomaterials. Biomaterials 2004;25(2):229-238.

43. Shapses SA, Cifuentes M, Spevak L, Chowdhury H, Brittingham J, Boskey AL, Denhardt DT. Osteopontin facilitates bone resorption, decreasing bone mineral crystallinity and content during calcium deficiency. Calcified Tissue International 2003;73(1):86-92.

44. Duvall CL, W.R. T, R.E. G. Osteopontin deficient mice display reduced vascular responce and altered bone properties during fracture healing. 2005; Vail, Colorado.

45. Boskey AL, Gadaleta S, Gundberg C, Doty SB, Ducy P, Karsenty G. Fourier transform infrared microspectroscopic analysis of bones of osteocalcin-deficient mice provides insight into the function of osteocalcin. Bone 1998;23(3):187-196.

46. Boskey AL, Mendelsohn R. Infrared analysis of bone in health and disease. Journal of Biomedical Optics 2005;10(3):031102.

47. Wang X, Shen X, Li X, Agrawal CM. Age-related changes in the collagen network and toughness of bone (vol 31, pg 1, 2002). Bone 2003;32(1):107-107.

48. Barth A. The infrared absorption of amino acid side chains. Progress in Biophysics & Molecular Biology 2000;74(3-5):141-173.

Nanomechanics and Raman Spectroscopy of Osteocalcin and Fibrillin 2 Knock-Out Mouse Bones

N.B.Kavukcuoglu[1], P.Patterson-Buckendahl[2], E. Arteaga-Solis[3], S. Lee-Arteaga[3], F.Ramirez[3], A.B.Mann[1,4]

[1]Materials Science & Engineering, Rutgers University, Piscataway, NJ 08854

[2]Center of Alcohol Studies, Rutgers University, Piscataway, NJ 08854

[3]Child Health Institute, UMDNJ-RWJMS, New Brunswick, NJ 08903

[4]Biomedical Engineering, Rutgers University, Piscataway, NJ 08854

Abstract

In healthy bone there is a balance between bone resorption and formation. When an imbalance occurs there is an overall loss of bone mass leading to an increased risk of fracture. The deterioration is typically accompanied by changes in the non-collagenous proteins in the bone. Osteocalcin (*OC*) is the most abundant noncollageneous bone matrix protein and it is believed to play a role in bone formation and resorption. Absence of Fibrillin 2 (*Fbn2*), another non-collagenous bone protein, causes a connective tissue disorder called congenital contractural arachnodactyly (CCA) and has been associated with decreased bone mineral density. Nanoindentation and Raman microspectroscopy have been used to correlate the mechanical and chemical properties of cortical bone from femora of *OC-/-* and *Fbn2-/-* deficient mice and their wild-type controls (*OC*+/+ and *Fbn2*+/+). We found significant intra-bone variations in mechanics and crystallinity especially in the mid-cortical section for *OC-/-* mice compared to *OC*+/+ mice. We also

found that *Fbn2-/-* bones have significantly lower hardness and elastic modulus compared to *Fbn2*+/+, but the crystallinity for *Fbn2-/-* bones is inversely correlated to their mechanical properties. Type-B carbonate substitution decreases significantly in the absence of both proteins. This appears to affect the hardness more than the elasticity.

Keywords: nanoindentation; raman; bone; osteocalcin; fibrillin

Introduction

Bone is a living and growing tissue which is constantly renewed by matrix resorption and formation throughout life. Bone resorption takes place by the action of specialized cells called osteoclasts whereas bone matrix formation is by cells called osteoblasts. In adults, bone mass is maintained by the coupling between the osteoclastic bone resorption and osteoblastic bone formation. However, when the activity levels of osteoclasts exceeds osteoblasts, uncoupling takes place causing a significant loss in bone mass and increased fragility. The reduced bone mineral density (BMD) is the main cause of the most common bone diseases, namely osteopenia/osteoporosis which is characterized by the microarchitectural deterioration of bone tissue and an increase in fracture risk [1]. Current treatments for osteoporosis and osteopenia focus on either increasing osteoblastic activity or reducing osteoclastic activity. In both cases there is a close link between bone cell activity and the presence of non-collagenous bone matrix proteins.

Bone is a composite tissue comprised of a mineral phase, an organic matrix and water. Although the organic phase of bone is 90% type I collagen, considerable amounts of non-collagenous bone proteins have been identified by researchers. Osteopontin, osteocalcin, osteonectin and bone sialoproteins are among the most abundant and most widely

investigated non-collageneous bone matrix proteins. Investigators have proposed that the mix of these proteins gives bone its characteristic properties, for instance its ability to mineralize compared to other tissues [2, 3]. It has been reported that the non-collageous proteins have both a role in bone turnover regulation [4] and contribute to the structural integrity of bone.

Osteocalcin (*OC*) is the most abundant non-collagenous bone matrix protein produced by osteoblasts. OC contains a γ-carboxyglutamic acid (GLA) residue that was shown to be involved in calcium and hydroxyapatite binding which has in turn drawn interest from researchers studying bone mineralization [5-7]. In vitro studies have shown that *OC* has a high affinity to HA [7, 8] with some in-vitro cell studies demonstrating that *OC* functions in the recruitment and differentiation of osteoclast precursors to bone resorbing cells suggesting its role in bone resorption [5, 9, 10]. On the other hand, bones from *OC* knockout mice (*OC*-/-) were found to contain more osteoclasts compared to wildtype mice (*OC*+/+) [11]. There have been contradictory results over the role of osteocalcin in bone mineralization. Ducy et al. demonstrated that OC deficiency caused an increase in bone density without any change in the bone resorption and mineralization [11]. However, there have been some studies showing positive correlation between the *OC* concentration and mineralization in *Ciprinus carpio (carp)* rib bone [12, 13] and increased mineral:organic matrix ratio for bones from ovariectomized *OC*-/- mice compared to *OC*+/+ [14]. Research on the mechanical properties of bones from *OC*-/- mice has demonstrated an increase in the failure load on the macro-scale compared to *OC*+/+ mice [11]. A recent study also suggested an inverse relationship between the *OC* concentration and both elastic modulus and hardness at the nano-scale [12].

Besides *OC*, mutations of other non-collagenous proteins can also have dramatic effects on the properties of bone. Fibrillin 1 and 2 are extracellular glycoproteins that constitute the major structural components of connective tissue microfibrils. Mutations in fibrillin 1 (*Fbn1*) and fibrillin 2 (*Fbn2*) cause the connective tissue disorders known as Marfan's syndrome and congenital contractural arachnodactyly, respectively [15, 16]. In addition to other manifestations, these two heritable disorders of the connective tissues have been associated with a reduction in bone mineral density [17-20]. The findings that fibrillin-rich microfibrils are widely distributed in the developing mouse and human skeleton has been interpreted to suggest key roles of these macromolecular aggregates in bone formation, growth and mineralization [21-23]. Furthermore, the fact that fibrillins are highly expressed by differentiating osteoblasts may also indicate a function in matrix adherence through interaction with the $\alpha_v\beta_3$ integrin [21, 24, 25]. Finally, fibrillin-rich microfibrils have been associated recently with modulating the activity of TGF-β, one of the major growth factors involved in bone physiology [26]. Consistent with these earlier lines of indirect evidence, unpublished data indicate that both fibrillin-1 and fibrillin-2 deficient mice are severely osteopenic due to distinct alterations in the balance of bone remodeling [27, 28]

The objective of the study presented here was to utilize nanoindentation and Raman spectroscopy to investigate how the absence of *OC* and *Fbn2* affects the mechanical and chemical properties of bones. The average properties of several bones were studied and then intra-bone variations in the properties were investigated and compared between cortical femora bones of knockout (*OC-/-*, *Fbn2-/-*) and wild-type (*OC*+/+, *Fbn2*+/+) mice.

Materials and Methods

Sample Preparation

This study has used 1 year old male C57Bl/6j osteocalcin (n=11) and 3 months old female 129/SvEv fibrillin-2 (n=9) knockout mouse models and their age, sex and background matched wild-type controls. *OC*-deficient mice (*OC-/-*) were created by simultaneously deleting both *OG1* and *OG2* genes using embryonic stem cell technology as described by Ducy et al. [11]. *OC-/-* and *OC+/+* mice were maintained in the vivarium of the Center of Alcohol Studies, Rutgers University, under climate controlled conditions (22°C, 12 h light/12 h dark) until they reached 1 year of age. At that time, they were killed by CO2 asphyxiation, and the hindlimbs removed and preserved in 70% ethanol at 4°C prior to analysis. Creation of fibrillin-2 null mice (Fbn2 -/-) has been already described [29] and the bones used in the present study were from animals of 129/SvEv genetic background. The research was approved by the Rutgers and UMDNJ-RWJMS Animal Care and Facilities Committees (Protocol # I 06-012-2 for the Fbn2-/- mice) and performed according to the NIH guidelines for the care and use of laboratory animals (NIH Publication #85-23 Rev. 1985). The left femoral bone from the mice for each genotype were selected for this study. The bones were then prepared for nanoindentation testing as described by Roy et. al [30]. Briefly, this involved dehydration in graded alcohol solutions (70-100%) and mounting in a low temperature cure epoxy (SPI supplies, West Chester,PA). After mounting, the included femora were sectioned transversely at mid-shaft using a diamond wafering saw. The surfaces were ground with silicon carbide paper of decreasing grit size (400, 600 and then 1200 particles per inch) followed by polishing with diamond paste down to ½ then ¼ μm grit size. After the

polishing, all specimens were cleaned ultrasonically to remove surface debris. Raman studies do not require any specific kind of sample preparation [31], so the same bones used for nanoindentation testing were used. It should be noted that embedding samples into epoxy has been shown to have no effect on the Raman data [32]. The locations for the nanoindentation and Raman spectroscopy measurements are shown in Fig. 1.

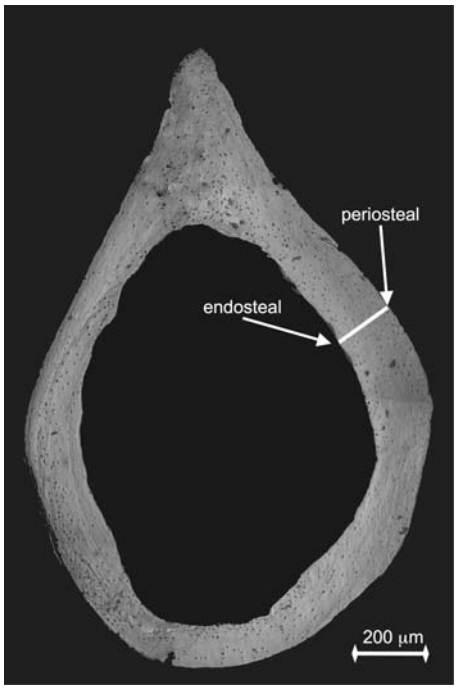

Fig. 1. Optical image (Leica, 5X) of a mouse femur's radial section. The white marks represent the nanoindentation and raman test locations.

Raman Microspectroscopy

Raman Spectroscopy is a non-destructive way of analyzing the molecular structure of the mineral components of bone at the microscopic level. Raman can characterize both the organic and inorganic component of bone by examining the vibrational spectra of the chemical bonds. It provides quantitative information on the changes in the mineral and matrix compositon as well as the nature and amounts of substituents in the mineral. These

advantages of Raman Spectroscopy have led to it gaining in importance as a method to study the compositional changes of bone due to aging, diseases and mechanical deformation.

A Renishaw inVia™ Raman microscope was used for this study with a 785 nm laser beam and a grating of 1200 1/mm. The laser was focused on each point of interest through a Leica DMLM, 50X/0.75 NA objective providing an approximately 2 μm spot size. All spectral acquisitions were performed in the 350-2000cm^{-1} range and the spots were spaced every 10 μm in the x- (radial) direction (see Fig.1). Signal to noise ratio and fluorescence background were minimized by employing 18 seconds of exposure time and 3 times of accumulation at each measurement point.

The Wire 2 software provided by Renishaw was used to remove sample background using cubic spline interpolation at each acquisition. A single spectrum for each sample point was obtained by averaging all the acquisitions per sample. An average spectrum was then obtained for each genotype by averaging the spectra from each individual sample. The software was then used to analyze the peaks after Gaussian-Lorentzian curve fitting. The intensities of the following peaks were measured: phosphate ν_1 at ~958 cm^{-1} (PO_4^{3-} symmetric stretching band), carbonate ν_1 at ~1071 cm^{-1} (CO_3^{2-} symmetric stretching band), CH_2 wag at ~1450cm^{-1} (C-H bending band), amide ~1667cm^{-1} (C=O stretching band), amide III at ~1243cm^{-1} (in-phase combination of the N-H bending and C-N stretching) and the width (full width at half maximum, FWHM) of phosphate ν_1 at around 958 cm^{-1}. A typical Raman spectrum for cortical mouse bone is shown in Fig. 2.

The degree of mineralization for each sample was calculated by taking the ratio of the intensities of the PO_4^{3-} ν_1/amide I peaks [33]. An increase in this ratio indicates a more mineralized matrix [34, 35]. In bone, two types of carbonate substitutions have been reported. Type-A carbonate substitution is when the CO_3^{2-} ion substitutes for the OH^- ion, and type-B carbonate substitution is when the CO_3^{2-} ion substitutes for the PO_4^{3-} ion [34, 36-38]. In the present study the type-B carbonate substitution was quantified by the ratio of the peak intensities for CO_3^{2-} (~1071 cm^{-1}) / PO_4^{3-} ν_1 (~958cm^{-1}). Type-A substitution, however, could not be quantified because the wavenumber for the vibrational signal for this substitution (~1108 cm^{-1}) was very weak and could not be observed with the Raman system. In addition, the bandwidth (FWHM) of the PO_4^{3-} ν_1 (~958 cm^{-1}) peak was calculated to assess the crystallinity of each sample. It has been reported by a number of researchers that as the mineral crystallinity improves (increase in the crystal size and/or atomic ordering) the bandwidth of the PO_4^{3-} ν_1 peak decreases [37, 39]. In addition to the mineral peaks, changes in the position and the area under the Amide I and Amide III peaks were investigated and compared between the genotypes. An increased area under Amide I peak corresponds to increased maturity in the collagen and, hence, collagen crosslinking [40]. The Amide I peak was analyzed after normalizing the Raman spectra with the CH_2 wag at ~1450cm^{-1} [41, 42].

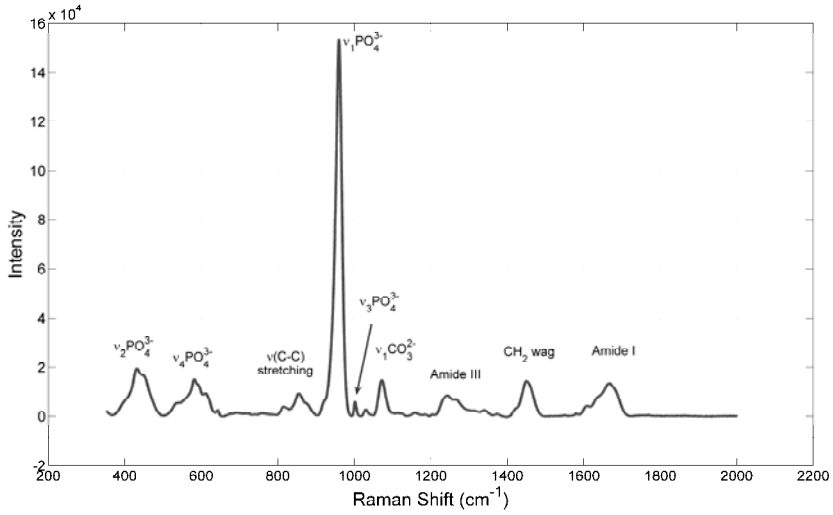

Fig. 2. Typical Raman spectrum of cortical bone from a mouse femur.

Nanoindentation

Nanoindentation has become the standard tool for characterizing the mechanics of materials at small length scales because of its ability to probe a surface and map its properties with a resolution smaller than 1 μm. Because of the small dimensions of mouse bones, this technique provides the most effective, even vital, measurements for bone mechanical properties [43-45].

In this study, the nanoindentation tests were performed using a Triboindenter^{TM} (Hysitron Inc., MN) in load control mode. All samples were tested in the ambient environment. Prior to testing the bones, the contact area, A_c, was determined by analysis of the load-depth curve and calibrating the tip on a standard material (fused quartz) as described by Oliver & Pharr [46]. The tip was nominally a diamond Berkovich pyramid and the loading direction was parallel to the long axis of the femur. For each indent a maximum load of 1000 μN was applied with a 2 second hold time at peak load. A grid pattern of approximately 300 indents was performed across the cortical radial sections of each bone

(Fig.1). The location of the indentation arrays were chosen to be at approximately the same location as the Raman spectral measurements to allow a comparison between the mechanical and chemical data for each sample.

Nanoindents were spaced every 2.5 μm and 10 μm in the x- (radial) and y- (tangential) directions, respectively. The Oliver & Pharr method [46] was used to determine the mechanical properties. This method uses the following equations to find the bone's elastic modulus, E, and hardness, H:

$$E_r = \frac{\sqrt{\pi}}{2}\frac{S}{\sqrt{A_c}} \qquad \mathrm{E} = \frac{1-\nu_s^2}{\frac{1}{E_r} - \frac{1-\nu_i^2}{E_i}} \qquad \mathrm{H} = \frac{P_{\max}}{A_c}$$

where, E_r is the reduced elastic modulus, S is the measured contact stiffness, $P_{\max}$ is the maximum load and A_c is the contact area. ν_i and ν_s are Poisson's ratio for the indenter and sample, respectively. The values for the diamond indenter tip are E_i = 1140 GPa, ν_i = 0.07 and the Poisson's ratio for the bone was taken to be ν_s = 0.3.

Statistical Analysis

The Raman spectra and the nanoindentations across the radial axis of each mutant (*OC-/-*, *Fbn2-/-*) and wild-type (*OC*+/+, *Fbn2*+/+) were examined to give the intra-bone variations for each genotype. Mechanical and chemical changes calculated at each measurement location were averaged for each set of mutant and wild-type bones, respectively. The data collected across the cortical thickness were then divided into seven equal sections. Sections I and II are the bone adjacent to periosteal (outer) surface. Sections III- V are the mid-cortical and sections VI -VII are the bone adjacent to the

endosteal (inner) surface (Fig. 1). Mechanical and chemical properties at each section were compared between the mutant and wild-type mice. Statistical tests were conducted to assess the significance of the differences between the mutant and wild-type mouse bones. Specifically, t-test was used for the normally distributed data. However, for the data that did not pass the normality and equal variance tests, Mann-Whitney U (M-W), a non-parametric alternative to the one-way analysis of variance (ANOVA) test was utilized. Pearson product moment test was used to calculate the correlation between the mechanical and chemical properties of each genotype. All tests used 95% minimum level of confidence and, statistically, $p \leq 0.05$ was considered significant.

Results

Osteocalcin

Nanoindentation

The mean values, standard deviations and standard errors for hardness (H) and Elastic Modulus (E) of both genotypes (*OC*-/- and *OC*+/+) were calculated. The average hardness for *OC*-/- and *OC*+/+ were calculated as 1.27 ± 0.006 GPa and 1.18 ± 0.009 GPa, respectively. The t-test analysis revealed that bones from *OC*-/- mice exhibited significantly higher H ($p<0.001$) values compared to *OC*+/+. On the other hand E did not change with genotype (30.08 ± 0.15 GPa for *OC*-/- and 30.48 ± 0.14 GPa for *OC*+/+). The intra-bone variations were assessed by examining the seven equal sections of the cortical segment described previously. The averages of the H and E data for both the *OC*-

/- and *OC*+/+ mouse bones in each section have been plotted as bar charts. This shows the variation of H and E across the radial axis of the cortical mouse femora bones for each genotype (Fig. 3). The results suggest that the H was significantly ($P<0.05$, M-W) higher in *OC* deficient bones at almost all locations, but especially at the mid-cortical section as shown by Fig. 3a. However, E for the *OC*-/- and *OC*+/+ mouse bones did not show any statistically significant difference across the cortical thickness. In addition, the H of the bones from *OC*-/- mice increased across the cortical thickness ($P<0.05$, M-W). For the *OC*+/+ mice bones H values dropped between the periosteal and mid-cortical regions ($P<0.05$, M-W) and increased slightly thereafter. E values calculated for the bones from *OC*+/+ mice did not change across the radial axis, but E did increase for *OC*-/- bones between the periosteal and mid-cortical sections ($p<0.05$, M-W).

Raman Analysis

The mean values, standard deviations and standard errors in the phosphate ν_1/amide I ratio, type-B carbonate/amide I ratio, and $1/\text{Phosphate}_{(\text{FWHM})}$ were calculated for each genotype (Table I). The statistical analysis revealed that there was a significant decrease in the type-B carbonate substitution ($p<0.05$) and an increase in the crystallinity of the bones from *OC*-/- mice compared to *OC*+/+ mice ($p=0.05$) in the center of the cortical section.

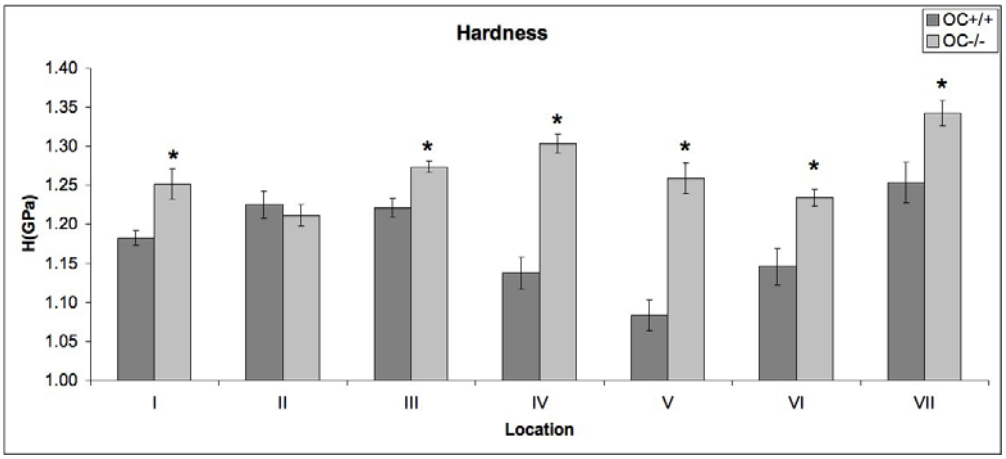

(a)

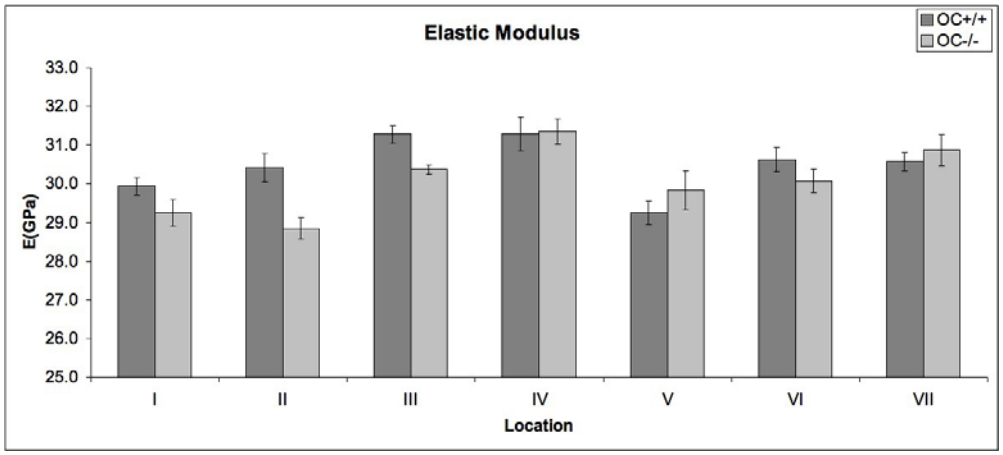

(b)

Fig. 3. Intra-bone variations in (a) hardness, H, and (b) elastic modulus, E, for femoral cortical bone from OC-/- and OC+/+ mice. The data is taken along a grid traversing between the outer periosteal and inner endosteal regions of the bone. The error bars are standard statistical errors. * denotes $p \leq 0.05$ when comparing OC-/- to OC+/+ mouse bones.

Table I: Average bone parameters and standard errors derived from Raman spectra of bones from *OC-/-* mice and *OC+/+* mice. * denotes p≤0.05 when comparing *OC-/-* to *OC+/+* mouse bones.

Genotype	PO_4^{3-} ν_1/amide I	CO_3^{2-}/PO_4^{3-} ν_1 *	1/ PO_4^{3-} $\nu_{1\ (FWHM)}$ *
OC-/-	13.78±0.10	0.1164±0.0007	0.05379±0.0001
OC+/+	13.58±0.14	0.1235±0.0017	0.05346±0.0001

The averaged intra-bone variations of type-B carbonate substitution and crystallinity were plotted along the radial axis of cortical femora (Fig. 4). Mineral:organic matrix ratio did not show any significant intra-bone variation between the genotypes (data not shown). However, the crystallinity of the *OC-/-* mouse bones was substantially higher at the mid-cortical ($p=0.05$, t-test), region IV on Fig. 4b, and remained slightly high towards the endosteal section compared to *OC+/+* mouse bones ($0.05<p<0.1$). Type-B carbonate substitution in *OC+/+* mouse bones was higher than that in *OC-/-* mouse bones in the mid-cortical ($p<0.05$, M-W) and endosteal ($p<0.05$, t-test) regions, regions III-VII in Fig. 4a.

The effects of OC deficiency on the collagen's maturity and cross-linking in the bones were analyzed by normalizing the average Raman spectra of each genotype with the intensity of the CH_2 wag at ~1450cm^{-1} (Fig. 5). The area under the Amide I peak did not show any difference between the genotypes. However, the area under the Amide III (~1243cm^{-1}) peak was higher for *OC+/+* mice bones. There was no statistically significant shift observed in the peak positions. The intensity of the phosphate ν_1 (~958

cm^{-1}) peak was higher and the carbonate ν_1 (~1071 cm^{-1}) peak was lower in the *OC-/-* mouse bones.

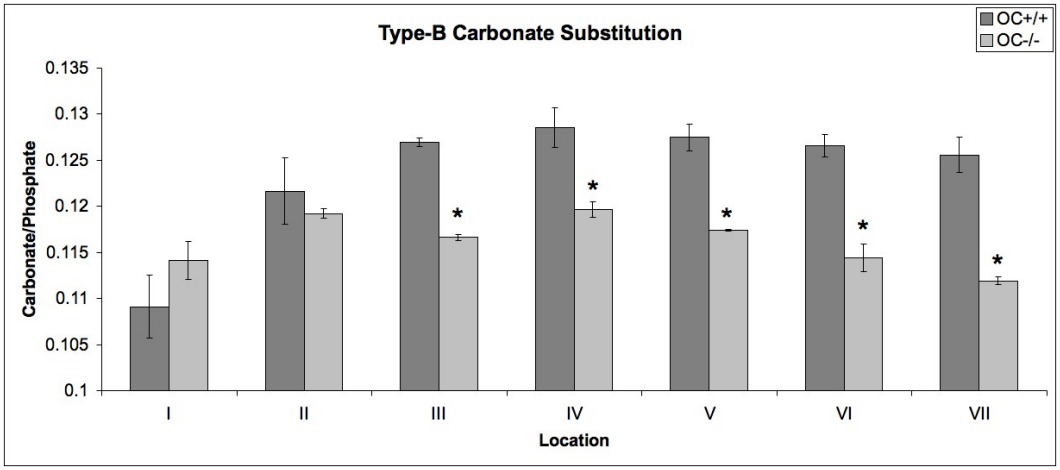

(a)

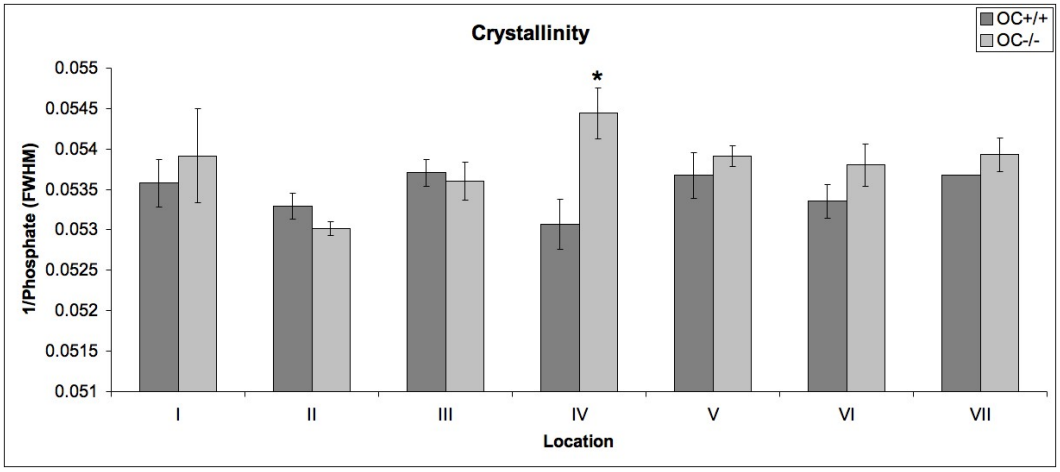

(b)

Fig. 4. Intra-bone variations in (a) type-B carbonate substitution and (b) crystallinity for femoral cortical bones from OC-/- and OC+/+ mice. The data were taken along a line traverse between the outer periosteal and inner endosteal regions of the bone. The error bars are standard statistical errors. * denotes $p \leq 0.05$ when comparing OC-/- to OC+/+ mouse bones.

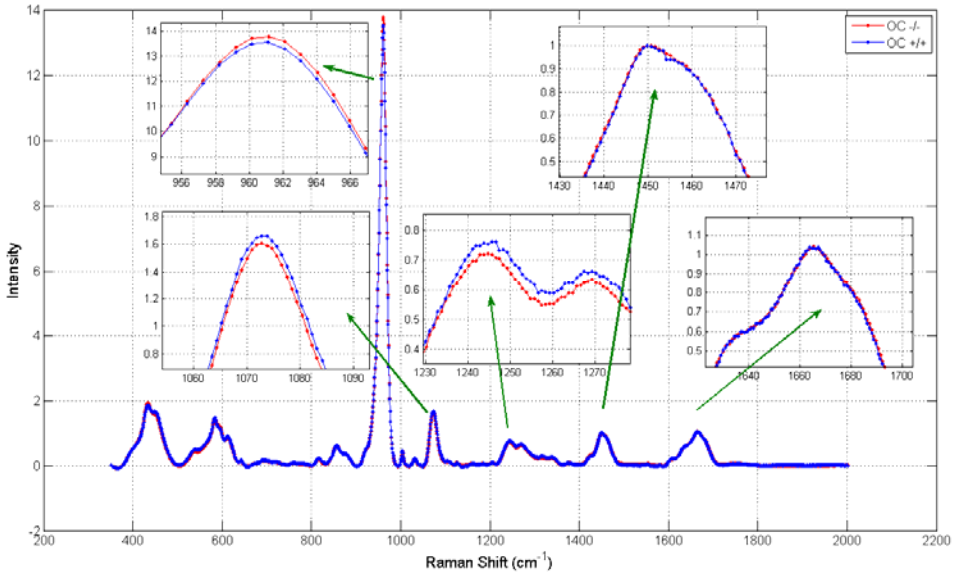

Fig. 5. Average Raman spectra normalized with CH_2 wag at 1450cm^{-1} for femoral cortical bones from *OC-/-* and *OC+/+* mice after baseline subtraction. The spectra were averaged over 20-25 measurements per sample that traverse between the outer periosteal and inner endosteal regions of the femur cortical bone.

Fibrillin-2

Nanoindentation

The mean values, standard deviations and standard errors in the cortical bones' H and E for both genotypes (*Fbn2-/-* and *Fbn2+/+*) were calculated. The t-test revealed that bones from *Fbn2-/-* mice exhibited significantly lower hardness and elastic modulus values compared to *Fbn2+/+* ($p<0.05$, M-W). The average H and E of *Fbn2-/-* mouse bones were 1.16 ± 0.008 GPa and 29.33 ± 0.177 GPa respectively. For *Fbn2+/+*, H was 1.23 ± 0.007 GPa and E was 31.79 ± 0.14 GPa. The intra-bone variation results were plotted as bar charts to show the variation of H and E with genotype across the radial axis of the cortical bone (Fig. 6). The results suggest that Fbn2 deficiency caused a very significant

decrease in both H and E of mouse bones at all locations from periosteal to endosteal cortical sections ($p<0.05$, M-W), though the difference was small close to the periosteal (region I on Fig. 6). The H values of bones from *Fbn2-/-* mice did not change significantly along the radial axis, but for the bones from *Fbn2+/+* mice, the H and E values increased significantly from the periosteal to mid-cortical sections followed by a decrease thereafter ($p<0.001$). Not surprisingly this was similar to the results for *OC+/+* mouse bones. However, deficiency in Fbn2 caused the E value to decrease substantially between the periosteal and mid-cortical bone, and increase thereafter ($p<0.05$).

Raman Analysis

The mean values, standard deviations and standard errors of the phosphate ν_1/amide I ratio, type-B carbonate/amide I ratio, and $1/\text{Phosphate}_{(FWHM)}$ are given in Table II. Type-B carbonate substitution decreases and the crystallinity increases in the Fbn2 deficient mouse bones ($p<0.05$).

Table II: Average bone parameters and standard errors derived from Raman spectra of bones from *Fbn2-/-* mice and Fbn+/+ mice. * denotes $p\leq0.05$ when comparing *Fbn2-/-* to *Fbn2+/+* mouse bones.

Genotype	PO_4^{3-} ν_1/amide I	CO_3^{2-}/PO_4^{3-} ν_1 *	$1/ PO_4^{3-}$ $\nu_{1\ (FWHM)}$ *
Fbn2-/-	14.92±0.1	0.110±0.0012	0.05274±0.00011
Fbn2+/+	14.63±0.12	0.115±0.0015	0.05236±0.00007

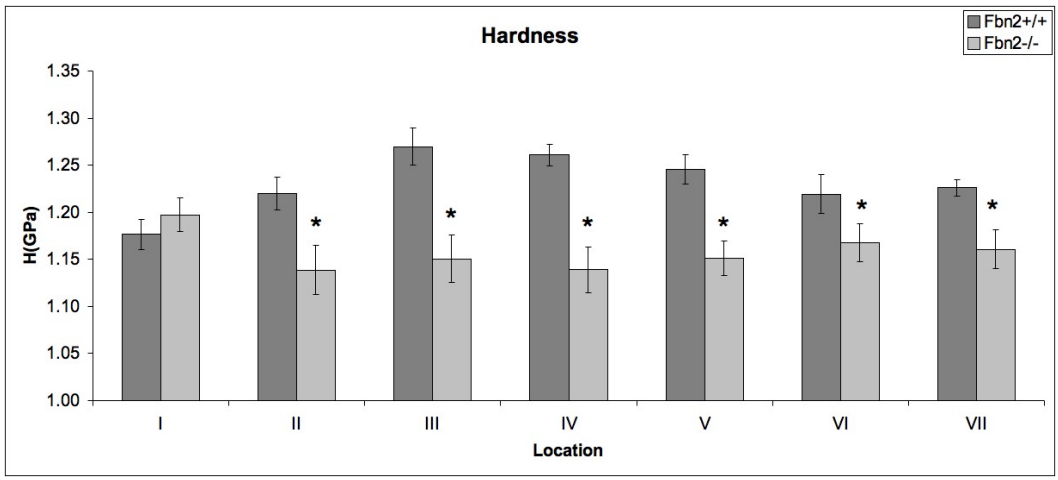

(a)

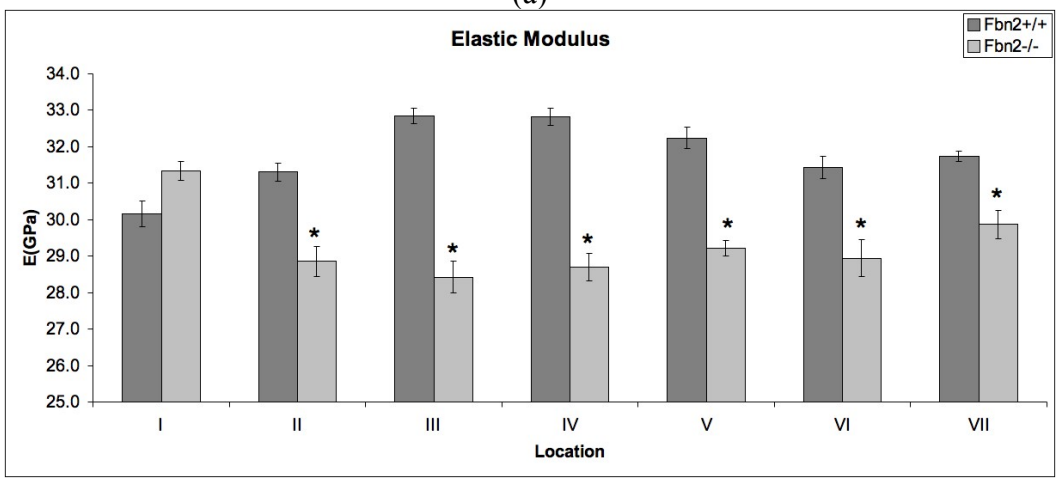

(b)

Fig. 6. Intra-bone variations in (a) hardness, H, and (b) elastic modulus, E, for femoral cortical bones from Fbn2-/- and Fbn2+/+ mice. The data were taken along a grid traverse between the outer periosteal and inner endosteal regions of bone. The error bars are standard statistical errors. * denotes $p \leq 0.05$ when comparing Fbn2-/- to Fbn2+/+ mouse bones.

Intra-bone variations of the bone parameters were plotted across the radial axis of the cortical mouse femora bones as shown in Figure 7. Bones from *Fbn2-/-* mice exhibited a similar mineral:organic ratio to bones from *Fbn2+/+* mice across the cortical section (data not shown). Type-B carbonate substitution, however, was significantly higher in *Fbn2-/-* mouse bones at locations near the periosteal and endosteal surfaces compared to

Fbn2+/+ mouse bones ($p<0.05$), as seen in regions II and VI of Fig. 7a. The crystallinity exhibited the greatest difference in the mid-cortical where it was significantly higher for *Fbn2-/-* mouse bones compared to *Fbn2*+/+ mouse bones (see regions III-V on Fig. 7b).

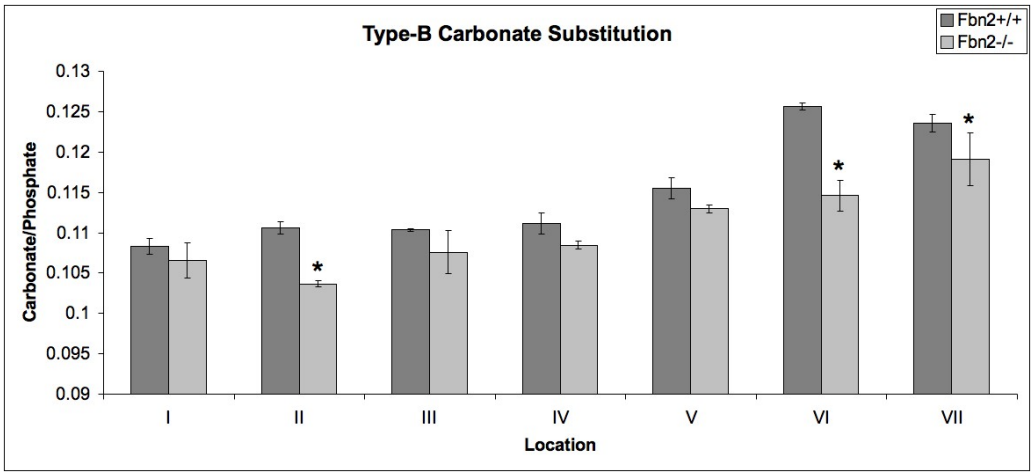

(a)

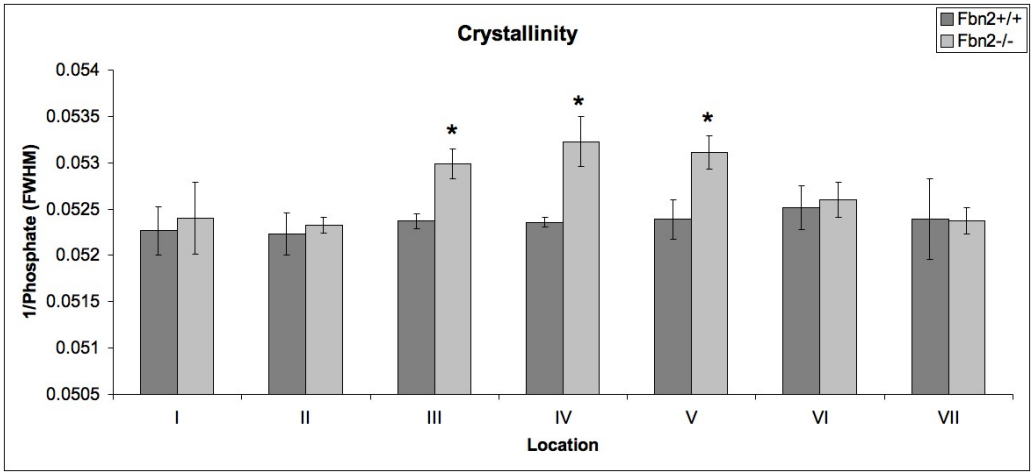

(b)

Fig. 7: Intra-bone variations in (a) type-B carbonate substitution and (b) crystallinity for femoral cortical bones from *Fbn2-/-* and *Fbn2*+/+ mice. The data were taken along a line traverse between the outer periosteal and inner endosteal regions of the bone. The error bars are standard statistical errors. * denotes $p \leq 0.05$ when comparing *Fbn2-/-* to *Fbn2*+/+ mouse bones.

The changes in the collagen's maturity and cross-linking for the bones from mice deficient in Fbn2 were examined by normalizing the average spectra of each genotype with the intensity of the CH_2 wag at ~1450cm^{-1} (Fig. 8). The area under the Amide I, Amide III and carbonate peaks all decreased slightly whereas, the phosphate ν_1 peak intensity did not change for the bones from *Fbn2-/-* mice compared to those from *Fbn2*+/+ mice.

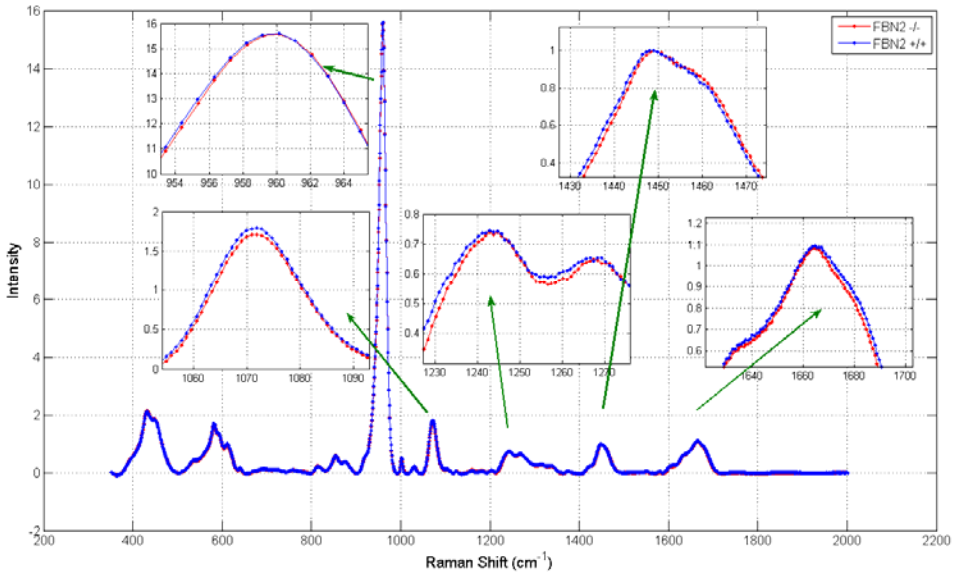

Fig. 8. Average Raman spectra normalized with CH_2 wag at 1450cm^{-1} for femoral bones from *Fbn2-/-* and *Fbn2*+/+ mice after baseline subtraction. The spectra are averaged over 20-25 measurements per sample that traverse between the outer periosteal and inner endosteal regions of the femur cortical bone.

Discussion

This study has investigated the role of two non-collagenous proteins, osteocalcin (OC) and fibrillin 2 (Fbn2), on the mechanical and chemical properties of cortical bone from mouse femora. Specifically, the intra-bone variations between the periosteal and

endosteal section of cortical bones were compared between the mutant and wild-type mice.

Deficiency of OC increased the average hardness of the mouse bones, while virtually no effect was seen for the elastic modulus. This agrees with an earlier study that reported no change in stiffness, but an increase in the failure load of bones from *OC*-/- mice when compared to *OC*+/+ mice [11]. It should be noted that the changes in H with genotype that were observed in the current study were not uniform across the entire bone. Some parts of the bone showed little difference while others show larger differences. A nanoindentation study by another group has reported a similar inverse correlation between OC concentration and the hardness of carp rib bone [12]. Unlike the present study, changes in E were also found in the carp bone.

In parallel to hardness, the crystallinity (crystal size and maturity) of the bones from *OC*-/- mice was higher compared to *OC*+/+ in the current study. An earlier FTIR study, however, indicated that the bones from *OC*+/+ mice had larger and more perfect crystals in comparison to bones from *OC*-/- mice [14]. The current study is in better agreement with a number of studies that have demonstrated osteocalcin's role in the recruitment of osteoclasts [5, 9, 10] and also in the inhibition of hydroxyapatite growth [3, 7, 8].

As well as the crystallinity, bones from *OC*-/- had lower type-B carbonate substitution compared to *OC*+/+ mice. Thus, OC deficiency alters the crystal stoichiometry. Boskey *et al.* found a similar relationship and speculated that the less mature bones of *OC*-/- mice might lead to a decrease in the carbonate/phosphate ratio [14]. The previous research when combined with the current findings may indicate that the apatite crystals become

larger and more perfect in *OC-/-* mouse bones compared to *OC+/+* mouse bones. The average Raman spectra (Fig. 5) for the current study exhibited a decrease in the collagen related peaks (Amide I and III) of *OC-/-* mouse bones. This suggests a slight increase in mineralization and possibly a decrease in collagen maturity in the *OC-/-* mouse bones.

Intra-bone variations in hardness, elastic modulus and crystallinity showed an increase when going from near-periosteal to near-endosteal sections of bone for *OC-/-* mice. This behavior could point to an alteration in the osteoclastic endosteal bone resorption. As reported elsewhere, the role of osteocalcin could be in bone remodeling [47] rather than bone formation [11].

The most significant finding for *OC* was the correlation between the hardness and crystallinity at the mid-cortical section which comprises the mature bone. That is, mature lamellar bone has properties which show a different dependence on *OC* than immature woven bone. The results suggest that *OC* may have the most impact in the fully mineralized matrix rather than early mineralization as was reported by Roach *et al*. [3]. Overall the results of the current study and previous studies showed some agreement and some contradictions with previously published data. This is most likely because the effects of *OC* are not uniform across the whole of the cortical bone and may even be completely different in trabecular bone.

Unlike *OC*, deficiency of *Fbn2* caused a significant decline in the average mechanical properties as shown by comparative nanoindentations of sex and age matched bones from mutant and wild-type littermates. Specifically, intra-bone variations revealed that bones from *Fbn2-/-* mice exhibited lower H and E in all sections across the cortical thickness

when compared to *Fbn2*+/+ mouse bones. However, we noted that crystal size and maturity of the bones from *Fbn2*-/- mice was increased when compared to *Fbn2*+/+ mouse bones. Therefore, there was a significant inverse correlation between the crystal size and mechanical properties of *Fbn2*-/- mouse bones. Interestingly the most significant alterations in crystallinity and mechanical properties of the bones from *Fbn2*-/- mice when compared to those from *Fbn2*+/+ mice were observed in mid-cortical section. This finding agrees with a previous suggestion based solely on a gene expression data of a structural role for microfibrils in the mature bone [21, 23, 48]. It is also consistent with the unpublished data indicating an increase in bone fragility in Fbn2-/- mice [28].

Conclusions

This study has demonstrated that at least at the nano-scale level the non-collagenous proteins *OC* and *Fbn2* are critical in determining the mechanical and chemical properties of bones. Increases in the mechanical properties typically correlate with increases in the crystallinity of the bones from *OC*-/- mice when compared to bones from *OC*+/+ mice. However, type-B carbonate substitution decreased in bones from *OC*-/- mice while hardness increased. Elastic modulus did not show the same dependence on carbonate substitution.

In bones from *Fbn2*+/+ mice, hardness and elastic modulus were higher in the mid-cortical region, but bones from *Fbn2*-/- mice had more uniform mechanical properties across the cortical section. In general mechanical properties would be expected to increase with increasing crystallinity, but crystallinity showed little variation in the mid-cortical section of the *Fbn2*+/+ bones, though it was higher in the *Fbn2*-/- bones. This

suggests that the fibrillin (microfibrils) in the *Fbn2*+/+ may be contributing to its mechanical properties. Carbonate substitution did not show a strong correlation with mechanical properties in *Fbn2-/-* or *Fbn2*+/+ bones.

In summary, the effects of mutations that remove *OC* and *Fbn2* on bone mechanical and chemical properties were not uniform across the width of cortical femora bone. The most significant difference between the genotypes was often observed in the mid-cortical sections. The present study has provided new insight into how non-collagenous proteins affect the nanomechanics and chemistry of bone tissue. This information is essential to the successful development of new treatments for osteopenia/osteoporosis and the avoidance of undesirable side-effects.

Acknowledgements

The authors would like to thank Prof. David Denhardt of Rutgers University, NJ and Prof. Nejat Guzelsu of UMDNJ, NJ for helpful discussions. Financial support for this research has been provided by NSF, ACS PRF, DOD DURIP, NJCHE, NIH and the Rutgers University Busch Bequest.

References

[1] P. Ammann, Therapie 58 (2003) 403.

[2] C. M. Gundberg, Osteoporosis International 14 (2003) S37.

[3] H. I. Roach, Cell Biology International 18 (1994) 617.

[4] M. T. Kaartinen, A. Pirhonen, A. LinnalaKankkunen and P. H. Maenpaa, Journal of Biological Chemistry 272 (1997) 22736.

[5] C. Chenu, S. Colucci, M. Grano, P. Zigrino, R. Barattolo, G. Zambonin, N. Baldini, P. Vergnaud, P. D. Delmas and A. Z. Zallone, Journal of Cell Biology 127 (1994) 1149.

[6] T. L. Dowd, J. F. Rosen, L. Li and C. M. Gundberg, Biochemistry 42 (2003) 7769.

[7] R. W. Romberg, P. G. Werness, B. L. Riggs and K. G. Mann, Biochemistry 25 (1986) 1176.

[8] P. A. Price, A. S. Otsuka, J. W. Poser, J. Kristaponis and N. Raman, Proceedings of the National Academy of Sciences of the United States of America 73 (1976) 1447.

[9] J. Glowacki, C. Rey, M. J. Glimcher, K. A. Cox and J. Lian, 45 (1991) 292.

[10] G. R. Mundy and J. W. Poser, Calcified Tissue International V35 (1983) 164.

[11] P. Ducy, B. F. Boyce, B. Story, C. Dunstan and G. Karsenty, Journal of Bone and Mineral Research 11 (1996) 43.

[12] M. E. Roy, S. K. Nishimoto, J. Y. Rho, S. K. Bhattacharya, J. S. Lin and G. M. Pharr, Journal of Biomedical Materials Research 54 (2001) 547.

[13] M. E. Roy, S. K. Nishimoto, J. Y. Rho, S. K. Bhattacharya and G. M. Pharr, Journal of Materials Science-Materials in Medicine 12 (2001) 699.

[14] A. L. Boskey, S. Gadaleta, C. Gundberg, S. B. Doty, P. Ducy and G. Karsenty, Bone 23 (1998) 187.

[15] E. A. Putnam, H. Zhang, F. Ramirez and D. M. Milewicz, Nature Genetics 11 (1995) 456.

[16] F. Quondamatteo, D. P. Reinhardt, N. L. Charbonneau, G. Pophal, L. Y. Sakai and R. Herken, Matrix Biology 21 (2002) 637.

[17] N. Carter, E. Duncan and P. Wordsworth, Rheumatology 39 (2000) 307.

[18] S. L. Dallas, D. R. Keene, S. P. Bruder, J. Saharinen, L. Y. Sakai, G. R. Mundy and L. F. Bonewald, Journal of Bone and Mineral Research 15 (2000) 68.

[19] P. F. Giampietro, M. Peterson, R. Schneider, J. G. Davis, C. Raggio, E. Myers, S. W. Burke, O. Boachie-Adjei and C. M. Mueller, Osteoporosis International 14 (2003) 559.

[20] L. Kohlmeier, C. Gasner, L. K. Bachrach and R. Marcus, Journal of Bone and Mineral Research 10 (1995) 1550.

[21] H. Zhang, W. Hu and F. Ramirez, Journal of Cell Biology 129 (1995) 1165.

[22] P. Plantin, M. Durigon, C. Boileau and J. M. Le Parc, Annales De Pathologie 20 (2000) 115.

[23] D. R. Keene, L. Y. Sakai and R. E. Burgeson, Human bone contains type III collagen, type VI collagen, and fibrillin: type III collagen is present on specific fibers that may mediate attachment of tendons, ligaments, and periosteum to calcified bone cortex, (1991) p. 59.

[24] F. Ramirez and L. Pereira, The International Journal of Biochemistry & Cell Biology 31 (1999) 255.

[25] H. Sakamoto, T. Broekelmann, D. A. Cheresh, F. Ramirez, J. Rosenbloom and R. P. Mecham, Journal of Biological Chemistry 271 (1996) 4916.

[26] E. R. Neptune, P. A. Frischmeyer, D. E. Arking, L. Myers, T. E. Bunton, B. Gayraud, F. Ramirez, L. Y. Sakai and H. C. Dietz, Nature Genetics 33 (2003) 407.

[27] K. B. Jones, P. D. Sponseller, G. Erkula, L. Sakai, F. Ramirez, H. C. Dietz, S. Kost-Byerly, K. H. Bridwell and L. Sandell, Symposium on the musculoskeletal aspects of marfan syndrome: Meeting report and state of the science, (2006) p. n/a.

[28] E. Arteaga-Solis et al., manuscript in preparation.

[29] E. Arteaga-Solis, B. Gayraud, S. Y. Lee, L. Shum, L. Sakai and F. Ramirez, Journal of Cell Biology 154 (2001) 275.

[30] M. E. Roy, J. Y. Rho, T. Y. Tsui, N. D. Evans and G. M. Pharr, Journal of Biomedical Materials Research 44 (1999) 191.

[31] M. D. Morris and W. F. Finney, Spectroscopy-an International Journal 18 (2004) 155.

[32] A. Carden and M. D. Morris, Journal of Biomedical Optics 5 (2000) 259.

[33] A. Boskey and R. Mendelsohn, Journal of Biomedical Optics 10 (2005).

[34] O. Akkus, F. Adar and M. B. Schaffler, Bone 34 (2004) 443.

[35] B. R. McCreadie, M. D. Morris, T.-c. Chen, D. Sudhaker Rao, W. F. Finney, E. Widjaja and S. A. Goldstein, Bone In Press, Corrected Proof.

[36] J. J. Freeman, B. Wopenka, M. J. Silva and J. D. Pasteris, Calcified Tissue International 68 (2001) 156.

[37] G. Penel, G. Leroy, C. Rey and E. Bres, Calcified Tissue International 63 (1998) 475.

[38] J. S. Yerramshetty, C. Lind and O. Akkus, Bone In Press, Corrected Proof.

[39] O. Akkus, A. Polyakova-Akkus, F. Adar and M. B. Schaffler, Journal of Bone and Mineral Research 18 (2003) 1012.

[40] E. P. Paschalis, K. Verdelis, S. B. Doty, A. L. Boskey, R. Mendelsohn and M. Yamauchi, Journal of Bone and Mineral Research 16 (2001) 1821.

[41] J. W. Ager, R. K. Nalla, K. L. Breeden and R. O. Ritchie, Journal of Biomedical Optics 10 (2005).

[42] R. K. Nalla, J. J. Kruzic, J. H. Kinney, M. Balooch, J. W. Ager and R. O. Ritchie, Materials Science & Engineering C-Biomimetic and Supramolecular Systems 26 (2006) 1251.

[43] M. P. Akhter, Z. Fan and J. Y. Rho, Calcified Tissue International 75 (2004) 416.

[44] Q. Chen, J. Y. Rho, Z. Fan, S. J. F. Laulederkind and R. Raghow, Calcified Tissue International 73 (2003) 387.

[45] M. J. Silva, M. D. Brodt, Z. Fan and J.-Y. Rho, Journal of Biomechanics 37 (2004) 1639.

[46] W. C. Oliver and G. M. Pharr, Journal of Materials Research 7 (1992) 1564.

[47] A. L. Boskey, M. F. Young, T. Kilts and K. Verdelis, Cells Tissues Organs 181 (2005) 144.

[48] S. Kitahama, M. A. Gibson, G. Hatzinikolas, S. Hay, J. L. Kuliwaba, A. Evdokiou, G. J. Atkins and D. M. Findlay, Bone 27 (2000) 61.

Effects of Osteopontin Deficiency and Aging on Nanomechanics of Mouse Bone

B. Kavukcuoglu[1], C. West[2], D.T. Denhardt[3], A. B. Mann[1, 2]

[1] Department of Ceramic and Materials Engineering, [2] Department of Biomedical Engineering,

[3] Department of Cell Biology and Neuroscience, Rutgers University, Piscataway, NJ

ABSTRACT

Osteopontin (OPN), a phosphorylated glycoprotein, is among the most abundant non-collageneous bone matrix proteins produced by osteoblasts and osteoclasts. OPN has been implicated in bone formation, resorption and remodeling. However, previous studies have presented contradictory results regarding the effect of OPN on the mechanics and microstructure of bone. This study has used nanoindentation to identify local variations in elastic modulus and hardness of OPN deficient (OPN -/-) and wild-type control (OPN+/+) mouse bones. Specifically, the study has looked at changes in the mechanical properties of OPN-/- and OPN+/+ mouse bones with the mouse's age. Cortical sections of femurs from different age groups ranging from 3 weeks to 58 weeks were tested and compared. The results suggest that there are large, abrupt variations in mechanical properties across the femur's radial section for 3-week-old mouse bone. The hardness (H) drops significantly towards the inner and outer sections so the cortical bone has a mean H=3.66 GPa with a standard deviation of 2.44 GPa. In contrast, the hardness of the 58-week-old mouse bone had a standard deviation of 0.35 GPa and a mean H=1.45 GPa. The hardness across the radial axis of the 58-week-old bone was found to be quite uniform.

The elastic modulus showed similar variations to the hardness with respect to age and position on the bone. We conclude that the mechanical properties of the mouse bones decrease substantially with maturity, and statistically the hardness and elastic modulus are more uniform in mature bones than young ones. Surprisingly we found a similar variation in both OPN-/- and OPN+/+ bones, with no statistically significant difference in the mechanical properties of the OPN -/- and OPN+/+ bones. The results for OPN-/- and OPN+/+ mouse bones are particularly important as control of OPN activity has been postulated as a potential treatment for bone pathologies that exhibit a change in the bone mineralization, such as osteoporosis, osteopetrosis and Paget's disease. Understanding the effects of OPN on bone mechanics is a vital step in the development of these new treatments.

INTRODUCTION

Osteoporosis means ‘porous bone’. It is a disease characterized by low bone mass, micro-architectural deterioration of bone tissue leading to enhanced bone fragility, and a consequent increase in fracture risk [1]. Increase in osteoclastic bone resorption causes loss of bone mineral in postmenopausal osteoporotic patients The osteoclastic bone resorption occurs as a result of attachment of osteoclasts to bone, forming a sealing zone. Once the sealing zone is formed, osteoclasts secrete hydrogen ions, creating an acidic environment causing the dissolution of bone mineral. Simultaneously, matrix metalloproteases are produced that degrade the bone’s collagen. It has been suggested that osteopontin (OPN), a major noncollageneous bone matrix protein, may possibly facilitate osteoclast attachment to the mineralized extracellular matrix during bone resorption [2] and, hence, it plays an important role in osteoporosis. There have been

many studies examining the role of OPN in bone mineralization and its effect on mineral crystal size.

Several studies have shown that in the absence of OPN (OPN-/-) female mice are resistant to ovariectomy-induced bone resorption (osteoporosis) when compared to OPN+/+ mice. Utilizing microcomputed tomography investigators have shown that OPN-/- mouse bone contains more mineral and larger mineral crystals. [3,4]. Another study that has used infrared imaging techniques to characterize the mineral in bones of two different genotypes revealed that the OPN-/- mouse bones are more mineralized than their background matched OPN+/+ controls [5]. It was recently demonstrated that OPN may play a key role in preventing bone loss due to reduced mechanical stress in bedridden patients and astronauts. Specifically, OPN-/- mice subjected to tail suspension showed no bone loss unlike OPN+/+ mice [2].

Although there are many studies of the action of OPN on bone mineralization, it is not clear how OPN deficiency affects the bone's mechanical properties. Accordingly, the primary objective of this study was to use nanoindentation to investigate the effects of OPN on hardness and elastic modulus of OPN-/- and OPN+/+ bones. The study was conducted on mice from different age groups in order to examine and compare the effects of aging on the mechanical properties of OPN+/+ and OPN -/- bones. Local variations in hardness and elastic modulus across the radial axis of cortical bone were also examined for both genotypes.

MATERIALS AND METHODS

Mice with targeted disruption of the OPN gene in a 129 background were developed at Rutgers University [3, 6 and 7]. Bones from mice between 3 and 58 weeks of age from both OPN -/- and OPN+/+ genotypes were used during the nanoindentation experiments. All mice were sacrificed humanely by CO_2 suffocation. The left femur from 2 or 3 mice in each age group and each genotype were excised and cleaned of soft tissue. The bones were then dehydrated in graded alcohol solutions (70-100%) and included in a low temperature cure epoxy (SPI supplies, West Chester, PA). Next, the included femora were sectioned transversely at a point just below the hip joint using a diamond wafering saw. The surfaces were ground with silicon carbide paper of decreasing grit size (400, 600 and 1200) followed by polishing with diamond paste down to ½ then ¼ µm grit. After the polishing all specimens were cleaned under water to remove surface debris.

Nanoindentation tests were done using a Triboindenter™ (Hysitron Inc., MN) in load control mode. All samples were tested in a dry state. Fused silica was used to calibrate the indenter. A berkovich diamond tip was used and the loading direction was parallel to the long axis of the femur. For each bone a grid pattern of approximately 300 indents were performed across the radial sections in the cortical bone. The results for hardness and elastic modulus were then averaged. For each indent a maximum load of 1000µN was applied with a 2 second hold time at peak load. The distance between indents was 2.5 µm and 10 µm in the x and y directions, respectively. The well known Oliver- Pharr method [8] was used for determining the elastic modulus and hardness. The following equations were used to find the bone's elastic modulus, E_s, and hardness, H:

$$E_r = \frac{\sqrt{\pi}}{2}\frac{S}{\sqrt{A_c}} \qquad E_s = \frac{1-\nu_s^2}{\frac{1}{E_r}-\frac{1-\nu_i^2}{E_i}} \qquad H = \frac{p_{\max}}{A_c}$$

where, E_r is the reduced elastic modulus, S is the measured contact stiffness, P_{max} is the maximum force and A_c the contact area. ν_i and ν_s are Poisson's ratio for the indenter and sample, respetively. The values for the diamond indenter tip are E_i = 1140 GPa, ν_i = 0.07 and Poisson's ratio for the bone was assumed to be ν_s = 0.3.

RESULTS AND DISCUSSION

The indents across the radial axis of each OPN+/+ femur and OPN-/- femur from matching age groups (between 3 and 58 weeks) were examined. Mechanical properties (H and E_s) were calculated for each indent and compared statistically between age groups as well as genotypes. The results suggest that there are large, abrupt variations in mechanical properties across the femur's radial section of young mouse bone (3 weeks) for both OPN-/- and OPN+/+ bones. However, for adult mouse bones (58 weeks) the mechanical properties were quite uniform across the radial axis for both genotypes (Figures 1 and 2).

As shown in Figure 1 the hardness (H) drops significantly towards the inner and outer sections of the cortical bone for 3 week old femora. Elastic modulus (E) shows similar variations along the radial axis of mouse bones. These findings suggest that the bones of younger mice are still in the process of growing and modeling. As a result the degree of mineralization is not the same at all points. In older bones it is known that during the process of remodeling there is a continuous deposition and turn over of bone. The most

recently deposited bone may be less mineralized than bone deposited earlier in life. As suggested by A. L. Boskey [9] and Goldman et. al. (2004) [10], one of the several microstructural variables known to affect the mechanical properties of bone is the degree of mineralization of the bone matrix [10].

The areas of apparently high mineralization and low mineralization within the same bone at 3 weeks may be due to the fact that the bone has not had sufficient time to be fully modeled. Consequently, there are abrupt variations in mineralization and, hence, in both H and E across the radial axis of femurs, as seen in our results (Figure 1). However, as the bones' become fully modeled and subsequently remodel over the mouse's lifespan, the variations in mineralization and mechanical properties diminish. Our results suggest that this maturation process increases the proportion of the bone with low mineralization. This gives cortical bone for 58 week old mice with more uniform and lower mechanical properties across the femur when compared with bone from 3 week old mice (Figure 2). It is important to note that both OPN-/- and OPN+/+ bones exhibited the same intra-bone variations and that the effects of aging were the same for both genotypes.

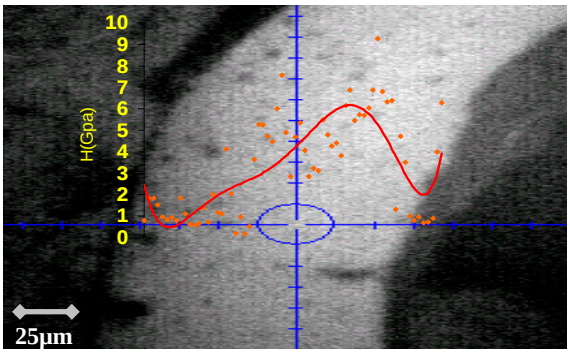

Figure 1. Optical image and hardness distribution of 3-week-old wild type mouse femur's radial section. A similar distribution is found for OPN (-/-) mouse bone of same age.

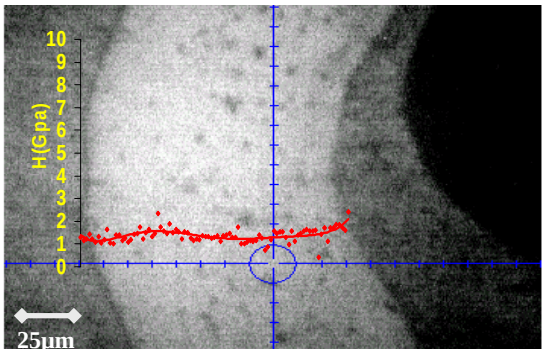

Figure 2. Optical image and hardness distribution of 58-week-old wild type mouse femur's radial section. A similar distribution is found for OPN (-/-) mouse bone of same age.

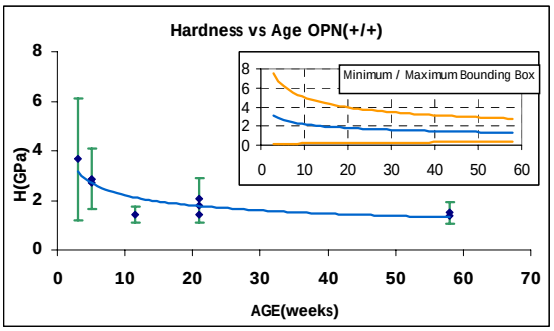

Figure 3. Change in mean Hardness as a function of age for wild type mouse femur. The error bars are standard deviations. The bounding box shows the minimum and maximum values of hardness for all age groups.

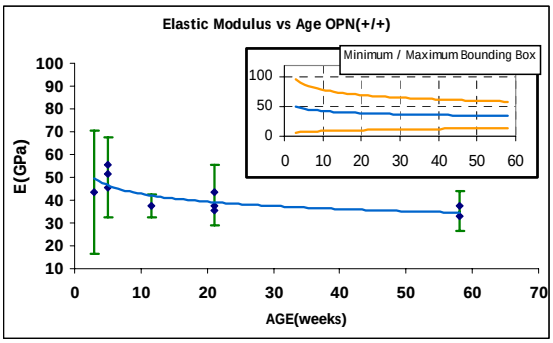

Figure 4. Change in mean Elastic Modulus as a function of age for wild type mouse femur. The error bars are standard deviations. The bounding box shows the minimum and maximum values of elastic modulus for all age groups.

Further examination of the mean values and standard deviations of H and E_s for each age group and genotype provided further information on the effects of aging and OPN on the mechanical properties of mouse bone. Figures 3 and 4 show the changes in mean hardness and elastic modulus for mouse femora due to aging of OPN +/+ mice.

Average hardness drops down significantly from 3.66 GPa (± 2.44) to 1.45 GPa (± 0.35) between the ages of 3 and 58 weeks. This is a very significant decrease in H and indicates that the degree of bone mineralization and the bone's structure change dramatically with

age. In addition there is an 87% drop in the standard deviation of hardness. The mean elastic modulus also decreased substantially with age from 43.5 GPa (±27.1) to 35.2 GPa (± 6.5) with a 76% decrease in standard deviation (Figure 4). Similar values were obtained for OPN-/- bone, as seen in Figures 5 and 6. For OPN-/- bone the mean hardness drops from 3.67 GPa (± 2.68) to 1.29 GPa (±0.36) with a 87.7% decrease in its standard deviation. The mean elastic modulus falls from 46.4 GPa (±21.8) to 37.7 GPa (±9.26) coupled with a 72.4% decrease in standard deviation.

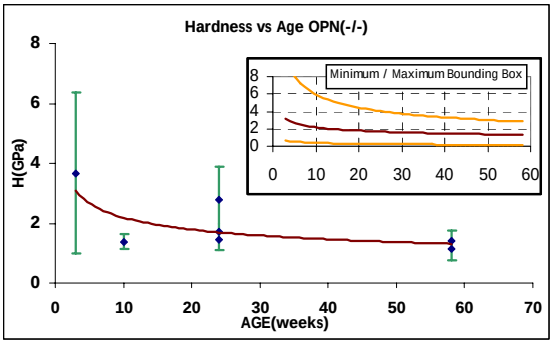

Figure 5. Change in mean Hardness as a function of age for OPN-deficient femora. The error bars are standard deviations. The bounding box shows the minimum and maximum values of hardness for all age groups.

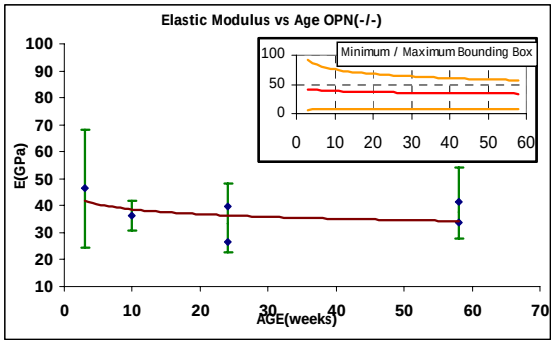

Figure 6. Change in mean Elastic Modulus as a function of age for OPN-deficient mouse femora. The error bars are standard deviations. The bounding box shows the minimum and maximum values of elastic modulus for all age groups.

Hardness and Elastic Modulus histograms present a better visualization of the changes that occur as the bone matures (Figures 7 and 8). In the figures y-axis shows the frequency, n, which indicates the number of indents on each sample. Accordingly; n = 423 (3 weeks OPN +/+), n = 327 (3 weeks OPN -/-), n = 882 (21 weeks OPN +/+), n = 867 (24 weeks OPN -/-), n = 431 (58 weeks, OPN +/+) and n = 584 (58 weeks OPN -/-).

There is an obvious shift in the curves towards smaller values with less scatter and a narrower range as the age increases. Thus there is an increase in homogeneity and a decrease in mechanical properties with age.

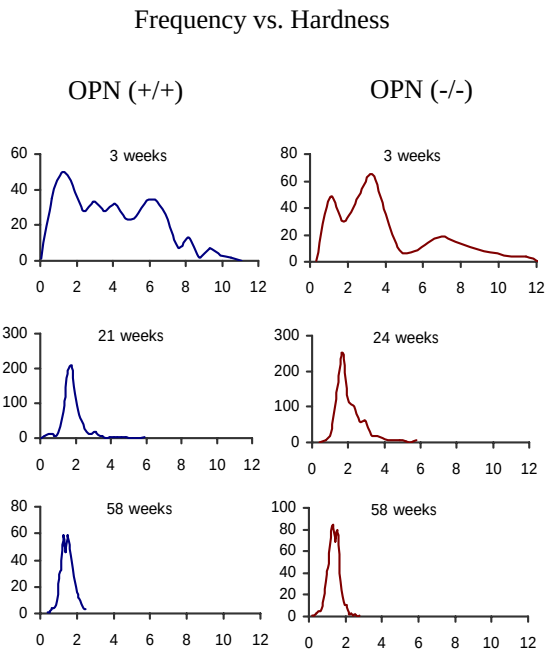

Figure 7. Hardness histograms for OPN +/+ and OPN -/- mouse bones of different ages (x axis is the hardness in GPa)

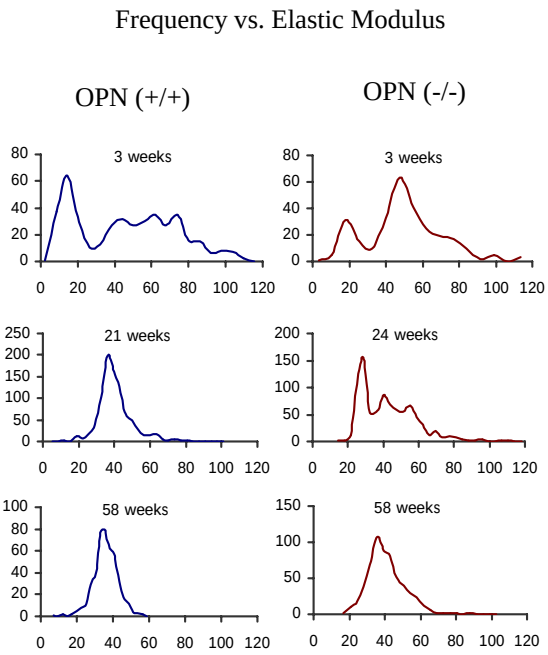

Figure 8. Elastic Modulus histograms for OPN +/+ and OPN -/- mouse bones of different ages (x axis is the elastic modulus in GPa)

CONCLUSIONS

Two main conclusions are suggested by our findings. First, as supported by the data in Figures 1 and 2, the mechanical properties diminished substantially with age. This is associated with a decrease in the variation of H and E_s in the cortical bone across the axis of the femur. That is the mechanical properties are more homogeneous in mature bones.

Another important finding was that there was no statistically important difference between the mechanical properties of OPN -/- mouse bone and its wild-type control

(OPN+/+). This is surprising given that earlier studies suggest an increase in the degree of mineralization in bones from OPN-deficient mice when compared with their wild-type controls [3, 4 and 5].

However, before it can be concluded that OPN does not affect the mechanical behavior of bone it is crucial that consideration be given to the viscoelastic nature of bone. These time-dependent properties are important in terms of preventing fracture and it is possible that the presence or absence of OPN has a more dramatic effect on these mechanical properties. As reviewed by P. Fratzl et.al (2004) [11] the mechanical behavior of the collagen mineral composite in bone depends remarkably on both components, mineral and viscoelastic collagen fibrils, and on their interaction. Accordingly, the contribution of the organic matrix to the mechanical properties of bone is critical. Small changes in mineralization may cause much greater changes in viscoelasticity because of the dependence on the organic matrix. That is a small increase in the amount of mineral present could dramatically change the ratio of organic to inorganic material in the bone. This may have little effect on H and E_s, but a noticeable effect on viscoelasticity. Further studies will be focused on the effect of OPN on the nanoscale viscoelasticity of bone.

The results for OPN -/- and OPN +/+ mouse bones are particularly important as control of OPN activity has been postulated [2, 3, 4 and 5] as a potential treatment for bone pathologies that exhibit a change in the bone mineralization. Understanding the effects of OPN on bone mechanics is a vital step in the development of these new treatments.

ACKNOWLEDGEMENTS

Mouse bones were provided by Dr. Susan Rittling (Rutgers University). Partial funding for this project was provided by the New Jersey Commission for Higher Education.

REFERENCES

1. P. Ammann, R Rizolli, Osteoporosis Int **14** (Suppl 3), 13 (2003).

2. M. Ishijima, S, Rittling, T, Yamashita, K Tsuji, H Kurusawa, A.Nifuji, D. Denhardt and M.Noda, J.Exp. Med., Vol **193**, Number **3**, 399 (2001).

3. S.A. Shapes, M. Clifuentes, L.Spevak, H. Chowdhury, J. Brittingham, A.L.Boskey, D.T. Denhardt, Calsif Tissue Int **73,** 86 (2003).

4. H. Yoshitake, S. R. Rittling, D.T. Denhardt and M. Noda, Proc. Nat. Acad. Sci. USA **96** 8156 (1999).

5. A. L. Boskey, L. Spevak, E. Pashalis, S.B. Doty, M.D. Mckee, Calcif Tissue Int. **71**, 145 (2002).

6. Rittling SR, Matsumoto HN, McKee MD, Nanci A, An XR, Novick KE et al. J Bone Min Res. **13(7)** 1101 (1998).

7. Soriano P, Montgomery C, Geske R, Bradley, A. Cell. **64(4),** 693 (1991).

8. W.C. Oliver, G.M. Pharr, J. Mater. Res. **7**, 1564, (1992)

9. A. L. Boskey, J Musculoskel Neuron Interact, **2 (6),** 532 (2002).

10. H. M. Goldman, T.G. Bromage, A. Boyde, C.D.L. Thomas and L.G. Clement, J. Anot. **203**, 243 (2003).

11. P. Frantzl, H.S. Gupta, E.P. Paschalls and R. Roschger, J. Mater. Chem. **14**, 2115 (2004).

Nanomechanics of Knockout Mouse Bones

N. B. Kavukcuoglu[1], A. B. Mann[1, 2]

[1] Department of Materials Science and Engineering,

[2] Department of Biomedical Engineering, Rutgers University, Piscataway, NJ

ABSTRACT

Osteocalcin (OC) and osteopontin (OPN) are among the most abundant non-collagenous bone matrix proteins. Both have drawn interest from investigators studying their function in osteoporosis and it is known that mutations of these proteins can also have dramatic effects on the properties of bone. Other proteins including fibrillin 1 and 2 (FBN2) have been less widely studied, but can be mutated in some individuals resulting in connective tissue disorders. It has been reported that abnormal fibrillin may play a role in decreased bone mass. In this study bones from osteopontin (OPN), osteocalcin (OC) and fibrillin-2 (FBN2) knockout mice have been investigated. The study has identified how these proteins affect the bone's nanomechanical properties (hardness and elastic modulus). Nanoindentation tests were performed on the radial axis of cortical femora bones from the knockout mice and their wildtype controls. The results showed that young (age< 12 weeks) OPN knock-out bones have significantly lower mechanical properties than wild-type bones indicate a crucial role for OPN in early bone mineralization. After 12 weeks of age, the OPN knockout and wild-type control bones did not show any statistical difference. In OC deficient mice the mechanical properties were found to increase in the cortical mid-shaft of femora from 1 year old mice, suggesting an increase in bone

mineralization, but 3 month old FBN2 deficient mice bones showed a decrease in mechanical properties across the cortical radial axis of the mid- femora.

INTRODUCTION

Osteoporosis is a bone disease in which bone mineral density (BMD) is reduced and the bone's microarchitecture deteriorates leading to an increased fragility [1]. The essential feature of osteoporosis is an increase in the ratio of osteoclastic bone resorption to osteoblastic bone formation. Simultaneously, there is a change in the amount and variety of non-collagenous proteins in the bone which suggests a link between bone mineralization/resorption and these proteins [2]. Osteopontin (OPN), a phosphorylated glycoprotein and Osteocalcin (OC), a γ-carboxyglutamic acid-containing protein (BGP), are among the most abundant non-collageneous bone matrix proteins. Because of their possible role in bone mineralization and crystal maturity, these proteins have drawn interest from many investigators [3-9]. Particularly, it has been indicated that OC functions as a signal in the recruitment of osteoclast pre-cursors to resorption sites and facilitates their differentiation to bone resorbing osteoclasts [2, 3]. Absence of OPN has been linked to a reduction in the effects of osteoporosis in small mammals [7, 9].

Moreover, bones from osteocalcin-deficient (OC-/-) mice were shown to have increased bone formation [4] and increased mineral to matrix ratio (for ovariectomized animals) [5]. Similar to the role of OC, several studies have shown the importance of OPN in bone resorption, remodeling, mineralization and osteoporosis [7,8,9] as well. It has been indicated that bones from OPN-/- mice have more mineral content and increased crystal size compared to their background matched OPN+/+ (wild-type) controls [8]. Besides

OC and OPN, mutations of other proteins can also have dramatic effects on the properties of bones. Fibrillins (fibrillin 1 and 2) are glycoproteins that constitute the major structural components of microfibrils. The fibrillin 2 (FBN2) gene located on chromosome 15q23-31 can be mutated in some individuals resulting in congenital contractural arachnodactyly (CCA) which is a connective tissue disorder [10]. It has also been associated with osteopenia. Some studies have reported that abnormal fibrillin could play a role in decreased bone mineral density and display reduced structural properties [11].

There are several studies on the effects of OPN, OC and FBN on bone mineralization, however their role on bone's mechanical properties on the submicron scale has not been investigated in any detail. This study has used mice of different genotypes to look at the effects of these noncollageneous proteins on the bone's nanomechanical properties (hardness and elastic modulus). In addition, because of the importance of OPN in bone remodeling and osteoporosis this study also examined mice from different age groups to identify the effects of aging on nanoscale mechanical properties.

MATERIALS AND METHODS

This study has used male osteopontin (OPN) and osteocalcin (OC) and female fibrillin-2 (FBN2) knockout mouse models and their age, sex and background matched wild-type controls. All mice were sacrificed by CO_2 suffocation. The left femur from the mice for each age group and genotype were excised and cleaned of soft tissue. Briefly, this involved dehydration in graded alcohol solutions (70-100%) and mounting in a low temperature cure epoxy (SPI supplies, West Chester,PA). After mounting, the included femora were sectioned transversely at a point just below the hip joint (for OPN studies)

and at mid-shaft (for OC and FBN studies) using a diamond wafering saw. The surfaces were ground with silicon carbide paper of decreasing grit size (400, 600 and then 1200 particles per inch) followed by polishing with diamond paste down to ½ then ¼ μm grit size. After the polishing, all specimens were cleaned ultrasonically to remove surface debris.

Nanoindentation tests were performed using a Triboindenter^{TM} (Hysitron Inc., MN) in load control mode. For each indent a maximum load of 1000 μN was applied with a 2 second hold time at peak load. The distance between indents was 2.5 μm and 10 μm in the x- (radial) and y- (tangential) directions, respectively. The Oliver-Pharr method [12] was used to determine the mechanical properties. The following equations were used to find the bone's elastic modulus, E and hardness, H:

$$E_r = \frac{\sqrt{\pi}}{2}\frac{S}{\sqrt{A_c}} \qquad \mathrm{E} = \frac{1-\nu_s^2}{\frac{1}{E_r} - \frac{1-\nu_i^2}{E_i}} \qquad \mathrm{H} = \frac{P_{\max}}{A_c}$$

where, E_r is the reduced elastic modulus, S is the measured contact stiffness, P*max* is the maximum load and A_c is the contact area. ν_i and ν_s are Poisson's ratio for the indenter and sample, respectively. The values for the diamond indenter tip are E_i = 1140 GPa, ν_i = 0.07 and the Poisson's ratio for the bone was taken to be ν_s = 0.3. The contact area, A_c, was determined by analysis of the load-depth curve and calibrating the tip on a standard material (fused quartz)

To gain statistically significant data for the aging study, bones from OPN-/- and OPN+/+ mice were divided into young (≤12 weeks old, n = 16), mature (12-50 weeks, n = 13) and

old (≥50 weeks old, n = 17). Effects of OC and FBN2 were measured on bones from 1 year (n=11) and 3 months (n=9) old mice, respectively. One-way analysis of variance (ANOVA) and non-parametric Mann-Whitney statistics tests was utilized to compare the mechanical properties measured for knock-out and wild-type animal models.

RESULTS AND DISCUSSION

The nanoindents were performed across the radial axis of each cortical femur to provide the intra- and inter-bone variations for each genotype and age (~300 indents/sample). The average values for each combination of genotype and age were also calculated. The variation in the mechanical properties with OPN deficiency and aging, OC and FBN2 deficiency and location across the cortical thickness (periosteal, mid-cortical and endosteal) were analyzed.

Effects of Osteopontin deficiency and aging

Hardness and Elastic modulus variations with age are shown in Figure 1a and 1b. Data from both OPN-/- and OPN +/+ showed no statistically significant difference with genotype for mature and old age groups ($F < F_{critical}$ and $P > 0.05$). However, for the young age group the mechanical properties of OPN-/- mice were significantly lower than those of the wild-type controls ($F > F_{critical}$ and $P < 0.05$). The mean H values for young OPN-/- and OPN+/+ mice were 1.52 ± 0.05 GPa and 2.64 ± 0.07 GPa, respectively. Similarly, the mean E for young OPN-/- mice was 30.84 ± 0.66 GPa, but 45 ± 0.98 GPa for OPN+/+ mice. These results are in agreement with the reported role for OPN in the earliest stages of bone formation, mineralization and osteoblast activity [13,14].

The results for the effects of aging on H and E show a significant difference between the genotypes. Bones from OPN-/- mice have been found to show very little variation in H and E with age, however bones from OPN+/+ mice show significant differences in H and E between the young and mature mice. The decrease in the mechanical properties of bone with age for OPN+/+ mice may be attributed to a change in the degree of bone mineralization.

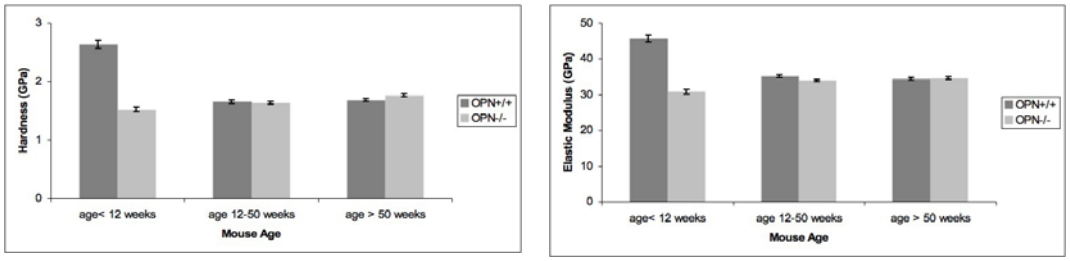

a. b.

Figure 1 Change in mean hardness (H) and Elastic Modulus (E) as a function of age groups for cortical femora from OPN+/+ and OPN-/- mice. The error bars are standard statistical errors

Effects of Osteocalcin deficiency

Figures 2a and 2b show the variations in hardness and elastic modulus across the cortical femoral sections from OC-/- and OC+/+ mice bones. Bones from OC-/- mice had higher hardness values in a statistically significant way, especially in the center and endosteal region of the cortical section ($p<0.01$). The average hardness for were calculated as 1.27 ± 0.007 GPa and 1.18 ± 0.01 GPa for OC-/- and OC +/+ mice bones respectively. On the other hand, OC deficiency did not have any significant effect on the elastic modulus of the bones. The average elastic modulus for OC-/- were measured as 30.1 ± 0.16 GPa and for OC+/+, it was 30.5 ± 0.14 GPa. Similar to these findings, another study has also used nanoindentation to correlate OC concentration to mechanical properties and reported an

inverse correlation between the OC concentration and the mechanical properties in the longitudinal plane of carpio rib bone [6].

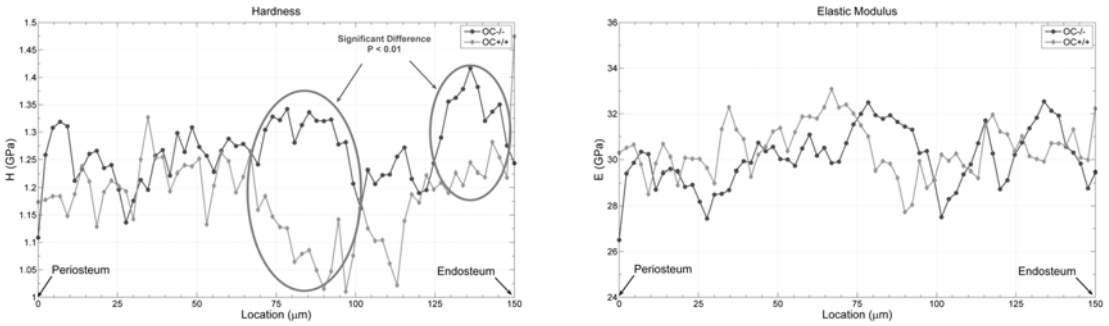

a. b.

Figure 2 Intra-bone variations in hardness (H) and Elastic Modulus (E) for femora from OC-/- and OC+/+ mice. The data is taken along a line traversing the radial section of the cortical bone. Each figure shows the averaged data from three lines of indents with regions of statistically significant difference highlighted.

Effects of Fibrillin-2 deficiency

Statistical analysis of the intra-bone variations in mechanical properties of bones from FBN2-/- and FBN2+/+ showed a significant decrease in hardness and elastic modulus with deficiency of FBN2 ($p<0.05$). The average hardness decreased from 1.23 ± 0.007 GPa to 1.15 ± 0.008 GPa and the average elastic modulus decreased from 31.8 ± 0.14 GPa to 29.3 ± 1.18 GPa between the FBN2+/+ and FBN2-/- mouse bones (Figure 3a, b). The decrease in the mechanical properties observed in this study can be related to the findings of a recent study that has indicated a reduction in bone mass and remodeling that is caused by mutations in the FBN2 gene [11].

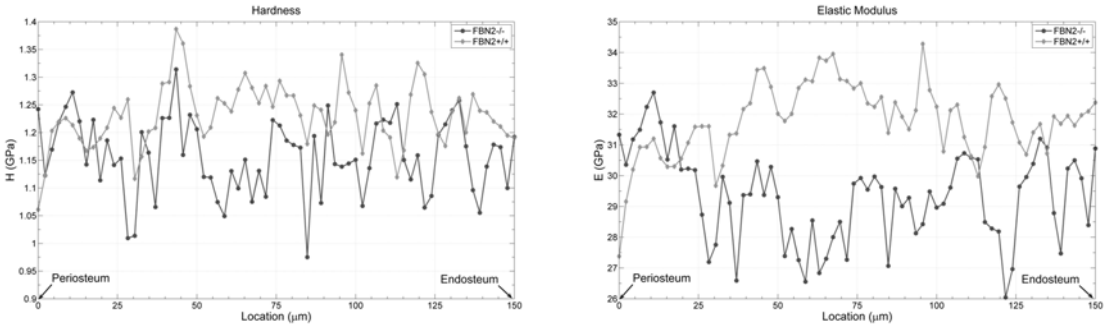

a. b.

Figure 3 Intra-bone variations in hardness (H) and Elastic Modulus (E) for femora from FBN2-/- and FBN2+/+ mice. The data is taken along a line traversing the radial section of the cortical bone. Each figure shows the averaged data from three lines of indents.

CONCLUSIONS

The results of this study indicated that the nanomechanical properties of bones from OPN, OC and FBN2 bones show a strong dependence on the presence or absence of those non-collagnous proteins. Specifically, the hardness and elastic modulus of bones from young OPN-/- mice are much lower than their background matched OPN+/+ equivalents. Deficiency of the other two non-collagenous proteins studied, OC and FBN2, causes a decrease in mechanical properties of the bones, but this is not uniform across the width of the bone. Thus, this study has shown that noncollagenous bone proteins are vital in determining the overall mechanical properties of bone.

In the future, new clinical approaches for the treatment of bone diseases such as osteopenia, osteoporosis and conditions such as Marfan's syndrome and congenital contractural arachnodactyly (CCA) may involve control of non-collagenous protein activity. This might be achieved for instance with antibodies that target the proteins or gene therapy that enables cells to express the protein. In each case knowledge of how the

proteins affect the nanomechanics of bone is essential to the successful development of these treatments and the avoidance of undesirable side-effects.

ACKNOWLEDGMENTS

The authors would like to thank the following for providing bone samples: David Denhardt and Pat Buckendahl (Rutgers University, NJ) and Francesco Ramirez (formerly of the Hospital for Special Surgery, NYC). Financial support was provided by the New Jersey Commission for Higher Education, the ACS Petroleum Research Fund and the Busch bequest (Rutgers University).

REFERENCES

1. L. Ginaldi, M.C. Benedetto, M.D. Martinis, Immunity and Ageing.2, 14 (2005)
2. H.I. Roach, Cell Biology International. 18, 6 (1994)
3. J.D. Malone, S.L. Teitelbaum, G.L. Griffin, R.M. Ssenior, A.J. Kahn. J. Cell Biol. 92, (1982)
4. D. Ducy, C. Desbois, B. Boyce, G. Pinero, B. Story, C. Dunstan, E. Smith, J, Bonadio, S. Goldstein, C. Gundberg, A. Bradley, G. Karsenty, Nature 382, (1996)
5. A. L. Boskey, S. Gadaleta, C. Gundberg, S.B. Doty, P. Ducy, G. Karsenty, Bone. 23,3 (1998)
6. M.E. Roy, S.K. Nishimato, J.Y. Rho, S.K. Bhattacharya, J.S.Lin, G.M. Pharr, J Biomed Mat Res. 54, 4 (2000)
7. M. Ishijima, S.R. Rittling, T. Yamashite, K. Tsuji, H. Kurosawa, A. Nifuji, D.T. Denhardt, M. Noda. J Exp Med. 193, (2001)
8. A.L. Boskey, L. Spevak, E. Pashalis, S.B. Doty, M.D. Mckee. Calcif Tissue Int. 71 (2002)
9. H Yoshitake, S.R. Rittling, D.T. Denhardt and M. Noda. Proc Natl Acad Sci. 96 (1999)
10. E.A. Putnam, H. Zhang, F. Ramirez, D.M. Milewicz. Nature Genetics. 11 (1995)
11. F. Ramirez. Matrix Biology 25 (2006)
12. W.C. Oliver, G.M. J. Mater. Res. 7 (1992)
13. T. Uemura, Y. Liu, A. Nemoto, T. Yabe, T. Ushida, H. Miyamoto, T. Tateishi. Mater Sci Eng C. 4 (1997)
14. S Kasugai, T Nagata, J Sodek. J Cell Biol. 152 (1992)

CURRICULUM VITA

Nadire Beril Kavukcuoglu

Born: 01/03/1976, Ankara, TURKEY

1993-1997: BS in Metallurgical and Materials Engineering, Middle East Technical University, Turkey

1997-1999: M.S. in Materials Science and Engineering, Rutgers University, NJ, USA

- Dissertation Topic – Development and Characterization of Piezoelectric Tube-array Actuators

2003-2007: Ph. D. Materials Science and Engineering, Rutgers University, NJ, USA

- Dissertation Topic – Characterization and Correlation of the Nano-scale Mechanical, and Chemical Properties of Knockout Mouse Bones

Publications

- Effects of Osteopontin Defficiency and Aging on Nanomechanics of Mouse Bone. N. B. Kavukcuoglu, D. Denhardt, N. Guzelsu, A.B. Mann; In Press, Journal of Biomedical Materials Research, 2006

- Nanomechanics of Knockout Mouse Bones, N. B. Kavukcuoglu, A.B. Mann; In Press, Materials Research Society Proceedings 2006.

- Effects of Osteopontin on Nanomechanics and Microstructure of Mouse Bones. B. Kavukcuoglu P, C. West, D. Denhardt, A.B. Mann; Materials Research Society Proceedings 2004; vol. 844, p. 99-104

- Raman Micro-spectroscopic Analysis of the Effects of Aging and Osteopontin-Deficiency on Mouse Bones. N. B. Kavukcuoglu, D. Denhardt, A.B. Mann; submitted to Calcified Tissue International, February 2007

- Nanomechanics and Raman Spectroscopy of Osteocalcin and Fibrillin-2 deficient Mouse Bones. N. B. Kavukcuoglu, A.B. Mann; submitted to Journal of Materials Science, December 2006.